

REMOTE POWER DELIVERY FOR HYBRID INTEGRATED BIO-IMPLANTABLE ELECTRICAL STIMULATION SYSTEM

A Thesis
Submitted to the Graduate Faculty of the
Louisiana State University and
Agricultural and Mechanical College
in partial fulfillment of the
requirements for the degree of
Master of Science in Electrical Engineering

in

The Department of Electrical and Computer Engineering

by
Venkat Reddy Gaddam
B.E., Bapuji Institute of Engineering and Technology, India, 2001
May 2005

Dedicated to:

my parents, sister, and brother-in-law

ACKNOWLEDGEMENTS

I would like to convey my deepest appreciation to my research advisor, Professor Pratul K. Ajmera for his valuable guidance, support and mentorship throughout my graduate studies at Louisiana State University. His deep insight, attention to detail and incredible common sense, both on my thesis and in general will always be an inspiration. I have learned tremendously from him. It has been my great pleasure to conduct research on a topic that has significant potential to better human health.

I would like to thank Dr. Ashok Srivastava and Dr. Jin-Woo Choi for serving on my thesis committee and for their valuable suggestions. Acknowledgements are due to Mr. Steve Schmeckpeper and Mr. James Breedlove for their hours of involvement in the project and help in coil winding. Special thanks to Mr. Golden Hwuang for his assistance in the use of laboratory equipment. I gratefully acknowledge the partial support that I received as a research assistant from the NSF and Louisiana Board of Regents through the EPSCoR research grant # 0092001.

I would like to extend my appreciation to Sunitha Kopparthi for introducing me to this project and her initial understanding of the subject involved. I will always be thankful to the support and guidance that I received from other student members of the Integrated Microsystems Group: Inhyouk Song, Tinghui Xin, Satish Kona, Jagadish Yernagula and Raghavendra Anantha.

I will forever be grateful to my parents for their unconditional love and support throughout my life. Last, but not the least, I am also grateful to my sister and brother-in-law for their encouragement and for supporting me during those initial days of struggle.

Thank you God for all my success is with your blessing.

TABLE OF CONTENTS

DEDICATION	ii
ACKNOWLEDGEMENTS	iii
LIST OF TABLES	vi
LIST OF FIGURES	vii
ABSTRACT	ix
CHAPTER 1. INTRODUCTION	1
1.1 Remote Power Delivery System (RPDS).....	1
1.2 Literature Review.....	2
1.3 Objectives and Scope of Thesis.....	6
1.4 Thesis Outline.....	7
CHAPTER 2. THEORY	9
2.1 Electric Field.....	9
2.2 Magnetic Field.....	10
2.2.1 Magnetic Field from a Circular Wire Loop.....	10
2.2.2 Magnetic Field in a Solenoid.....	12
2.2.3 Magnetization and Magnetic Materials.....	13
2.2.4 Magnetic Induction.....	14
2.3 RPDS Overview.....	20
2.3.1 Transmitter Coil Driver.....	20
2.3.2 Coil Setup.....	21
2.3.3 Link Efficiency and Coil Compensation.....	21
2.3.4 Rectifier Circuit.....	22
2.3.5 Voltage Regulator.....	22
2.3.6 Implant Circuitry.....	23
CHAPTER 3. RPDS DESIGN	24
3.1 Coil Design.....	24
3.1.1 Transmitter Coil Design.....	26
3.1.2 Receiver Coil Design.....	27
3.1.3 Operating Frequency.....	28
3.2 Link Efficiency.....	28
3.2.1 Link Efficiency for the Uncompensated Case.....	29
3.2.2 Link Efficiency for the Compensated Case.....	32
3.2.3 Link Efficiency for the Compensated Case-Considering Parasitic Coil Capacitance.....	37
3.3 RPDS Overall Efficiency and Other Design Aspects.....	45

CHAPTER 4. SIMULATIONS AND RESULTS	51
4.1 RPDS Simulation.....	51
4.2 Coil Parasitics, Skin and Proximity Effects Model.....	54
4.3 Results.....	58
CHAPTER 5. SUMMARY AND FUTURE WORK	63
5.1 Summary and Discussions.....	63
5.2 Future Work.....	64
REFERENCES	65
APPENDIX A: TABLE FOR VALUES OF Y_1 AND Y_2	69
APPENDIX B: LINK EFFICIENCY FOR THE UNCOMPENSATED CASE	70
APPENDIX C: MATLAB CODE FOR THE UNCOMPENSATED CASE	73
APPENDIX D: LINK EFFICIENCY FOR THE COMPENSATED CASE	74
APPENDIX E: MATLAB CODE FOR THE COMPENSATED CASE	81
APPENDIX F: LINK EFFICIENCY FOR THE COMPENSATED CASE – CONSIDERING COIL PARASITIC CAPACITANCES	83
APPENDIX G: MATLAB CODE FOR THE COMPENSATED CASE – CONSIDERING COIL PARASITIC CAPACITANCES	88
APPENDIX H: LI-ION BATTERY RATINGS	90
APPENDIX I: MATLAB CODE TO CALCULATE POWER DELIVERED TO THE LOAD	91
APPENDIX J: TABLE AND CHART FOR SKIN EFFECT MODEL	93
APPENDIX K: PERFORMANCE CHARACTERISTICS OF SKIN EFFECT MODEL	95
VITA	96

LIST OF TABLES

3.1	Copper coil wire specifications from MWS Wire Industries.....	26
3.2	Parameter values for the designed transmitter and receiver coils.....	28
4.1	Variation in load voltage V_{dc} and load power P_{dc} with radial coplanar displacement X of the coil axes at 20 kHz and 40 kHz. $V_{IN} = 19.81$ V rms and $R_L = 65 \Omega$	60
A.1	Values of y_1 and y_2 for use in Eqn. (3.1). After reference [27].....	69
H.1	Polymer Li-ion battery (PR-042025) ratings from TCL Hyperpower Batteries Inc....	90
J.1	Values for functions H and G. After reference [27].....	94

LIST OF FIGURES

2.1	Magnetic field at point P due to a circular wire loop.....	11
2.2	Magnetic field lines in a solenoid.....	12
2.3	Magnetic materials chart.....	14
2.4	Lumped equivalent model for an inductor.....	16
2.5	Schematic arrangement of two coaxial coils.....	18
2.6	Schematic arrangement of two concentric, coplanar and coaxial loops.....	19
2.7	Block diagram for a transcutaneous power delivery system.....	20
3.1	Short multiple layered coil of solenoidal form.....	25
3.2	Schematic illustration of hexagonally close-packed cross-section along thickness of the coil. Diameter of the coil wire is d_w	25
3.3	An inductively coupled circuit and its equivalent transmitter circuit.....	30
3.4	Link efficiency η as a function of frequency for the uncompensated case.....	31
3.5	Circuit schematic for coil compensation topologies with external capacitors C_T and C_R . a) series compensation, b) parallel compensation.....	33
3.6	Link efficiency η as a function of coil operating frequency when transmitter coil is series compensated and receiver coil is both series and parallel compensated (C_{R-}). Semi-log scale.....	38
3.7	Link efficiency η as a function of coil operating frequency when transmitter coil is series compensated and receiver coil is both series and parallel compensated (C_{R-}). Logarithmic scale.....	38
3.8	Link efficiency η as a function of coil operating frequency when transmitter coil is series compensated and receiver coil is both series and parallel compensated (C_{R+}). Semi-log scale.....	39
3.9	Link efficiency η as a function of coil operating frequency when transmitter coil is series compensated and receiver coil is both series and parallel compensated (C_{R+}). Logarithmic scale.....	39

3.10	Link efficiency η as a function of coil operating frequency when transmitter coil is series compensated and receiver coil is parallel compensated (C_{R+} and C_{R-}). Semi-log scale.....	40
3.11	Link efficiency η as a function of coil operating frequency when transmitter coil is series compensated and receiver coil is parallel compensated (C_{R+} and C_{R-}). Logarithmic scale.....	40
3.12	Circuit schematic of an inductively coupled system. Transmitter coil is series compensated and receiver coil is parallel compensated.....	41
3.13	Link efficiency η as a function of coil operating frequency, considering parasitic coil capacitances. Transmitter coil is series compensated and receiver coil is parallel compensated (C_{RE+} and C_{RE-}).....	44
3.14	Lumped equivalent circuit for the front end of the RPDS with a voltage doubler circuit.....	45
3.15	Block diagram of battery charging chip MIC 79050.....	47
3.16	Simplified version of Fig. 3.14 from power dissipation consideration.....	48
4.1	Load power delivered as a function of resonance frequency. Analytical model considers parasitic coil capacitances $C_{ST} = 47.63$ pF and $C_{SR} = 2.1$ pF. $V_{IN} = 1.55$ V rms, $R_L = 35 \Omega$	52
4.2	Load power delivered as a function of resonance frequency for different values of parasitic capacitances C_{ST} and C_{SR} . $V_{IN} = 1.55$ V rms, $R_L = 35 \Omega$	53
4.3	Load power delivered as a function of resonance frequency for different values of coil resistances R_T and R_R . $V_{IN} = 1.55$ V rms, $R_L = 35 \Omega$	53
4.4	Variation in the transmitter coil resistance with frequency (skin/proximity effects).....	56
4.5	Variation in the receiver coil resistance with frequency (skin/proximity effects).....	56
4.6	Load power delivered as a function of resonance frequency with and without using skin effect. $V_{IN} = 1.55$ V rms, $R_L = 35 \Omega$	57
4.7	Link efficiency as a function of resonance frequency with and without using skin effect. $V_{IN} = 1.55$ V rms, $R_L = 35 \Omega$	58

4.8	Power delivered to the load as a function of radial coplanar displacement X of the receiver coil axis with respect to the transmitter coil axis.....	59
4.9	Schematic illustration of the radial coplanar displacement of the coil axes X	59
4.10	Circuit layout for the RPDS consisting of the lumped equivalent model, a voltage doubler circuit and a battery charger circuit. Transmitter coil is series compensated and receiver coil is parallel compensated.....	61
4.11	Variation in battery voltage and charging current with time. Resonance frequency of the coils is 20 kHz and radial coplanar displacement of the coil axes $X = 6$ inches....	62
B.1	Inductively coupled circuit with equivalent transmitter and receiver circuits.....	70
B.2	Equivalent transmitter circuit.....	70
D.1	Inductively coupled circuit with equivalent series compensated transmitter and receiver circuits.....	74
D.2	Inductively coupled circuit with equivalent series compensated transmitter and parallel compensated receiver circuits.....	78
F.1	Inductively coupled circuit with series compensated transmitter and parallel compensated receiver coils.....	83
F.2	Equivalent circuit on the transmitter side of an inductively coupled circuit.....	86
J.1	Plots for various values of K for multilayer coils. After reference [27] reproduced by permission.....	93
K.1	The performance characteristics of an Ultralife polymer rechargeable battery. The actual battery used for experimental purposes was a similar Powerizer polymer Li-ion rechargeable battery. No data sheets were made available by Powerizer for their product.....	95

ABSTRACT

Bio-implantable devices such as heart pacers, gastric pacers and drug-delivery systems require power for carrying out their intended functions. These devices are usually powered through a battery implanted with the system or are wired to an external power source. In this work, a remote power delivery system (RPDS) is considered as a means to charge rechargeable batteries that power a Bio-implanted Electrical Stimulation System (BESS). A loosely coupled inductive power transmitter and receiver system has been designed to recharge batteries for a bio-implanted gastric pacer.

The transmitter coil is periodically worn around the waist. The receiver coil, rechargeable batteries, battery-charging chip and the chip containing electrical stimulation circuitry form a bio-implanted hybrid integrated microsystem. The link efficiency between a transmitter coil and the implanted receiver coil when the diameters are markedly different is analyzed. A design methodology for RPDS is proposed based on the load and voltage required at the load. An analytical model is developed with the help of simple Matlab coding. A full wave rectifier with a voltage doubler circuit is used for the conversion of ac voltage to the required dc voltage. This dc voltage supplies power to a battery charging chip which is used to safely and appropriately charge a rechargeable Li-ion battery.

For an input supply voltage of 17.67 V rms, operating frequency of 20 kHz and radial coplanar displacement between the coil axes of 7.5 inches, the maximum dc voltage and power obtained across a 65 Ω load resistor are 9.65 V and 1.33 W respectively. For a radial coplanar displacement between the coil axes of 6 inches, a 3.7 V nominal, 150 mAh polymer lithium ion battery has been successfully charged in 1 hour and 40 minutes from an initial voltage of 3.39 V to 4.12 V with an input voltage of 19.81 V rms at 20 kHz.

An attempt has been made to model coil parasitics at high frequency. Variations in the load power as a function of frequency and radial coplanar displacement of the axes are examined. Design strategies to optimize power delivery with given geometric constraints are considered.

CHAPTER 1

INTRODUCTION

1.1 Remote Power Delivery System (RPDS)

The development in implantable electronics for biomedical applications is scaling new heights. As miniaturization of these implants keeps increasing, so also does the complexity in designing power supplies for such systems.

Most bio-implants have a bio-compatible electronic interface such as electrodes or sensors which serve either in current/voltage stimulation or in micro/nano drug delivery systems. From the early pacemaker designs of the 1930's with external protruding electrodes and leads coming out of the skin to the latest cochlear implants with RF power delivery system, power supply has always been a significant practical issue to contend with. Quality of life for the patient, implant life time and risk of infection through wires protruding out of skin are among the factors instrumental in the choice of wireless power supply for bio-implants.

Power for a bio-implant can be delivered from an external power source or through an energy source contained within the body such as glucose, thermal or kinetic energy or from implanted batteries. With the production of miniature rechargeable polymer lithium-ion batteries, wireless power supply systems are now a viable option for uninterrupted operation of bio-implanted microsystems. This approach avoids periodic surgery necessary for battery replacement and also does not tie a person to an external power source at all times. Inductively coupled power delivery systems at frequencies ranging from a few kHz to a few MHz have been designed for various power requirements for bio-implanted microsystems. Inductively coupled power sources have been considered for artificial heart system, auditory prosthesis, neuromuscular stimulation and measurement of intraocular pressure.

Inductive power delivery system though utilized for a very long time in power transmission and other applications, remains a relatively new technology for supplying power to microsystems. The research reported here is a part of a project for developing a hybrid integrated Bio-implantable Electrical Stimulation System (BESS) and deals with design and implementation of a remote power delivery system (RPDS) for the same.

1.2 Literature Review

Schuder, et al. [1] developed an inductively coupled system for transportation of electromagnetic energy. Coupling between two pancake shaped coils was used for this purpose. A coil of internal diameter (id) 4 cm and outside diameter (od) of 11 cm was implanted in the chest wall of a dog. A similar external coil was placed coaxially outside the body on the skin surface and a cooling system was developed for it. At a frequency of 428 kHz, 1 kW of electromagnetic power was delivered to the internal coil. This system might find applications in charging of internal energy storage units of artificial heart systems. It was found that temperature rise in the adjoining tissues was related to losses observed in the coil.

Radio-frequency (RF) power was also utilized for miniature and long term implant telemetry systems by Ko et al. [2]. A secondary receiver coil picks up transmitted RF power and is subsequently converted into a regulated DC supply. A design procedure was developed based on load, coil spacing and radio frequency.

Hochmair [3] designed a transcutaneous signal transmission system for an auditory prosthesis with minimized dependence on the relative spacing between the coils by employing critical coupling. Optimizing coil geometries and prevention of the RF output amplifier from saturating were necessary to approximately maintain critical coupling despite placement tolerances within a reasonable range.

Smith et al. [4] have developed an externally powered, multichannel implantable muscle stimulator to control paralyzed muscles. A single 10 MHz RF carrier was used with closely coupled transmitter and receiver coils. Upto eight independently controlled output channels are provided. Both laboratory and animal evaluations had been performed.

Donaldson [5] showed theoretically that inductively coupled series resonant systems can be rendered insensitive to coil separation and misalignment over a useful range.

Schuder and Stephenson [6] showed that efficiency of energy transport in a system, involving inductive coupling between an external and an internal coil with a low initial value of efficiency, can be increased by the utilization of a suitable ferrite core in the implanted coil. The analysis indicates that unless the almost field-free region within the ferrite shell is utilized to advantage, increased efficiency of energy transport can probably be achieved more easily by increasing the diameter of the coreless coil than by the utilization of a ferrite core.

Soma et al. [7] presented a cohesive analytical derivation for mutual inductance and analyzed theoretical effects due to lateral and angular misalignments in RF coil systems designed for use extensively in implantable devices for transdermal power and data transmission. A design procedure is established to maximize coil coupling for a given configuration.

Zierhofer and Hochmair [8] presented a new approach for optimizing the overall efficiency of a transmission scheme consisting of an RF oscillator, power amplifier, and inductively coupled link which were used in a high efficiency, coupling insensitive transcutaneous power and data transmission system. The paper aimed at optimizing the transmission scheme with respect to two criteria, overall efficiency and tolerance to misalignment. Experimental and theoretical results were in good agreement.

Ghahary and Cho [9] designed a transcutaneous energy transmission system using a full bridge, zero voltage switched, series resonant converter. This converter could power an artificial heart through skin by utilizing a transformer with an air gap of 1–2 cm between the primary and secondary coils. The design procedure allows for variable air gap as well as a variable output power. A small signal analysis of the transcutaneous DC-DC converter has also been characterized.

Schuylenbergh, and Puers [10], showed that an inductively coupled system to deliver power is fully compatible with a hospital environment. Multiple automatic tuning loops were incorporated to handle component tolerances and coil movements. Moreover the results could be expanded to other remote power delivery applications characterized by difficult coil coupling conditions, such as miniature implanted stimulators and telemetry in artificial knee or hip joint.

Ziaie et al. [11], developed a single-channel implantable microstimulator for functional neuromuscular stimulation, with reduced number of hybrid components, lead wires, and bulky packaging. This device is $2 \times 2 \times 10 \text{ mm}^3$ in dimension and can be inserted into tissue by expulsion from a hypodermic needle. The microstimulator is powered and controlled through an inductive telemetry link driven by a class E power amplifier at 2 MHz. A fully functional circuitry for this purpose has been fabricated using $3 \text{ }\mu\text{m}$ linewidth bi-CMOS technology.

Hirai et al.[12] have proposed the use of inductive transmission of power and information for safe and intelligent battery charging in electric vehicles and mobile robot systems.

Puers et al. [13], described an implantable system with low power consumption and miniaturization for detecting hip prosthesis loosening, based on a mechanical vibration analysis method. The system consists of a circuit along with the receiver coil that is embedded in a cavity inside the prosthesis. The circuit detects the vibration and converts it to electrical signal. The

transmitter coil is placed around the patient's leg. It uses two wireless links, one to power the implant and the other to monitor transmitted electronic signals from the implant.

Covic and Green [14] have examined stability and control of inductively coupled power transfer systems. Along with the operation of such a system, they have investigated its limiting factors and system stability. Theoretical developments are then compared with practical measurements from a prototype system.

Wu et al. [15] demonstrated a simple wireless power scheme for MEMS devices, which utilizes a transformer with an air gap. The transformer secondary was fabricated on-chip and was made detachable from the primary. Transformer operated at frequencies less than a few MHz and handled high voltages of $223.4 V_{pp}$ and also delivered high power of $4.5 W_{rms}$ to the load.

Puers and Vandevoorde [16] developed design strategies for wireless energy transfer for stand alone systems providing comparison between low and high power applicability. Optimization of power transfer efficiency for given geometric constraints was considered. Finally, an inductive link capable of transferring 20 W of power over a distance of 1 cm with an overall efficiency of 80 % was presented.

Covic and Stielau [17] described a design methodology for loosely coupled inductive power transfer systems. Level of compensation as well as compensation topologies and design tradeoffs were discussed in the paper.

Covic et al. [18] developed a high order mathematical model for power transfer capability and bifurcation phenomena (multiple operating modes) in loosely coupled inductive power transfer systems consisting of both primary and secondary resonant circuits. A contactless electric vehicle battery charger was developed to validate the theory.

Covic et al. [29] discussed about load models and their application in the design of loosely coupled inductive power transfer systems. The models evaluate the sensitivity of the system to variations in operational frequency and load.

Mokwa and Schnakenberg [20] presented monolithically and hybrid mounted implantable microdevices based on CMOS compatible processes. Microsystems were developed to measure intraocular pressure and monitor in situ strain on femoral nailplates. A very complex system for stimulating the nerve cells of the retina of patients suffering from retinitis pigmentosa was also developed.

1.3 Objectives and Scope of Thesis

The primary objective of this thesis is to design and implement a loosely coupled inductive power delivery system than can safely recharge a bio-implanted polymer lithium ion battery. An optimal coil set is chosen based on the power requirement, operating conditions and patient's comfort level. The transmitter coil is to be worn periodically as a belt by the patient. The receiver coil is bio-implanted outside the stomach wall and will be encapsulated with rest of the receiver and implant circuitry. It is important that the collective size of the implant circuitry be small. This imposes a significant constraint on the achievable efficiency of the inductive link. Available literature in RPDS mostly deal with coils of similar diameters placed coaxially, usually separated by a small distance.

In this work, coupling between transmitter and receiver coils with markedly different diameters is examined along with rigorous testing of the coils in the operating frequency range. A design procedure is established based on the power and voltage required at the load. An analytical model is developed with the help of a simple Matlab code and simulated results are matched with practical measurements. Coil parasitics at high frequency are accounted for in this

model. Optimization of power delivery to the load is necessary owing to poor efficiency inherent in loosely coupled inductive coils. Various compensation techniques and rectifier circuits are considered for optimum power delivery. Finally the system is tested for reliable power delivery to the load.

Research and analysis of coil behavior under actual bio-implanted conditions is beyond the scope of this thesis. The Bio-Implanted Electrical Stimulation System (BESS) IC chip with a modified design has been fabricated and a prototype system is actually ready for hybrid integration in our laboratory. Final tests will be run on the integrated microsystem soon.

1.4 Thesis Outline

In this chapter, concept of a RPDS is introduced. A literature review of related research is given. The goals and scope of present research are provided.

In chapter 2, required background theory concerning important laws governing electric and magnetic fields is discussed. This theory is applied to the problem of inductive coupling and remote power delivery. Finally, the RPDS is explained in detail.

In chapter 3, design procedures for the transmitter and receiver coil system design are discussed. Reflected impedance of the receiver on the transmitter coil and link efficiency of the coil are analyzed. An overall design methodology for RPDS is proposed.

In chapter 4, Matlab simulation results are matched with practical results. Coil parasitics are calculated and a model is developed considering skin effect. A rectifier circuit is chosen and explained. The battery charger chip is explained. Finally, battery charging ability of the RPDS is demonstrated.

Chapter 5 provides summary and suggested future work on this area of research.

Appendices provide detailed derivations and Matlab codes for the analytical models introduced in chapter 3.

CHAPTER 2

THEORY

2.1 Electric Field

The study in electrostatics begins with introduction to the two fundamental laws namely 1) Coulomb's law and 2) Gauss's law. Interaction between two charges at rest is known as electrostatic force. Coulomb's law describes this electrostatic force \mathbf{F}_{12} between two point

charges Q_1 and Q_2 in vacuum. $\mathbf{F}_{12} = \frac{Q_1 Q_2}{4\pi\epsilon_0 r^2} \hat{\mathbf{r}}$. Here, $\hat{\mathbf{r}} = \frac{\mathbf{r}}{r}$ is a unit vector along \mathbf{r} , ϵ_0 is the

permittivity of free space and r is the distance between Q_1 and Q_2 . When there are more than two charges, the principle of superposition is used to determine the force acting on a particular charge. The net force acting on a charge is, hence, the vector sum of the forces exerted on that

charge by all other charges. The net force on charge Q_j is expressed as $\mathbf{F}_j = \sum_{i=1}^N \mathbf{F}_{ij}$ [21]. Each

charge creates an electric field of its own that acts on other charges. The electric field intensity or electric field strength \mathbf{E} is the force acting on a unit test charge when placed in this electric field.

i.e. $\mathbf{E} = \lim_{Q \rightarrow 0} \frac{\mathbf{F}}{Q}$ or $\mathbf{E} = \frac{\mathbf{F}}{Q}$ for small magnitudes of Q [22]. The electric flux density \mathbf{D} in vacuum

is given by $\mathbf{D} = \epsilon_0 \mathbf{E}$. Electric flux Ψ is given by $\psi = \int \mathbf{D} \cdot d\mathbf{s}$ where s is area. Electric potential V

at a distance r from a point charge can be defined as the work done per unit charge in transferring a test charge from infinity to that point, assuming the potential at infinity to be zero. It is

expressed as $V = -\int_{\infty}^r \mathbf{E} \cdot d\mathbf{l}$. Here, \mathbf{l} is distance.

Gauss's law states that the total electric flux through any closed surface is equal to the total charge enclosed by that surface. Thus $\psi = Q_e$ where Q_e is charge enclosed by surface s .

Gauss's law in integral form is given by $\oint \mathbf{D} \cdot d\mathbf{s} = Q_e$.

2.2 Magnetic Field

Magnetic field \mathbf{H} is always associated with moving charges. Hence the sources of magnetic fields are currents. If the velocity \mathbf{V} of a charge Q given by $\mathbf{V} = 0$, then $\mathbf{E} \neq 0$ but $\mathbf{B} = 0$; and if $\mathbf{V} \neq 0$, then $\mathbf{E} \neq 0$ and $\mathbf{B} \neq 0$. Here, \mathbf{B} is magnetic flux density. Now, when a particle of charge Q is moving with a velocity \mathbf{V} , the magnetic force exerted on the particle is proportional to both Q and \mathbf{V} . The magnetic force $\mathbf{F} = Q(\mathbf{V} \times \mathbf{B})$. The major difference between forces generated by electric fields and magnetic fields is that the force acting on a charge in an electric field is in the direction of the electric field and the force acting on a charge in a magnetic field depends on the velocity component of the charge and is perpendicular to the direction of the magnetic field and the direction of motion. Magnetic force \mathbf{F} on a wire carrying current I placed in a magnetic flux density \mathbf{B} is given by $d\mathbf{F} = I d\mathbf{l} \times \mathbf{B}$ i.e. $\mathbf{F} = \oint I d\mathbf{l} \times \mathbf{B}$.

Biot-Savart's law helps in the calculation of the magnetic flux density at a point, a distance r away from a current carrying wire. This magnetic flux density can be expressed as

$$d\mathbf{B} = \frac{\mu_0}{4\pi} \frac{I d\mathbf{l} \times \hat{\mathbf{r}}}{r^2} \text{ i.e. } \mathbf{B} = \frac{\mu_0}{4\pi} \int_{\text{wire}} \frac{I d\mathbf{l} \times \hat{\mathbf{r}}}{r^2}. \text{ Here } \mu_0 \text{ is the permeability of free space and.}$$

2.2.1 Magnetic Field from a Circular Wire Loop

Using Biot-Savart's law, the magnetic flux density \mathbf{B} at a point P which is at a height of Z on the axis of a current carrying circular wire loop of radius R , as shown in Fig. 2.1 can be

calculated as $\mathbf{B} = B_{\hat{z}} = \frac{\mu_0 I R_l^2}{2(R_l^2 + Z^2)^{3/2}} \hat{z}$. Here \hat{z} is the unit vector along z direction and $B_{\hat{z}}$ is the magnetic field in the z direction. The magnetic fields in x and y directions cancel out. Also, when $Z=0$, the resultant magnetic field in the z direction on the xy plane is given by $B_{\hat{z}} = \frac{\mu_0 I}{2R_l}$.

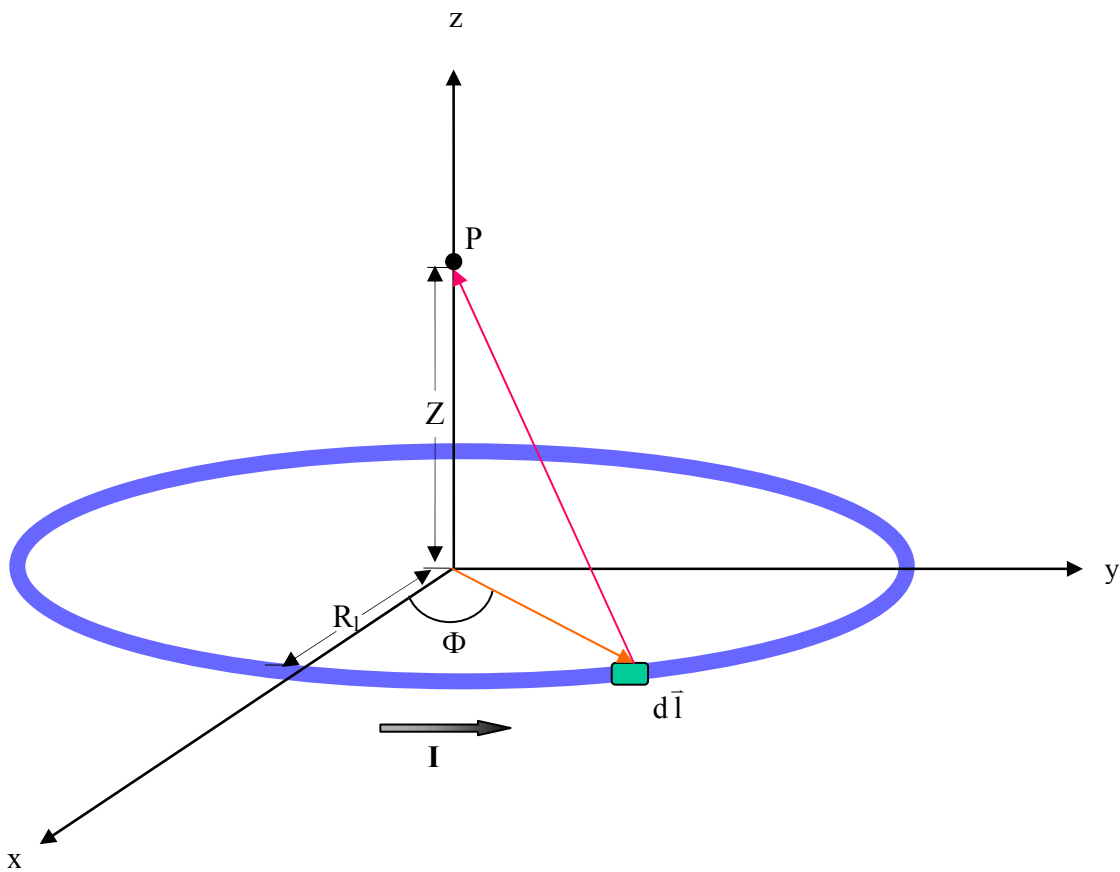


Figure 2.1: Geometry to determine magnetic field at point P due to a circular wire loop.

2.2.2 Magnetic Field in a Solenoid

A solenoid is a long helically wound coil of insulated wire. Figure 2.2 shows the magnetic field generated by a solenoid carrying a uniform current I . The magnetic field is concentrated and uniform at the center of a long solenoid and is weak outside the solenoid. Applying the result obtained in the previous section to a solenoid, the magnetic field at the center

of the solenoid of length l and radius R_l is $B_z = \frac{\mu_0 NI}{\sqrt{l^2 + 4R_l^2}}$.

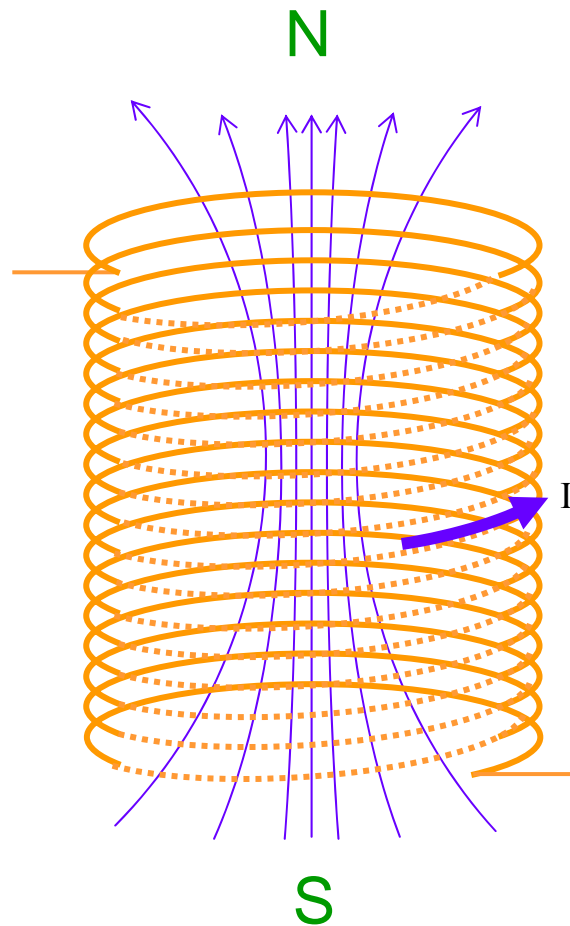


Figure 2.2: Magnetic field lines in a solenoid.

For radius $R_l \gg$ length l , the magnetic field at the center of such a solenoid is $B_z = \frac{\mu_0 NI}{2R_l}$. Ampere's law relates I and \mathbf{B} and is given by: $\oint \mathbf{B} \cdot d\mathbf{l} = \mu_0 \mathbf{I}_e$ where path l encloses current \mathbf{I}_e .

2.2.3 Magnetization and Magnetic Materials

In every material, each magnetic dipole has its own magnetic field. Magnetization \mathbf{M}_M is the net dipole moment per unit volume of that material and can be expressed as $\mathbf{M}_M = \frac{1}{V} \sum \mathbf{v}$ or $\mathbf{M}_M = N \frac{\mathbf{v}}{V}$. Here, N is the number of dipoles per unit volume and \mathbf{v} is the net dipole moment per dipole. The average magnetic flux density due to all the dipoles in a material is given by $\mathbf{B}_{avg} = \mu_0 \mathbf{M}_M$. Hence the total magnetic field experienced by any material when placed in an external magnetic field \mathbf{B}_{ext} is: $\mathbf{B} = \mathbf{B}_{ext} + \mathbf{B}_{avg}$ i.e. $\mathbf{B} = \mu_0 (\mathbf{H} + \mathbf{M}_M)$ or $\mathbf{B} = \mu_0 (1 + \chi_m) \mathbf{H}$. Here, $\mathbf{M}_M = \chi_m \mathbf{H}$ and χ_m is known as the magnetic susceptibility of the medium. χ_m is a dimension less quantity. Also, $\mathbf{B} = \mu_0 \mu_r \mathbf{H}$ i.e. $\mathbf{B} = \mu \mathbf{H}$. Where $\mu = \mu_0 \mu_r$ is the permeability of the medium and $\mu_r = 1 + \chi_m$, a dimension less quantity and is known as relative permeability of the material.

Figure 2.3 shows the division of all magnetic materials into linear and nonlinear categories. Linear materials are again divided into paramagnetic ($\mu_r > 1$) and diamagnetic materials ($\mu_r < 1$). Ferromagnetic materials ($\mu_r \gg 1$) are nonlinear and require a hysteresis curve to describe the relation between B and H .

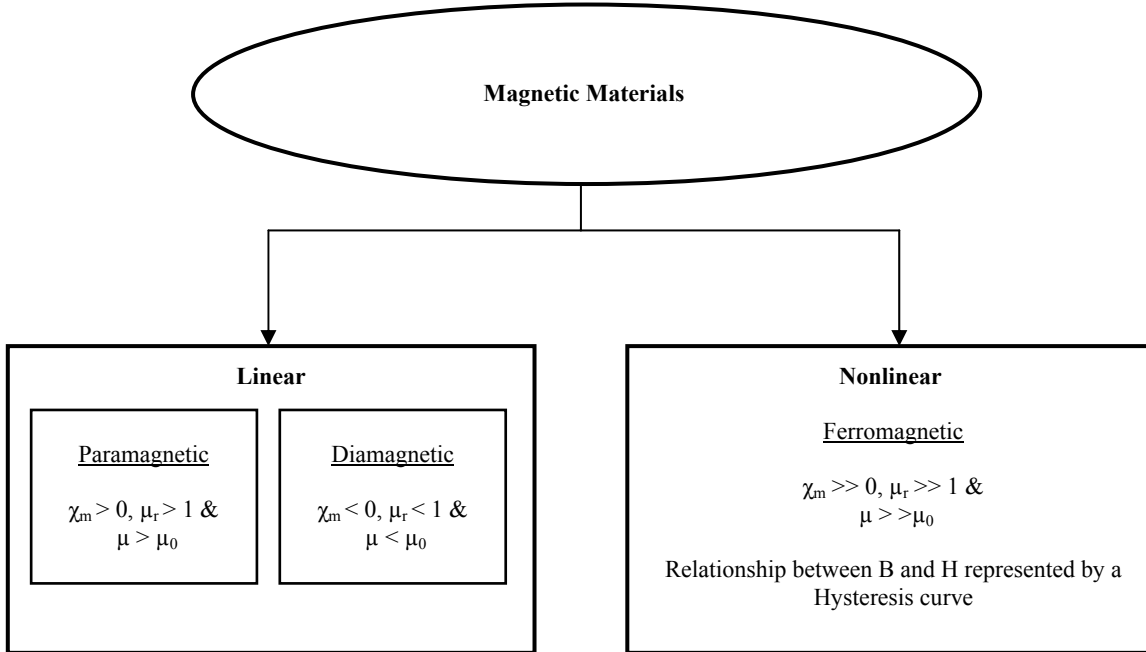


Figure 2.3: Magnetic materials chart.

2.2.4 Magnetic Induction

Faraday's law of induction

In 1831 Michael Faraday discovered that a static magnetic field produced no current but a time varying magnetic field generated an electric field. Faraday's law states that the induced emf E in a closed circuit is proportional to the rate of change of magnetic flux Φ_M and can be

expressed as $E = -\frac{d\Phi_M}{dt}$. For any coil that consists of N loops, $E = -N \frac{d\Phi_M}{dt}$.

Lenz's law

Lenz's law states that the induced current tends to produce a magnetic field that opposes any change in the magnetic field that induced that current.

Inductor

An inductor L is a linear element that opposes any change in current. Inductance can be defined as a measure of how much magnetic energy is stored in the magnetic field of an inductor. It can also be defined as the ratio of the flux linkage to the current flowing through the inductor.

$$L = \frac{\Lambda}{I} = N \frac{\Phi_M}{I} = \frac{NBA}{I}. \quad (2.1)$$

Here, Λ is the total flux linkage, N is the number of turns and A is the area of the inductor. From the above equation, $L = N \frac{d\phi}{di}$ and $V = -N \frac{d\phi}{dt}$. Hence, $V = \left(N \frac{d\phi}{di} \right) \left(\frac{di}{dt} \right) = L \frac{di}{dt}$. Here, V is the induced voltage.

As established in the previous section, permeability of a material is the ease with which magnetic lines of force can pass through it. The reluctance R_M against these magnetic lines of force is given by: $R_M = \frac{l}{\mu A}$ where l is length of the magnetic path, and A is its cross-sectional area.

Magnetomotive force M_F , also known as magnetic potential gives the strength of the magnetic field in a coil. It is proportional to the product of the number of turns N around the core (in which the flux is to be established) and the current I through the turns. $M_F = NI$ ampere-turns. Magnetomotive force per unit length is known as the Magnetizing force, given

$$\text{by } H = \frac{M_F}{l} = \frac{NI}{l}. \text{ Now, from Eqn. (2.1), } L = \frac{NBA}{I}. \text{ For a solenoid, } L = \frac{N \left(\frac{\mu_0 NI}{\sqrt{(l^2 + 4R_l^2)}} \right) A}{I}$$

$$\text{or } L = \frac{\mu_0 N^2 A}{\sqrt{(l^2 + 4R_l^2)}}. \text{ Here, } R_l \text{ is the radius of the solenoid, } l \text{ is the length of the solenoid and } A$$

is the cross-sectional area of the solenoid. When $R_l \gg l$ such as in our case of

interest:
$$L = \frac{\mu_0 N^2 A}{2R_l}.$$

The inductor however cannot store energy as well as a capacitor because there is always some winding resistance in the coil that quickly dissipate energy. Figure 2.4 shows a lumped equivalent model for an inductor L consisting of the turn resistance R and parasitic capacitance C . The resonance frequency for the inductor and its parasitic capacitance is known as the self resonance frequency of the inductor. The energy stored by an inductor W_M in its magnetic field

is given by $W_M = \frac{1}{2} LI^2$ joules.

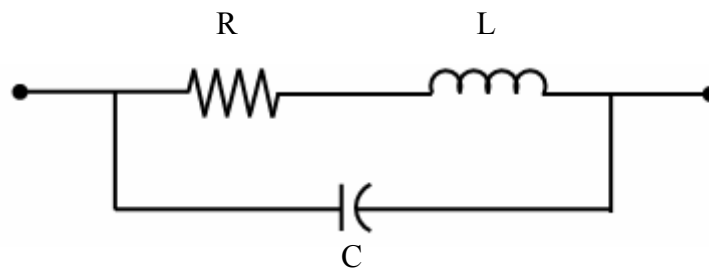


Figure 2.4: Lumped equivalent model for an inductor.

Mutually coupled coils

When all the flux linkages in an inductor are produced by that inductor then it exhibits self inductance. Two coils are said to be coupled when there is an exchange of energy electromagnetically between them. Mutual inductance M between two coils may be defined as the number of flux linkages in the secondary coil per unit current in the primary coil or vice versa i.e. mutual inductance exists between two magnetic circuits when they share a common

flux linkage. $M = L_{12} = \frac{\text{Flux linking coil 2 due to current in coil 1}}{\text{Current in coil 1}}$ or $M = \frac{\Lambda_{12}}{I_1}$. Here, Λ_{12} is the

flux linking coil 2 due to the current flowing in coil 1 and I_1 is the current flowing in coil 1. The flux linking coil 2 will induce a voltage V_{ind} in coil 2 if the flux changes with time. The

magnitude of this induced voltage is given by $|V_{ind}| = M \frac{dI_1}{dt}$.

The maximum value of mutual inductance between two coils of inductance L_1 and L_2 is $M = \sqrt{L_1 L_2}$. The coefficient of coupling between two coils is given by $K = \frac{M}{\sqrt{L_1 L_2}}$

and $0 \leq K \leq 1$. If $K > 0.5$ then the coils are said to be tightly coupled. If $K \leq 0.5$ then the coils are said to be loosely coupled. $K = 1$ indicates unity coupling. In this latter case, all existing flux is mutual flux. There is no leakage flux. Figure 2.5 shows two mutually coupled coaxial coils.

Mutual inductance between two concentric, coplanar and coaxial coils

Figure 2.6 shows a schematic arrangement of two concentric, coplanar and coaxial coils. Coil 1 has N_1 number of turns with I being the current flowing through coil 1. Radius R_1 of coil 1 is much greater than its length l_1 . Coil 2 has N_2 number of turns with its radius R_2 also much greater than its length l_2 and $R_1 \gg R_2$. Magnetic flux density at the center of coil 1 along the axis

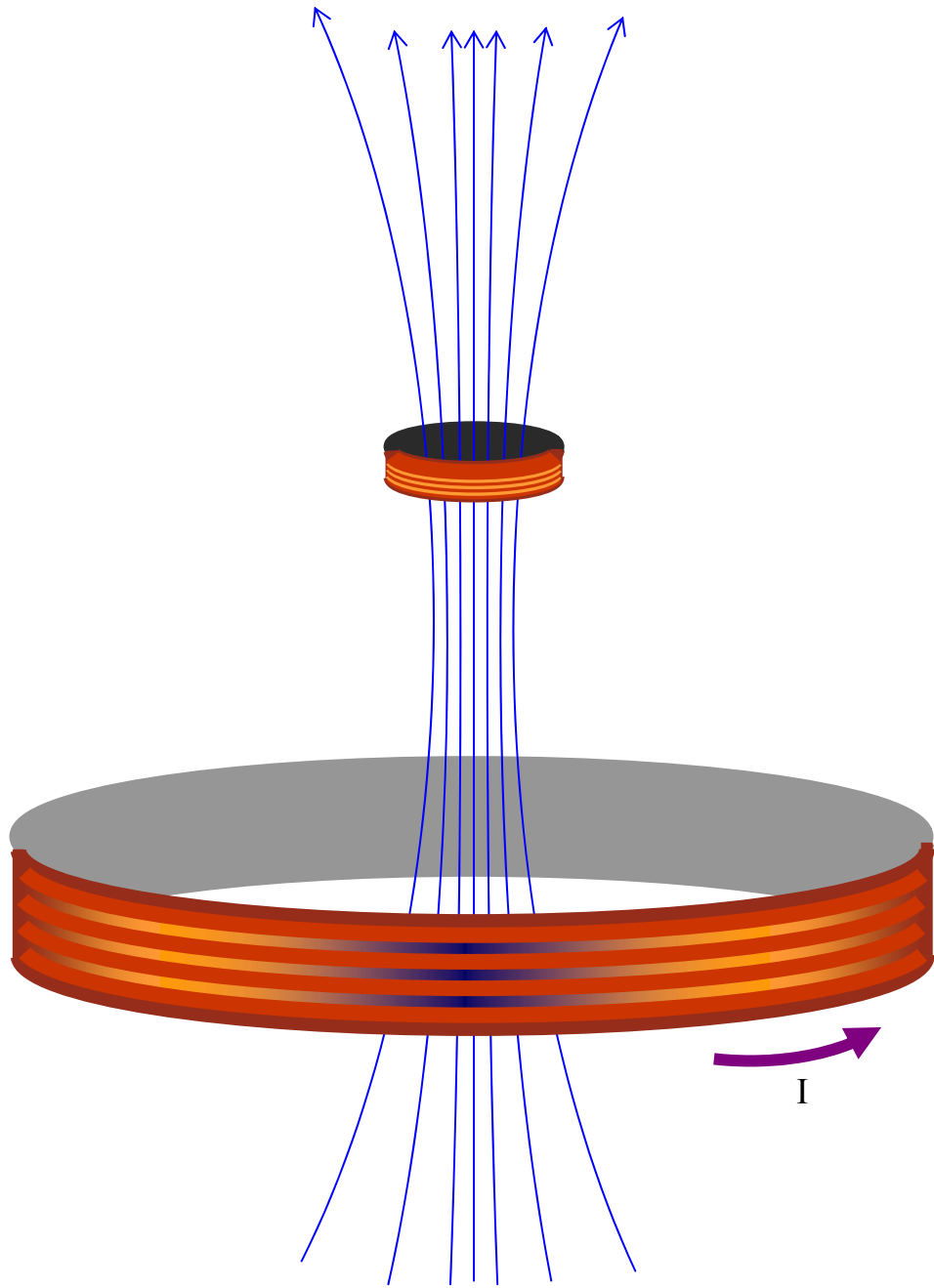


Figure 2.5: Schematic arrangement of two coaxial coils.

is $B_1 = \frac{\mu_0 N_1 I}{\sqrt{l_1^2 + 4R_1^2}}$ or $B_1 \approx \frac{\mu_0 N_1 I}{2R_1}$ since $R_1 \gg l_1$. Since $R_1 \gg R_2$, we assume that the magnetic

flux density through the smaller coil is also B_1 . Then, the flux linking coil 1 and coil 2 is

$\Phi_{12} = B_1 N_2 A_2$ or $\Phi_{12} = \left(\frac{\mu_0 N_1 I}{2R_1}\right) N_2 (\pi R_2^2)$. Here, A_2 is cross-sectional area of coil 2. It is

known that mutual inductance $M = \frac{\Phi_{12}}{I}$. Hence,

$$M = \frac{\mu_0 \pi N_1 N_2}{2} \left(\frac{R_2^2}{R_1}\right) \quad (2.2)$$

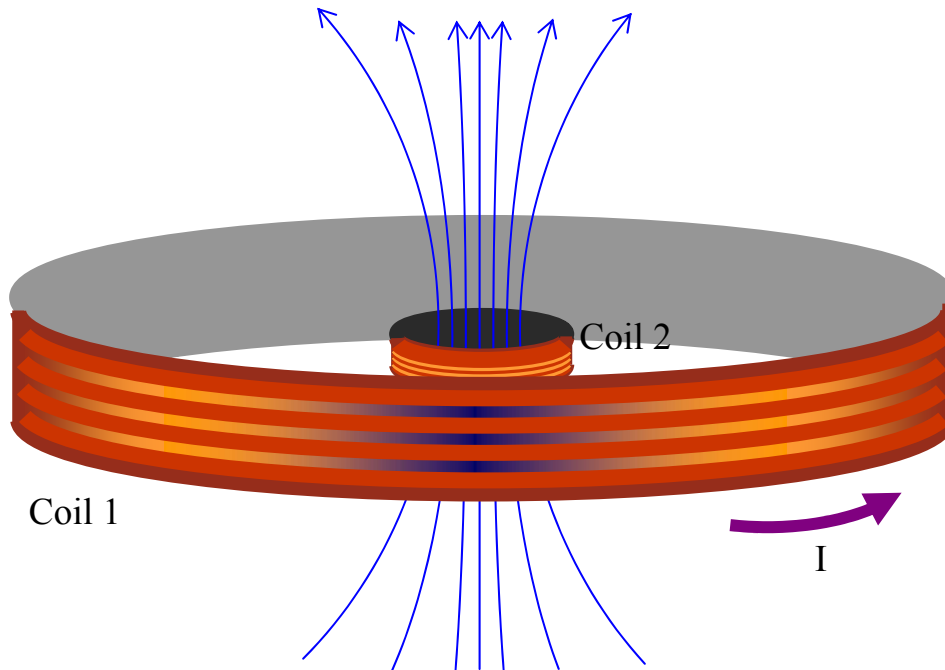


Figure 2.6: Schematic arrangement of two concentric, coplanar and coaxial coils.

2.3 RPDS Overview

Figure 2.7 shows the basic elements of the RPDS. The basic technique in this RPDS is to establish magnetic coupling between a remotely located receiver coil and a transmitter coil driven by an alternating current. The induced voltage in the receiver coil is then rectified and regulated. This dc voltage is then used to power the bio-implanted circuitry. Hybrid integration is employed for the bio-implantable part of the system.

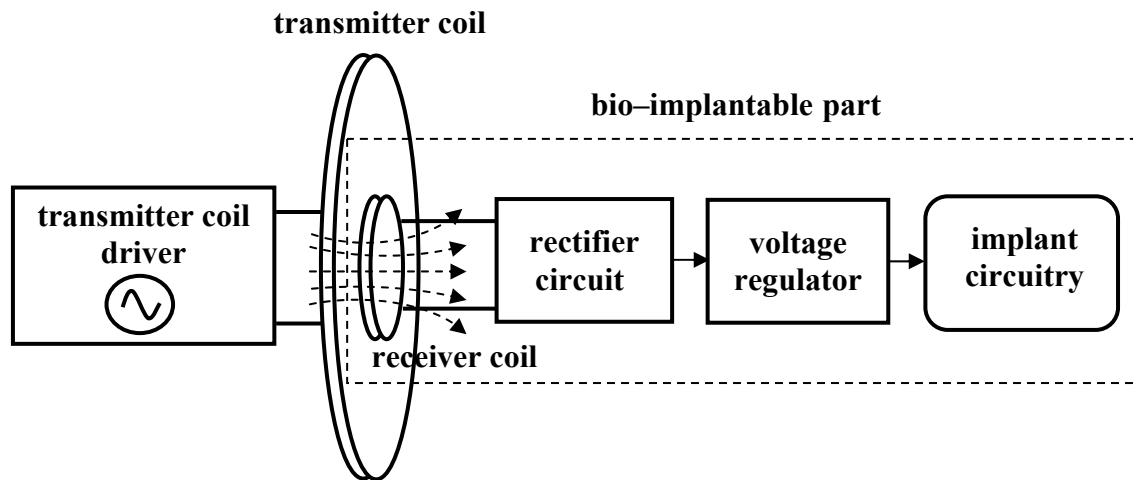


Figure 2.7: Block diagram for a transcutaneous power delivery system.

2.3.1 Transmitter Coil Driver

In most loosely coupled inductive power delivery systems, the transmitter coil driver is usually a resonant power supply. Switch-mode amplifiers of class C, class D and class E topologies with very high efficiencies and minimum dissipation are utilized. Here, transistors in the amplifier are used as switches and draw current at zero voltages while relaying real power only. Since the coupling between the transmitter and the receiver is low, there is no need for closed loop drivers [16].

2.3.2 Coil Setup

The RPDS designed in this work has a receiver coil of diameter 1.34” positioned coplanar and concentric with the transmitter coil of diameter 16.05”. This marked difference in coil dimensions renders it a loosely coupled inductive power delivery system. This setup was chosen for use in a gastric pacer system. The receiver coil will be implanted outside the stomach wall and the transmitter coil is periodically worn by the patient as a belt to safely and appropriately charge the rechargeable polymer lithium-ion batteries in the implanted circuitry. The maximum voltage supplied to the transmitter coil is restricted such that the maximum current through the coil is not more than 0.1 times the fusing current [23]. The receiver coil has to be bio-implanted for gastric pacing and has to be as small as possible. The load and power required at the load also influence the coil selection. A final tradeoff has to be achieved between the electromagnetic geometry and the electrical requirements of the system. The actual coil design process is described in further detail in section 3.1

2.3.3 Link Efficiency and Coil Compensation

In a loosely coupled inductive system, the fraction of the flux produced by the transmitter coil that links with the receiver coil is very small. This implies a low value for coupling factor in the range of 1 – 10 %. The coil sizes and separation among other parameters characterize the coupling factor. The flux linkage between the transmitter and the receiver coil determines the power transfer efficiency of the inductive link. The link efficiency of an inductively coupled circuit is the product of the transmitter and receiver coil efficiencies. The efficiency of each coil in the coupled system can be individually calculated as the ratio of the power delivered to the next stage to the power handled by the coil. The power transfer efficiency and coil power capacity depend on the link efficiency, operating frequency and VA rating of the receiver coil.

Since, in loosely coupled inductive links, the transmitter and receiver coil leakage inductances are high, it is common practice to cancel out the effect of this leakage inductance by connecting an external capacitor either in series or in parallel with the circuit. The process of addition of a resonant capacitor is known as coil compensation. Henceforth, in this text, *coil compensation* refers to compensation of both transmitter and receiver coils unless otherwise indicated. The optimization of link efficiency is of utmost importance in loosely coupled inductive systems since this link efficiency usually determines the overall system efficiency. Link efficiency for the uncompensated case, the compensated case and the compensated case with more accurate modeling of coil parasitics will be discussed in further detail in section 3.2.

2.3.4 Rectifier Circuit

In loosely coupled systems, the restricted receiver coil geometry and low flux linkage efficiency may make it difficult to achieve a high induced voltage or power transfer in the receiver. In the former case, the voltage drop across the rectifier becomes an important design criterion in the selection of a rectifier topology. It is for this reason that a full wave rectifier to provide doubling of the rectified voltage magnitude is preferred. Since the overall system efficiency usually depends on the link efficiency, the rectifier efficiency is of secondary concern. The full wave rectifier circuit with voltage doubling is discussed in further detail in section 3.3.

2.3.5 Voltage Regulator

In the present case, the output of the rectifier circuit is fed to a lithium-ion battery charger chip (MIC 79050 from MICREL). The latter provides a simple cost effective solution for voltage regulation for battery charging. The charging chip specifications require a minimum voltage of 4.7 V dc and a current of 100 mA. This implies an effective load of 47 Ω and load power of 470 mW. Considering power losses in the receiver coil, the design power is estimated to be 670 mW.

The regulated output voltage of the battery charger chip is 4.2 volts at 100 mA. The battery charger chip is discussed in further detail in section 3.3.

2.3.6 Implant Circuitry

The implant circuitry which has been initially designed by Kona [24] and subsequently refined by Gaddam et al. [25] consists of the signal conditioning circuit for a remotely rechargeable, bio-implantable, Battery-powered Electrical Stimulation System (BESS) [24]. A rechargeable lithium ion battery with a voltage of 3.7 V powers the proposed circuit. The desired output, which goes directly to the electrodes, is a series of 10 V, 100 Hz pulses with a duty cycle of 4.5 %. A second rechargeable lithium ion battery serves as a back-up. The two batteries work in tandem i.e. when one battery powers the IC the other gets recharged and vice versa thereby providing an uninterrupted output. The IC uses a series of charge pumps to get the required boost in voltage. The IC also includes voltage detector circuits to detect battery voltages, voltage regulator, pulse generator circuits, logic circuits and necessary switches. Hybrid packaging is considered for integrating the implantable electrical stimulation and the remote power delivery system [26].

CHAPTER 3

RPDS DESIGN

3.1 Coil Design

Inductance value L of short multiple-layer coils of the solenoidal form, for low RF frequency applications, is given in [25] and reproduced here for convenience. For $l > t$:

$$L = 0.03193rN^2 \left[2.303 \left\{ 1 + \frac{l^2}{(32r^2)} + \frac{d^2}{(96r^2)} \right\} \log_{10} \left(\frac{8r}{d} \right) - y_1 + \frac{l^2 y_2}{(16r^2)} \right]. \quad (3.1)$$

Here, l and t are the axial length and radial thickness of the winding and r is the mean radius, d is the diagonal of the winding cross section as shown in Fig. 3.1, y_1 and y_2 are constants depending upon the ratio l/t and are given in reference [27] and reproduced here in Table A.1 in Appendix A. For short multiple layer coils, the axial length l is smaller than radius r of the coil ($l \ll r$) as shown in Fig. 3.1.

For a coil of length l and thickness t , wound with a wire of diameter d_w , the number of turns along length of the coil N_l in each layer is given by $N_l \approx l / d_w$ and the number of layers N_t that can be fit in thickness t is given by $N_t \approx t / (0.866 \times d_w)$ as indicated in Fig. 3.2. Table 3.1 gives the copper wire specifications for both the transmitter and receiver coils. For the transmitter coil, a 10 AWG plain enamel heavy insulated copper wire is used. The receiver coil is wound from a 20 AWG plain enamel single insulated copper wire. The wire gauge size selection is based on the load power requirement. The maximum allowable current through the coils in this design is 10 % of the fusing current. The fusing current for the 10 AWG transmitter coil is 333 A and that for the 20 AWG receiver coil is 58.4 A [23].

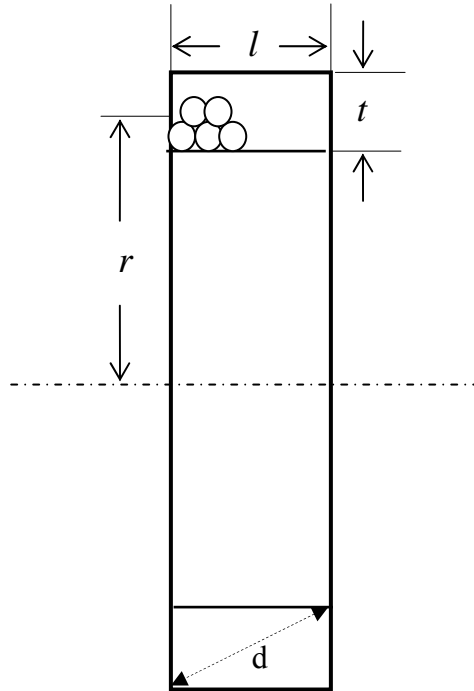
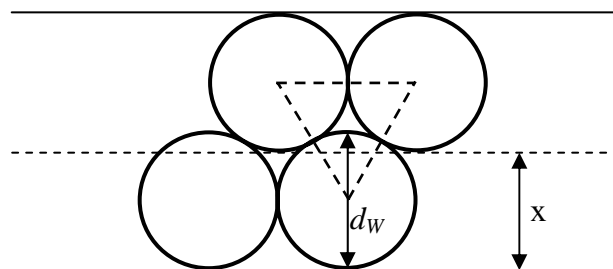


Figure 3.1: Short multiple layered coil of solenoidal form.



$$x = (3)^{1/2} d_w / 2, \text{ i.e. } x = 0.866 d_w$$

Figure 3.2: Schematic illustration of hexagonally close-packed cross-section along thickness of the coil. Diameter of the coil wire is d_w .

Table 3.1: Copper coil wire specifications from MWS Wire Industries.

Gauge Size	Diameter d_w (inches)			Resistance ρ_w (Ω /1000 feet)			Length w (feet/lb)
	Min	Nom	Max	Min	Nom	Max	
10 AWG (bare)	0.1009	0.1019	0.1029	0.9795	0.9988	1.019	31.82
10 AWG (plain enamel, heavy insulation)	0.1040	0.1051	0.1061	-	-	-	31.5
20 AWG (bare)	0.0317	0.0320	0.0323	9.941	10.13	10.32	323
20 AWG (plain enamel, single insulation)	0.0329	0.0334	0.0339	-	-	-	318.4

3.1.1 Transmitter Coil Design

The transmitter coil is a 10 AWG enamel coated heavy insulation copper wire. The coil is a hollow cylinder with inner radius of 7.875" and outer radius of 8.175". The radius of the transmitter coil R_t is approximated to 8.025" which makes the diameter of the transmitter coil D_t 16.05". The axial length or height l_t and the thickness t_t of the transmitter coil were chosen to be 2" and 0.3" respectively [23]. For a 10 AWG plain enamel, heavy insulation transmitter coil wire, number of turns along 2" length of the coil $N_l \approx 2"/0.1051" = 19.02 \approx 19$. Number of turns along 0.3" thickness of the coil $N_t \approx 0.3"/(0.1051 \times 0.866) = 3.29 \approx 3$. Hence, total turns of transmitter coil is N_T is $19 \times 3 = 57$. Resistance of the transmitter coil $R_T = \pi D_t N_T \rho_w / (1000 \times 12) = (3.14 \times 16.05 \times 57 \times 0.9988) / (1000 \times 12) = 0.24 \Omega$. Weight of the coil wire $W_T \approx \pi D_t N_T / w = (3.14 \times 16.05 \times 57) / (31.50 \times 12) \approx 7.6$ lb. Here, values for ρ_w and w are obtained from Table 3.1. Inductance of the transmitter coil L_T from Eqn. (3.1) for r_t/l_t ratio = 4.0125 is given by $L_T \approx$

2.5 mH. Here $D_t = 2r_t$. Parasitic capacitance of the coil $C_{ST} \approx 5.2 \times 10^{-14} D_T N_T = 5.2 \times 10^{-14} \times 16.05 \times 57 \approx 47.63$ pF [23]. Self resonance frequency of the transmitter coil is given by:

$$f_{srt} = \frac{1}{2\pi} \sqrt{\frac{1}{L_T C_{ST}}} = \frac{1}{2 \times 3.14} \sqrt{\frac{1}{2.5 \times 10^{-3} \times 47.6 \times 10^{-12}}} \approx 462 \text{ kHz.}$$

3.1.2 Receiver Coil Design

The receiver coil is made from a 20 AWG plain enamel coated single insulation copper wire and it has an inner radius of 0.64” and an outer radius of 0.703”. The radius of the receiver coil R_r is approximated to 0.67” which makes the diameter of the receiver coil $D_r = 1.34$ ”. The axial length or height l_r and the thickness t_r of the receiver coil were chosen to be 0.5” and 0.0625” respectively [23]. For a 20 AWG receiver coil, number of turns along 0.5” length of the coil $N_l = 0.5"/0.0334" = 14.97 \approx 15$. Number of turns along 0.0625” thickness of the coil $N_t = 0.0625"/(0.0334" \times 0.866) = 2.16 \approx 2$. Hence, total number of turns for the receiver coil is $N_R = 15 \times 2 = 30$. Resistance of the coil wire $R_R = \pi D_r N_R \rho_w / (1000 \times 12) = (3.14 \times 1.343 \times 30 \times 10.13) / (1000 \times 12) = 0.107 \Omega$. Weight of the coil wire $W_R = \pi D_r N_R / (w \times 12) = (3.14 \times 1.343 \times 30) / (318.4 \times 12) = 0.033 \text{ lb} = 14.79 \text{ gm}$. Here, values for ρ_w and w are obtained from Table 3.1. Inductance L_R of the receiver coil from Eqn. (3.1) is given by $L_R = 39 \mu\text{H}$. Parasitic capacitance of the coil $C_{SR} \approx 5.2 \times 10^{-14} D_T N_T = 5.2 \times 10^{-14} \times 1.343 \times 30 \approx 2.1$ pF [23]. Self resonance frequency of the receiver coil is given by:

$$f_{srr} = \frac{1}{2\pi} \sqrt{\frac{1}{L_R C_{SR}}} = \frac{1}{2 \times 3.14} \sqrt{\frac{1}{39 \times 10^{-6} \times 2.1 \times 10^{-12}}} = 17.6 \text{ MHz.}$$

The coil set is designed using formulae provided in reference [27]. The measured values and the calculated values for the coil set are found to be a good match. The mutual inductance M between two concentric coplanar and coaxial coils can be described from Eqn. (2.2) as:

$M = \frac{\mu_0 \pi N_T N_R}{2} \left(\frac{R_r}{R_t} \right)^2$. Here, R_t and R_r are the radii of the transmitter and receiver coils

respectively. Mutual inductance calculated in the above manner is found to be 4.796 μ H and matches with values obtained from other calculation methods given in reference [28]. The

coupling coefficient k is given by $k = \frac{M}{\sqrt{L_T L_R}} = 1.54 \%$. Table 3.2 shows values for designed

transmitter and receiver coils.

Table 3.2: Parameter values for the designed transmitter and receiver coils.

	Transmitter coil (10 AWG)	Receiver coil (20 AWG)
Diameter (inches)	16.05	1.34
Length (inches)	2	0.5
Thickness (inches)	0.3	0.0625
Weight (lbs)	7.5	0.044
Inductance (mH)	2.5	39×10^{-3}
Coil resistance (ohms)	0.24	0.107
Parasitic capacitance (pF)	47.6	2.1
Mutual inductance (mH)	4.796×10^{-3}	4.796×10^{-3}
Coupling coefficient	0.0154	0.0154

3.1.3 Operating Frequency

The self resonance frequency of the designed receiver coil is very high. The self resonance frequency of the transmitter coil then sets a limit for maximum operating frequency. In order to eliminate self resonance effect in both the transmitter and the receiver coils, the operating frequency in this work is set at least a factor of 10 below the lower self resonance frequency of 462 kHz. Hence, 40 kHz is tentatively set as the upper operating frequency limit.

3.2 Link Efficiency

In a loosely coupled system, the link efficiency essentially determines the power transfer efficiency of an inductive link. In the present case, due to extremely small receiver coil diameter,

the fraction of the flux produced by the transmitter coil, linking the receiver coil is very small. This implies a very low coupling factor of 1.54 %. The link efficiency in a coupled system is in turn calculated as the product of the transmitter and receiver coil efficiencies. The transmitter coil efficiency can be calculated as the ratio of the power delivered to the receiver coil to the power handled by the transmitter coil. The receiver coil efficiency can be calculated as the ratio of the power delivered to the load to the power handled by the receiver coil.

3.2.1 Link Efficiency for the Uncompensated Case

In loosely coupled inductive systems, the coupling coefficient is in the range of 1 – 10 %. The mutual inductance between the transmitter and receiver coils is small and a large uncoupled flux exists. The uncoupled flux gives rise to a leakage inductance. It is a common practice to cancel out this leakage inductance in order to increase power transfer efficiency. This is achieved by connecting an external capacitor either in series or in parallel with the coil. The process of addition of such a resonant capacitor is known as coil compensation. The capacitance will compensate for the reflected receiver coil reactance along with the transmitter coil leakage inductance thereby reducing the VA rating of the coil driver. This also provides incentive to set the coil operating frequency to the receiver coil resonance frequency. Receiver coil compensation effectively cancels the receiver coil reactance there by reflecting only a resistance into the transmitter coil. The optimization of link efficiency is of utmost importance in loosely coupled inductive systems since this link efficiency usually determines the overall system efficiency. Figure 3.3 shows an inductively coupled, uncompensated circuit and its equivalent transmitter circuit. The behavior of inductively coupled circuits can be analyzed by considering the reflected impedance of the coupled receiver circuit in series with the transmitter coil.

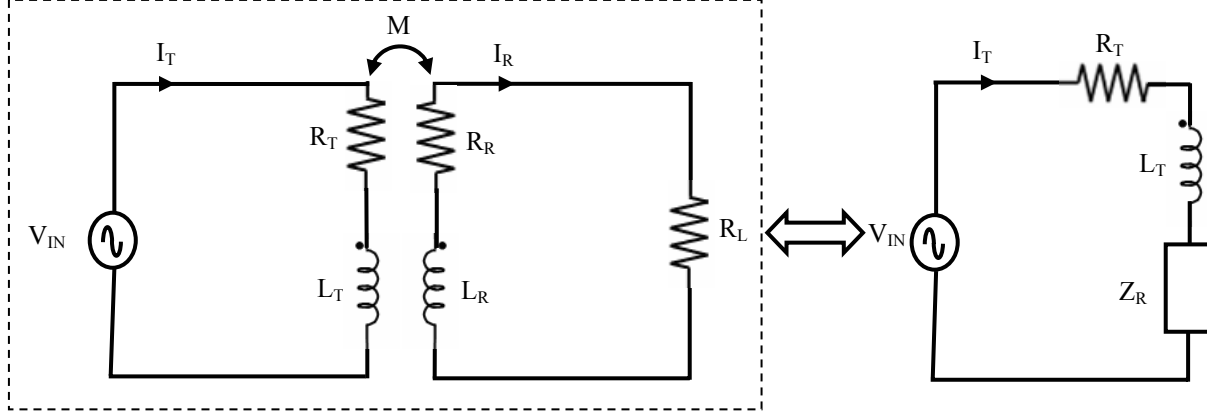


Figure 3.3: An inductively coupled circuit and its equivalent transmitter circuit.

Parasitic capacitors for the transmitter and the receiver coils have not been considered for simplicity. The receiver coil impedance is expressed as $Z_{REC} = (R_R + R_L) + j(\omega L_R)$. For a sinusoidal steady state case, the reflected impedance Z_{REF} of the receiver circuit into the transmitter can be expressed as:

$$Z_{REF} = \frac{\omega^2 M^2 (R_R + R_L)}{(R_R + R_L)^2 + \omega^2 L_R^2} + j \left[-\frac{\omega^3 M^2 L_R}{(R_R + R_L)^2 + \omega^2 L_R^2} \right]. \quad (3.2)$$

Here, L_T and L_R are the self inductance values for the transmitter and the receiver coils respectively, R_T and R_R are the resistances of the coil winding wire of L_T and L_R respectively, ω is angular frequency and R_L is the load resistance. The link efficiency η for the case shown in Fig. 3.3 can be represented as:

$$\eta = \frac{\omega^2 M^2 R_L}{R_T [(R_R + R_L)^2 + \omega^2 L_R^2] + \omega^2 M^2 (R_R + R_L)}. \quad (3.3)$$

A detailed derivation for the above expressions is given in Appendix B. This expression for link efficiency has been further optimized in terms of the transmitter coil and the receiver coil quality factors in reference [14]. It is evident that the link efficiency depends on coupling coefficient and

is generally low for weak coupling such as in the present case. In loosely coupled inductive power delivery systems, the link efficiency dominates the overall efficiency of the system. Hence, further optimization of this link efficiency is essential for a viable RPDS.

Figure 3.4 shows a plot for variation in link efficiency with operating frequency for the uncompensated case. It is evident from the plot that link efficiency tends to increase with frequency. Inset shows a plot for the same data in a logarithmic scale. Theoretical values have been used to plot these curves. Actual variations in the coil parasitics with frequency have not been considered while plotting this curve. The Matlab code used to generate these plots is given in Appendix C.

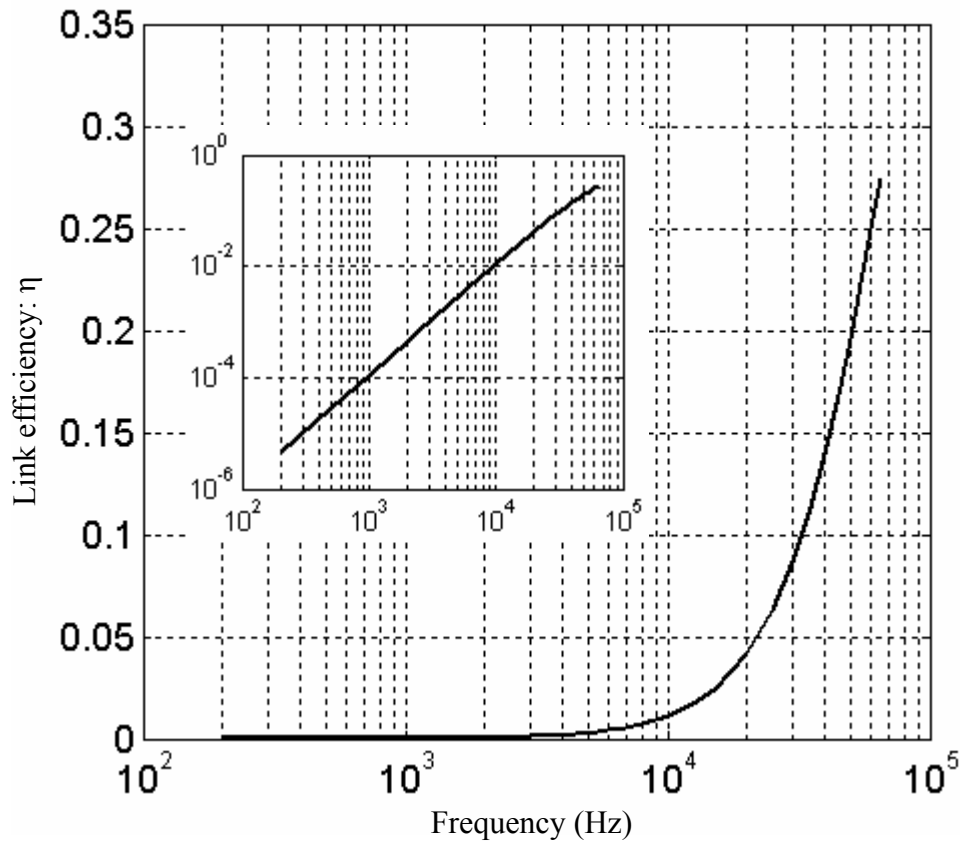


Figure 3.4: Link efficiency η as a function of frequency for the uncompensated case.

3.2.2 Link Efficiency for the Compensated Case

The large leakage inductances of the transmitter coil and the receiver coil call for adequate compensation. Both the transmitter and the receiver circuits can be compensated either in series or in parallel. Series compensation has been chosen for the transmitter circuit as this reduces the required voltage rating of the transmitter coil driver [17]. The choice between series or parallel compensation for the receiver coil depends on the optimum link efficiency obtained in each case. Practical considerations such as the receiver coil geometry size limitations [16] can set a limit to the obtainable inductance and the frequency of operation of the coupled system. Figure 3.5 shows a schematic circuit representation of a loosely coupled inductive power delivery system with different topologies for transmitter and receiver circuit compensations. Here, L_T , R_T and C_{ST} constitute a high frequency model for the transmitter coil and L_R , R_R and C_{SR} constitute a high frequency model for the receiver coil, where L_T and L_R are the self inductance values for the transmitter and the receiver coils respectively, R_T and R_R are the parasitic turn resistances of L_T and L_R respectively, C_{ST} and C_{SR} are the parasitic turn capacitances associated with the transmitter and receiver coils respectively and C_T and C_R are respectively the compensation capacitors for the transmitter and the receiver side respectively. R_L is the load resistance. C_T and C_R are chosen such that both transmitter and receiver coils resonate at the same operating frequency ω_0 . Also in the present RPDS model, $\omega_0 \ll \omega_{srt} \ll \omega_{srr}$ where, ω_{srt} and ω_{srr} are the self resonance frequencies of the transmitter coil and the receiver coil respectively. Analytical models have been developed for this circuit that consider series compensation for the transmitter circuit and both series and parallel compensation for the receiver circuit.

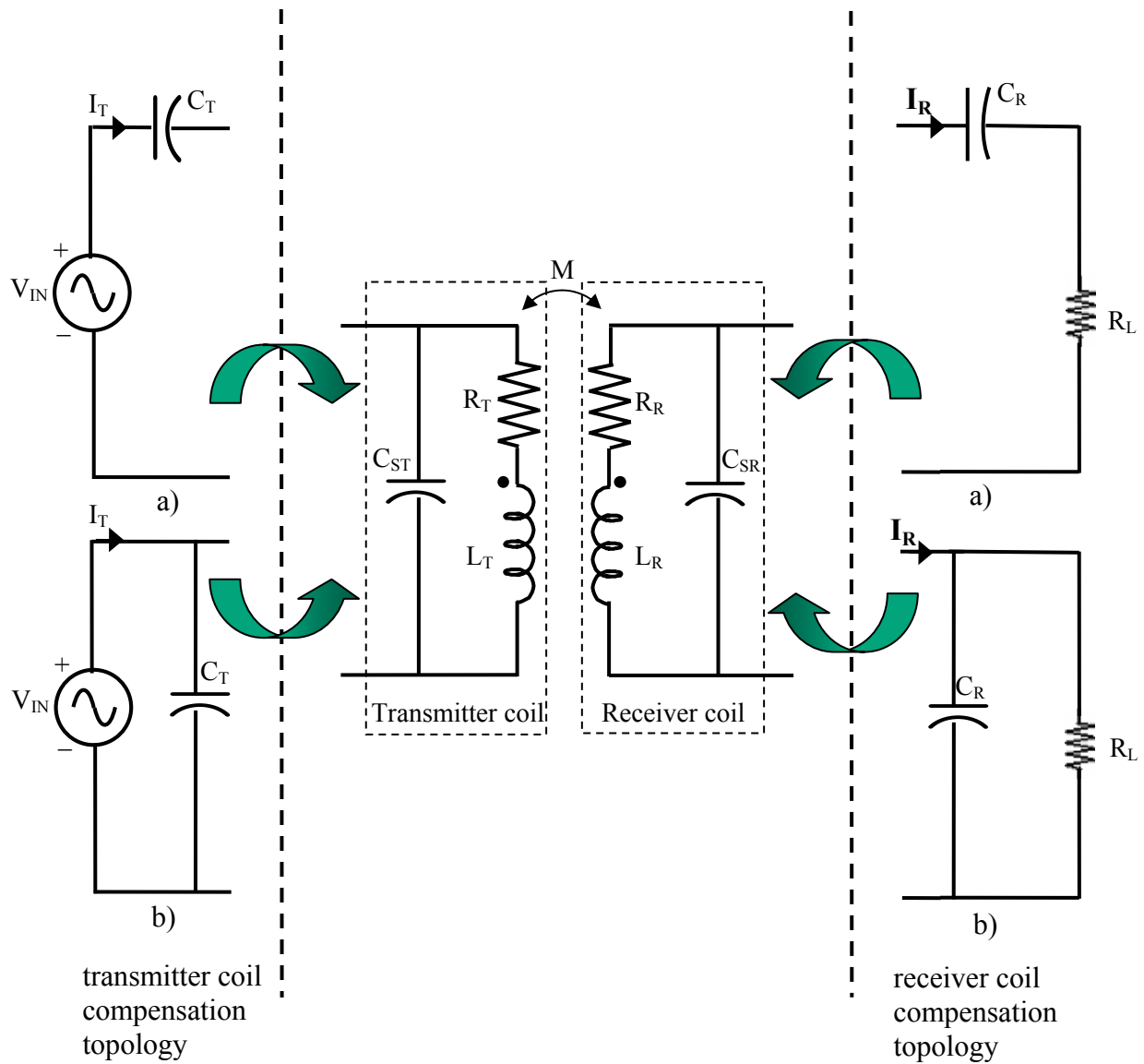


Figure 3.5: Circuit schematic for coil compensation topologies with external capacitors C_T and C_R . a) series compensation, b) parallel compensation.

Transmitter coil series compensation and receiver coil series compensation

In this analysis, for simplicity, the parasitic capacitors C_{ST} and C_{SR} for the transmitter and the receiver coils respectively are neglected. The receiver circuit impedance Z_{REC} from Fig. 3.5

a) is given by: $Z_{REC} = (R_R + R_L) + j\left(\omega L_R - \frac{1}{\omega C_R}\right)$. As in the previous section, the reflected

impedance Z_{REF} of the receiver circuit into the transmitter circuit can be expressed in this case as:

$$Z_{REF} = \frac{\omega^2 M^2 (R_R + R_L)}{(R_R + R_L)^2 + \left(\omega L_R - \frac{1}{\omega C_R}\right)^2} - j \left[\frac{\omega^2 M^2 \left(\omega L_R - \frac{1}{\omega C_R}\right)}{(R_R + R_L)^2 + \left(\omega L_R - \frac{1}{\omega C_R}\right)^2} \right]. \quad (3.4)$$

Here, C_T and C_R are the compensation capacitors for the transmitter and the receiver coils respectively ω is the angular frequency. A detailed derivation for this case is given in Appendix

D. The link efficiency η for this case can be represented as:

$$\eta = \frac{\omega_0^2 M^2 R_L}{R_T \left[(R_R + R_L)^2 + \left(\omega_0 L_R - \frac{1}{\omega_0 C_R}\right)^2 \right] + \omega_0^2 M^2 (R_R + R_L)} \quad \text{or}$$

$$\eta = \frac{M^2 R_L}{(R_R + R_L) \left[R_T L_R C_R (R_R + R_L) + M^2 \right]}. \quad (3.5)$$

The angular resonance frequency for the receiver circuit $\omega_{0r} = \frac{1}{\sqrt{L_R C_R}}$. The coil operating

frequency ω_0 in this case is taken to be the same as the resonance frequencies of the transmitter and receiver circuits. Hence, $\omega_0 = \omega_{0t} = \omega_{0r}$. Here, ω_{0t} is the transmitter coil resonance

frequency. For a chosen value of ω_0 , $C_R = \frac{1}{\omega_0^2 L_R}$ and $C_T = \frac{1}{\omega_0^2 L_T}$.

Another model that considers the effect of the parasitic capacitances is derived in the next sub-section. The expression for link efficiency has been further optimized in terms of the transmitter and the receiver coil quality factors in reference [14]. The link efficiency depends on the coupling coefficient and is generally low for weak coupling from the latter model as well.

Transmitter coil series compensation and receiver coil parallel compensation

From Fig. 3.5 b), neglecting parasitic capacitances C_{ST} and C_{SR} , the receiver circuit impedance at angular frequency ω is given by:

$$Z_{REC} = \frac{R_R + R_L + \omega^2 R_R C_R^2 R_L^2}{1 + \omega^2 C_R^2 R_L^2} + j \left[\frac{\omega L_R - \omega C_R R_L^2 + \omega^3 L_R C_R^2 R_L^2}{1 + \omega^2 C_R^2 R_L^2} \right].$$

A detailed derivation is provided in Appendix D. As in the previous section, the general expression for the reflected impedance Z_{REF} of the receiver circuit into the transmitter circuit can be expressed in this case as:

$$Z_{REF} = \frac{\omega^2 M^2 (\omega^2 R_R C_R^2 R_L^2 + R_R + R_L)}{(R_R + R_L - \omega^2 L_R C_R R_L)^2 + (\omega L_R + \omega R_R C_R R_L)^2} + j \left[\frac{\omega^2 M^2 (\omega C_R R_L^2 - \omega^3 L_R C_R^2 R_L^2 - \omega L_R)}{(R_R + R_L - \omega^2 L_R C_R R_L)^2 + (\omega L_R + \omega R_R C_R R_L)^2} \right] \quad (3.6)$$

At resonance, $\omega = \omega_0 = \omega_{0t} = \omega_{0r}$, and the link efficiency η as derived in Appendix D and can be represented as:

$$\eta = \frac{\omega_0^2 M^2 R_L}{R_T \left\{ (R_R + R_L - \omega_0^2 L_R C_R R_L)^2 + (\omega_0 L_R + \omega_0 R_R C_R R_L)^2 \right\} + \omega_0^2 M^2 (R_R + R_L + \omega_0^2 R_R C_R^2 R_L^2)} \quad (3.7)$$

or
$$\eta = \frac{M^2 R_L}{R_T \left\{ \frac{L_R (L_R + R_R C_R R_L)^2}{(C_R R_L^2 - L_R)} + (L_R + R_R C_R R_L)^2 \right\} + M^2 \left\{ \frac{(R_R + R_L) L_R + (C_R R_L^2 - L_R) R_R}{L_R} \right\}}. \quad \text{Here,}$$

$$\omega_{0r} = \sqrt{\frac{C_R R_L^2 - L_R}{L_R C_R^2 R_L^2}}, \quad \omega_0 \text{ is the coil operating frequency and } \omega_0 = \omega_{0t} = \omega_{0r}. \text{ As before, } \omega_{0t} \text{ and}$$

ω_{0r} are the transmitter coil and receiver coil resonance frequencies. At a chosen value for ω_0 ,

$$C_R = \frac{R_L \pm \sqrt{R_L^2 - 4\omega_0^2 L_R^2}}{2\omega_0^2 L_R R_L} \quad (3.8)$$

and $C_T = \frac{1}{\omega_0^2 L_T}$. For physically realizable case, Eqn. (3.8) for C_R is valid when $\omega_0 \leq \frac{R_L}{2L_R}$. For

our case, $L_R = 39 \mu\text{H}$ and R_L is the ac rms equivalent load resistance and has a value of 32.5Ω (for a DC load resistance of 65Ω). For these values for the given case gives $\omega_0 \leq 66.32 \text{ kHz}$.

Henceforth in this thesis, C_{R+} refers to C_R when $C_R = \frac{R_L + \sqrt{R_L^2 - 4\omega_0^2 L_R^2}}{2\omega_0^2 L_R R_L}$ and C_{R-} refers to C_R

$$\text{when } C_R = \frac{R_L - \sqrt{R_L^2 - 4\omega_0^2 L_R^2}}{2\omega_0^2 L_R R_L}.$$

A model that considers the effect of the parasitic capacitors is derived in the next subsection. This expression for link efficiency has been further optimized in terms of the transmitter coil and the receiver coil quality factors in reference [14]. It is evident here also that the link efficiency depends on coupling coefficient and is low for weak coupling.

Receiver coil: series compensation vs parallel compensation

It is necessary to evaluate the link efficiency for both compensation topologies in the receiver coil utilizing C_{R+} and C_{R-} . A compensation topology will be chosen based on a higher link efficiency obtained for the frequencies of interest. Figures 3.6 and 3.7 show plots for variation in link efficiency as a function of operating frequency on semi-log and logarithmic scales respectively. Here, series compensation has been chosen for the transmitter circuit and a comparison is made between series and parallel compensation (C_{R-}) for the receiver circuit. It is evident from the plots that parallel compensation in the receiver circuit delivers a higher

efficiency for this case in the frequency range of interest. Figures 3.8 and 3.9 are a set of two other plots similar to the ones mentioned above, but in this case parallel compensation in the receiver circuit is achieved with C_{R+} . Again, it is evident that for this case also parallel compensation in the receiver circuit produces a higher efficiency in the frequency range of interest. Figures 3.10 and 3.11 show plots for variation in the link efficiency as a function of operating frequency on semi-log and logarithmic scales respectively. Here, the transmitter coil is series compensated and the receiver coil is compensated in parallel (C_{R+} and C_{R-}). It is evident from the plots that C_{R+} compensation of the receiver coil yields higher link efficiency than C_{R-} compensation in the frequency range of interest.

Theoretical data has been used in plotting these curves. On extending these plots to higher frequencies (100 MHz), it is observed that the link efficiency levels off to 1 in the frequency range of 4.5 MHz for transmitter coil series compensation and receiver coil series and parallel (C_{R+} and C_{R-}) compensation. Simulation at such high frequencies is not always accurate as the theoretical data used does not consider coil parasitics. Also, Eqn. (3.8) does not stand at frequencies higher than 66.32 kHz. The Matlab code used to generate the above plots is given in Appendix E.

3.2.3 Link Efficiency for the Compensated Case – Considering Parasitic Coil Capacitance

In the previous section, expressions for link efficiency for the uncompensated case and the compensated case have been derived and plotted as a function of operating frequency. It is observed that implementation of series compensation for the transmitter circuit and parallel compensation for the receiver circuit results in higher link efficiency. In the previous section it is assumed that

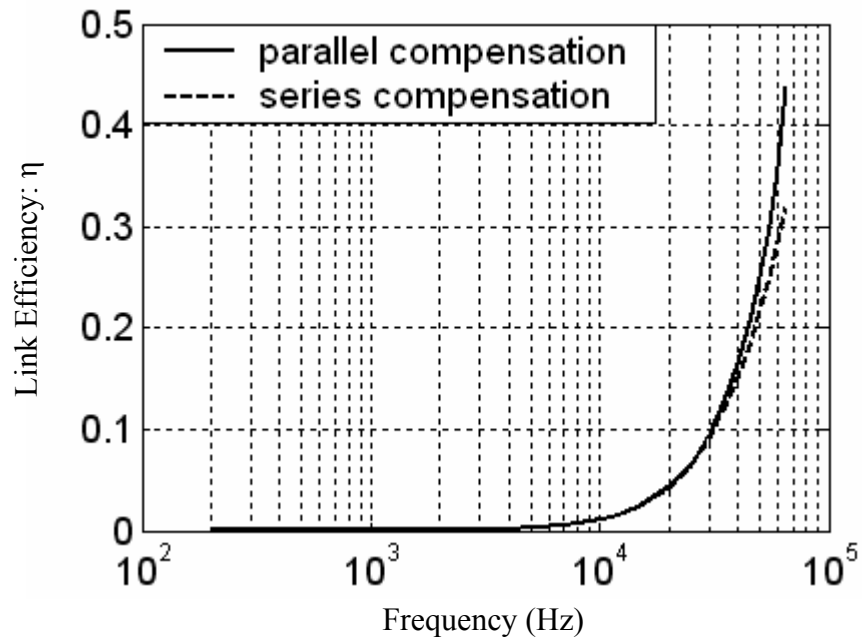


Figure 3.6: Link efficiency η as a function of coil operating frequency when transmitter coil is series compensated and receiver coil is both series and parallel compensated (C_R). Semi-log scale.

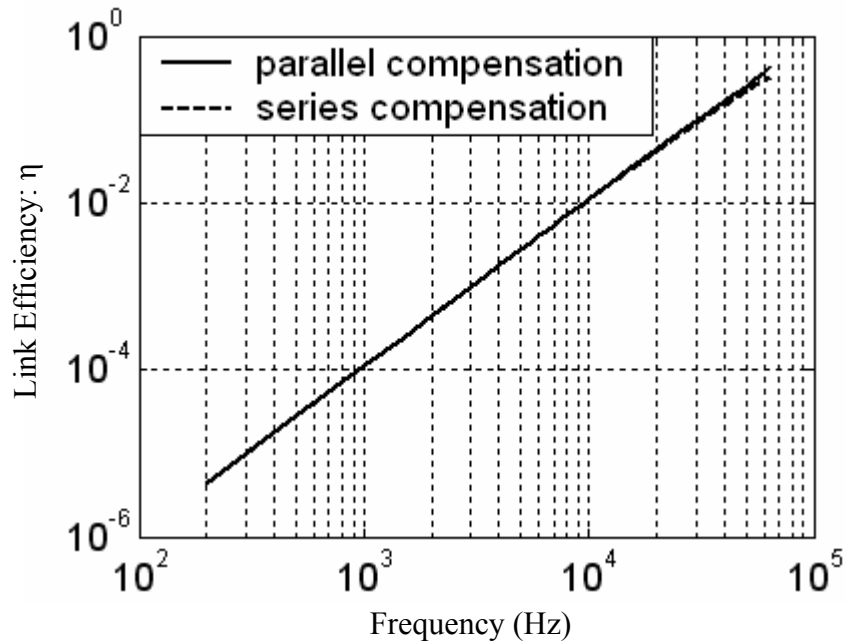


Figure 3.7: Link efficiency η as a function of coil operating frequency when transmitter coil is series compensated and receiver coil is both series and parallel compensated (C_R). Logarithmic scale.

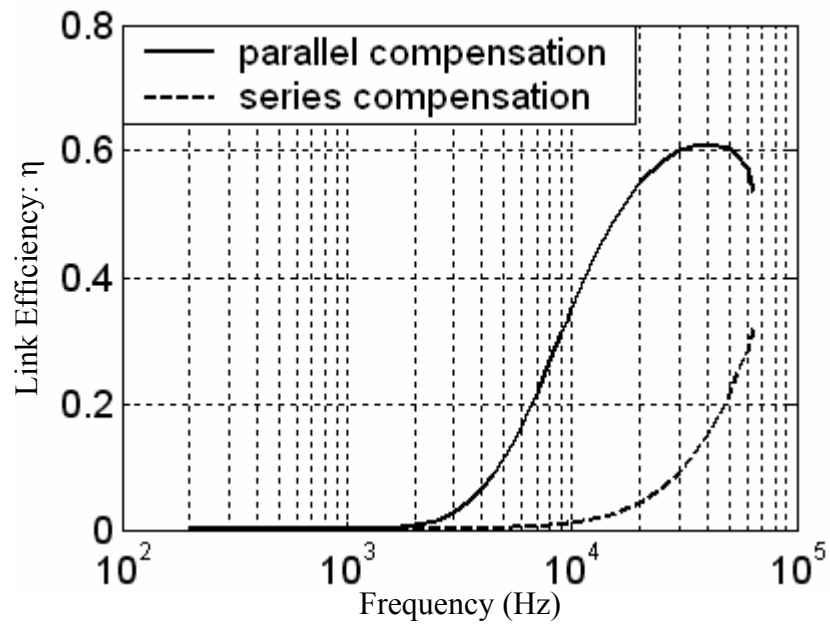


Figure 3.8: Link efficiency η as a function of coil operating frequency when transmitter coil is series compensated and receiver coil is both series and parallel compensated (C_{R+}). Semi-log scale.

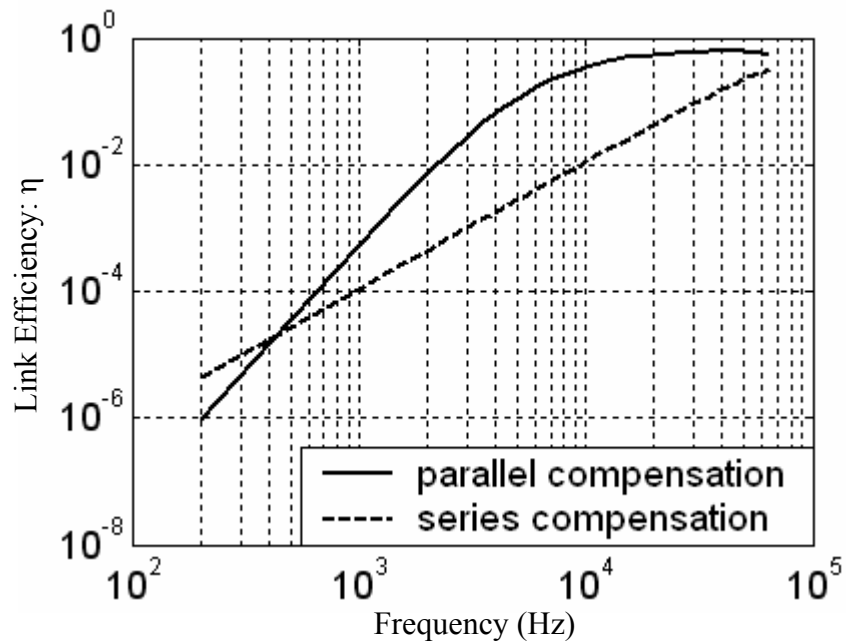


Figure 3.9: Link efficiency η as a function of coil operating frequency when transmitter coil is series compensated and receiver coil is both series and parallel compensated (C_{R+}). Logarithmic scale.

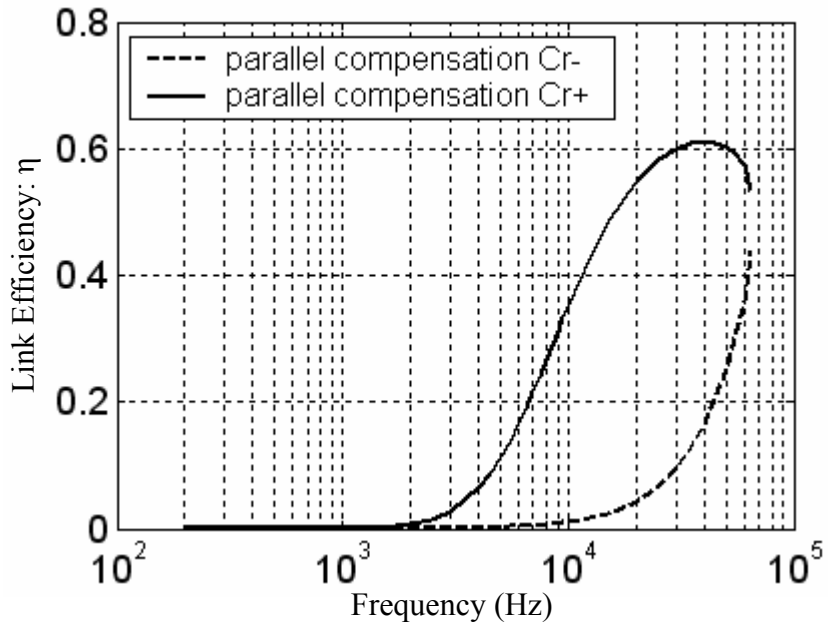


Figure 3.10: Link efficiency η as a function of coil operating frequency when transmitter coil is series compensated and receiver coil is parallel compensated (C_{R+} and C_{R-}). Semi-log scale.

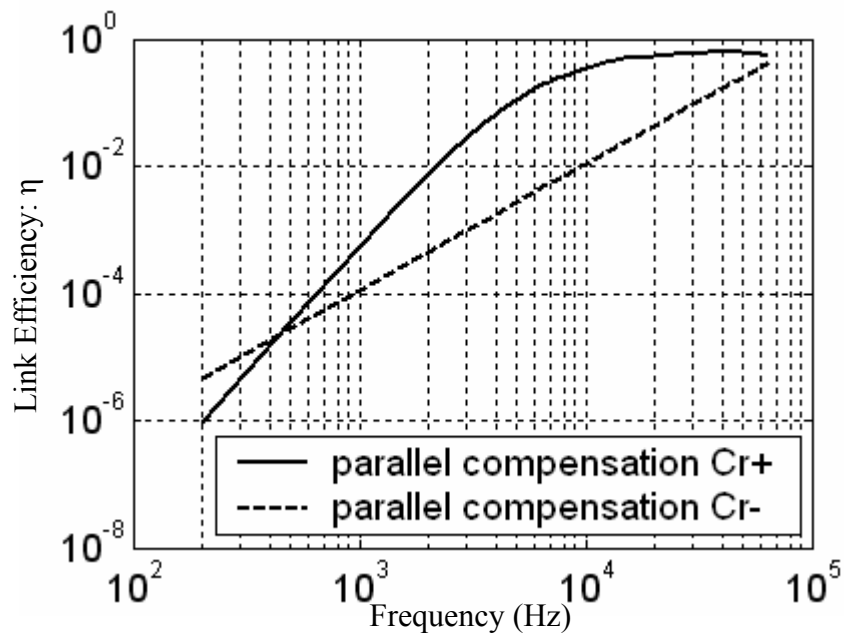


Figure 3.11: Link efficiency η as a function of coil operating frequency when transmitter coil is series compensated and receiver coil is parallel compensated (C_{R+} and C_{R-}). Logarithmic scale.

the operating frequency is almost a factor of ten below the self resonance frequency $f_{srr} = 462$ kHz of the transmitter coil. The self resonance frequency of the receiver coil $f_{srr} = 17.6$ MHz is much higher. This assumption allowed for elimination of both the transmitter coil and the receiver coil parasitic capacitances. In this section, an analytical model is developed that considers the effect of these parasitic capacitances on the link efficiency of the system. Figure 3.12 shows the circuit schematic for an inductively coupled system with the transmitter circuit compensated in series and the receiver circuit compensated in parallel. Also shown in this figure are the high frequency models for the transmitter and the receiver coils. Here, C_{ST} and C_{SR} are the parasitic capacitances of the transmitter coil and the receiver coil respectively.

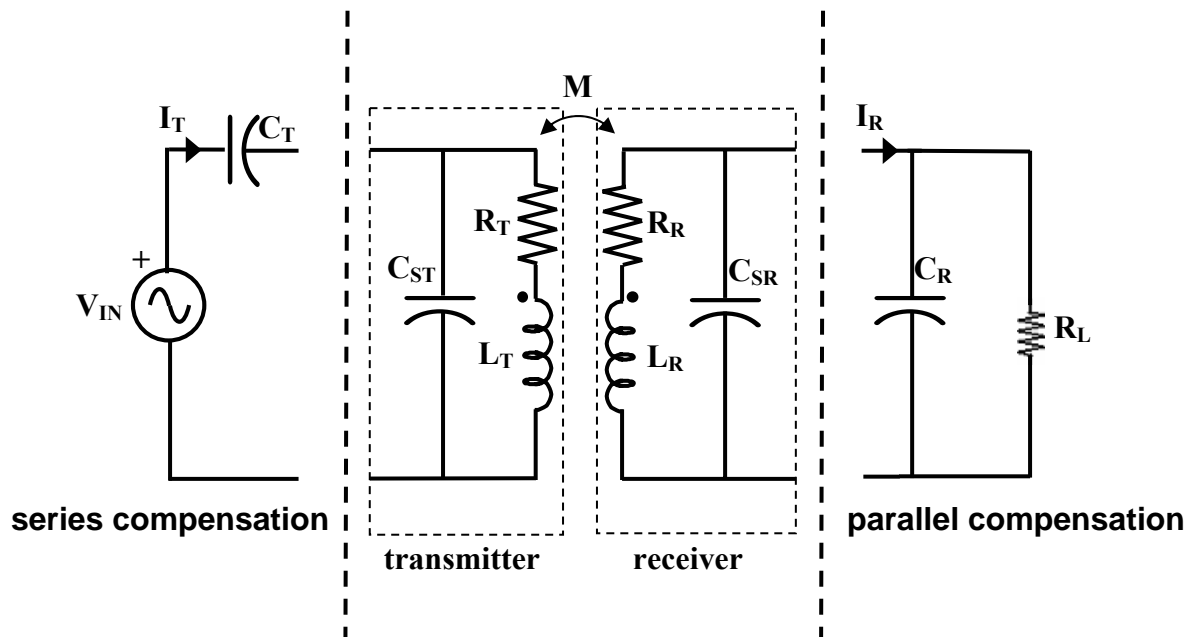


Figure 3.12: Circuit schematic of an inductively coupled system. Transmitter coil is series compensated and receiver coil is parallel compensated.

The receiver coil impedance is obtained by replacing the external compensation capacitor C_R by $C_{RE} = C_R + C_{SR}$ in equations derived for receiver coil parallel compensation case earlier. Hence,

$$Z_{REC} = \frac{R_R + R_L + \omega^2 R_R C_{RE}^2 R_L^2}{1 + \omega^2 C_{RE}^2 R_L^2} + j \left[\frac{\omega L_R - \omega C_{RE} R_L^2 + \omega^3 L_R C_{RE}^2 R_L^2}{1 + \omega^2 C_{RE}^2 R_L^2} \right].$$

Here, $R_{REC} = \frac{R_R + R_L + \omega^2 R_R C_{RE}^2 R_L^2}{1 + \omega^2 C_{RE}^2 R_L^2}$ and $X_{REC} = \frac{\omega L_R - \omega C_{RE} R_L^2 + \omega^3 L_R C_{RE}^2 R_L^2}{1 + \omega^2 C_{RE}^2 R_L^2}$ are the

receiver coil resistance and reactance respectively as seen in section 3.2.2 and Appendix D. The general expression for the receiver circuit reflected impedance into the transmitter circuit can be expressed from Eqn. 3.6 as

$$Z_{REF} = \frac{\omega^2 M^2 (\omega^2 R_R C_{RE}^2 R_L^2 + R_R + R_L)}{(R_R + R_L - \omega^2 L_R C_{RE} R_L)^2 + (\omega L_R + \omega R_R C_{RE} R_L)^2} + j \left[\frac{\omega^2 M^2 (\omega C_{RE} R_L^2 - \omega^3 L_R C_{RE}^2 R_L^2 - \omega L_R)}{(R_R + R_L - \omega^2 L_R C_{RE} R_L)^2 + (\omega L_R + \omega R_R C_{RE} R_L)^2} \right]$$

Here, $R_{REF} = \frac{\omega^2 M^2 (\omega^2 R_R C_{RE}^2 R_L^2 + R_R + R_L)}{(R_R + R_L - \omega^2 L_R C_{RE} R_L)^2 + (\omega L_R + \omega R_R C_{RE} R_L)^2}$ and $X_{REF} = \frac{\omega^2 M^2 (\omega C_{RE} R_L^2 - \omega^3 L_R C_{RE}^2 R_L^2 - \omega L_R)}{(R_R + R_L - \omega^2 L_R C_{RE} R_L)^2 + (\omega L_R + \omega R_R C_{RE} R_L)^2}$

are the receiver circuit reflected resistance and reactance respectively. The resonance frequency

ω_{or} of the receiver coil is obtained as $\omega_{or} = \sqrt{\frac{C_{RE} R_L^2 - L_R}{L_R C_{RE}^2 R_L^2}}$. Here, $\omega_0 = \omega_{0t} = \omega_{0r}$. The receiver

coil net parallel capacitance is expressed as $C_{RE} = \frac{R_L \pm \sqrt{R_L^2 - 4\omega_0^2 L_R^2}}{2\omega_0^2 L_R R_L}$ or

$$C_R = \frac{R_L \pm \sqrt{R_L^2 - 4\omega_0^2 L_R^2}}{2\omega_0^2 L_R R_L} - C_{SR}. \quad (3.9)$$

In order to limit C_{RE} to real values, $R_L^2 - 4\omega_0^2 L_R^2 \geq 0$ or $\omega_0 \leq \frac{R_L}{2L_R}$ i.e. $\omega_0 \leq 66.32$ kHz. As

seen previously, C_{RE+} refers to C_{RE} when $C_{RE} = \frac{R_L + \sqrt{R_L^2 - 4\omega_0^2 L_R^2}}{2\omega_0^2 L_R R_L}$ and C_{RE-} refers to C_{RE} when

$C_{RE} = \frac{R_L - \sqrt{R_L^2 - 4\omega_0^2 L_R^2}}{2\omega_0^2 L_R R_L}$. A more detailed analysis of this case is given in Appendix F. The

transmitter coil impedance from Appendix F is expressed as:

$$Z_{TRA} = \frac{\omega^2 (R_T + R_{REF}) C_T (1 - \omega^2 L_T C_{ST}) (C_T + C_{ST}) - [1 - \omega^2 L_T (C_T + C_{ST})] [\omega^2 C_T C_{ST} (R_T + R_{REF})]}{\omega^2 C_T^2 (1 - \omega^2 L_T C_{ST})^2 + \omega^4 C_T^2 C_{ST}^2 (R_T + R_{REF})^2} - j \left(\frac{\omega^3 C_T C_{ST} (R_T + R_{REF})^2 (C_T + C_{ST}) + \omega C_T [1 - \omega^2 L_T (C_T + C_{ST})] (1 - \omega^2 L_T C_{ST})}{\omega^2 C_T^2 (1 - \omega^2 L_T C_{ST})^2 + \omega^4 C_T^2 C_{ST}^2 (R_T + R_{REF})^2} \right).$$

$$\text{Here, } R_{TRA} = \frac{\omega^2 (R_T + R_{REF}) C_T (1 - \omega^2 L_T C_{ST}) (C_T + C_{ST}) - [1 - \omega^2 L_T (C_T + C_{ST})] [\omega^2 C_T C_{ST} (R_T + R_{REF})]}{\omega^2 C_T^2 (1 - \omega^2 L_T C_{ST})^2 + \omega^4 C_T^2 C_{ST}^2 (R_T + R_{REF})^2}$$

$$\text{and } X_{TRA} = - \left(\frac{\omega^3 C_T C_{ST} (R_T + R_{REF})^2 (C_T + C_{ST}) + \omega C_T [1 - \omega^2 L_T (C_T + C_{ST})] (1 - \omega^2 L_T C_{ST})}{\omega^2 C_T^2 (1 - \omega^2 L_T C_{ST})^2 + \omega^4 C_T^2 C_{ST}^2 (R_T + R_{REF})^2} \right) \text{ are the}$$

transmitter coil resistance and reactance respectively. The transmitter coil compensation

capacitor C_T is expressed as: $C_T = \frac{2\omega_0^2 L_T C_{ST} - \omega_0^2 C_{ST}^2 (R_T + R_{REF})^2 - \omega_0^4 L_T^2 C_{ST}^2 - 1}{\omega_0^2 C_{ST} (R_T + R_{REF})^2 + \omega_0^4 L_T^2 C_{ST} - \omega_0^2 L_T}$. The

link efficiency η for the transmitter coil and receiver coil can be obtained as $\eta = \eta_T \times \eta_R$. Here,

η_T and η_R are the transmitter coil and receiver coil efficiencies respectively. From Appendix F,

$$\eta_T = \frac{\omega_0^2 M^2 (\omega_0^2 R_R C_{RE}^2 R_L^2 + R_R + R_L)}{\omega_0^2 M^2 (\omega_0^2 R_R C_{RE}^2 R_L^2 + R_R + R_L) + R_T \left[(R_R + R_L - \omega_0^2 L_R C_{RE} R_L)^2 + (\omega_0 L_R + \omega_0 R_R C_{RE} R_L)^2 \right]}$$

$$\eta_R = \frac{R_L}{R_R + R_L + \omega_0^2 R_R C_{RE}^2 R_L^2}.$$

The overall link efficiency η is now given as:

$$\eta = \frac{M^2 R_L}{R_T \left\{ \frac{L_R (L_R + R_R C_{RE} R_L)^2}{(C_{RE} R_L^2 - L_R)} + (L_R + R_R C_{RE} R_L)^2 \right\} + M^2 \left\{ \frac{(R_R + R_L) L_R + (C_{RE} R_L^2 - L_R) R_R}{L_R} \right\}}.$$

Since, we have obtained the expression for link efficiency for the compensated case considering coil parasitics, it now becomes necessary to compare this efficiency with the efficiency obtained for the compensated case without considering parasitic coil capacitances. Figure 3.13 shows the plot for variation in link efficiency (for a series compensated transmitter circuit and a parallel compensated receiver circuit considering coil parasitics) with operating frequency for the case of C_{RE+} and C_{RE-} . Comparing Fig. 3.13 with Figs. 3.6 and 3.8 (parallel case), it is seen that the variation in link efficiency with operating frequency (when transmitter coil is compensated in series and receiver coil in parallel) is the same with and without consideration of parasitic coil capacitances C_{ST} and C_{SR} . This implies that the assumption in the previous section (of not considering parasitic coil capacitance) is valid and applicable for the frequency range of interest. The effect of the parasitic capacitances C_{ST} and C_{SR} is to obtain accurate values of C_T and C_R from Eqns. (F8) and (3.9) respectively. The Matlab code generated for this simulation is given in Appendix G.

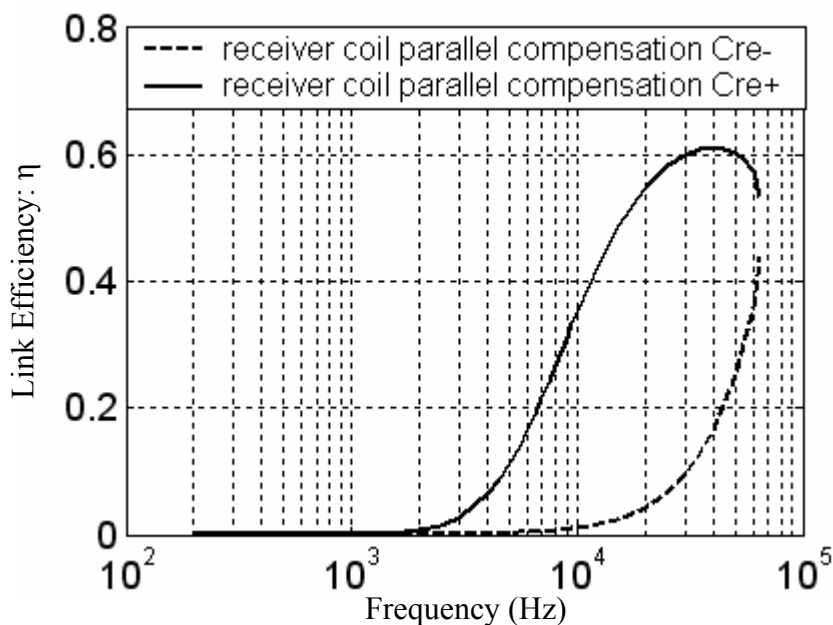


Figure 3.13: Link efficiency η as a function of coil operating frequency, considering parasitic coil capacitances. Transmitter coil is series compensated and receiver coil is parallel compensated (C_{RE+} and C_{RE-}).

3.3 RPDS Overall Efficiency and Other Design Aspects

Now that the coil design parameters, link efficiency and compensation topology of the RPDS have been established, it is necessary to consider other system design aspects such as overall system efficiency, rectifier and regulator topologies. Figure 3.14 shows a lumped equivalent model for the front end of the RPDS with a voltage doubler circuit. The overall system efficiency of such an RPDS is given by $\eta_{RPDS} = \eta_{CD} \times \eta_{link} \times \eta_{RECT}$. Here, η_{RPDS} is the RPDS efficiency, η_{CD} is the transmitter coil driver efficiency, η_{link} is the link efficiency and η_{RECT} is the rectifier circuit efficiency. Also, $\eta_{link} = \eta_T \times \eta_R$. Here, η_T and η_R are the transmitter coil and receiver coil efficiencies respectively as described in section 3.2. In loosely coupled inductive systems, the link efficiency is very small when compared to the coil driver efficiency and the rectifier efficiency and hence dominates the overall system efficiency. Unlike the case of tightly coupled systems, where power delivered is high, here, η_{CD} and η_{RECT} can be neglected. Hence,

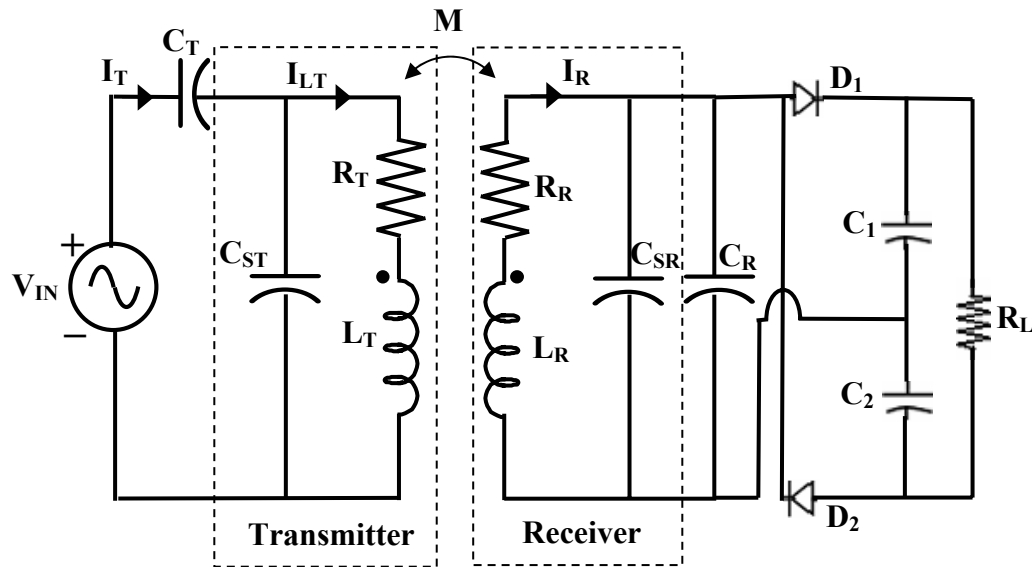


Figure 3.14: Lumped equivalent circuit for the front end of the RPDS with a voltage doubler circuit.

optimization of the link efficiency is of primary importance in order to increase the overall system efficiency.

The voltage doubler and rectifier circuit is used instead of the conventional full wave bridge rectifier in the receiver circuitry. It is possible to obtain a rectified voltage that is double the voltage obtained using a bridge rectifier. This usually occurs at high load values. For loosely coupled inductive power delivery systems the voltage doubler circuit is commonly recommended. In the positive half of the input cycle diode D_1 is forward biased and the voltage appears across capacitor C_1 . During the negative input cycle, diode D_2 is forward biased and this voltage now appears across capacitor C_2 . These voltages appear in series across the load. The ripple obtained here is the same as a full wave rectifier. This rectifier topology transforms the dc load (65Ω in the present case) at its output to an equivalent ac load at its input assuming that the rectifier efficiency is high enough to rectify the peak value of voltage across $C_{RE} = C_{SR} + C_R$ and make it appear as a direct voltage across R_L . If the dc power dissipated in R_L , is equal to the ac power dissipated in the equivalent resistor placed directly in parallel with C_R and L_R , then the value of the equivalent resistor is $R_L/2$.

The output of the voltage doubler circuit is fed to a lithium-ion battery charger chip (MIC79050, MICREL). The MIC79050 is a high-accuracy, linear battery charging circuit designed for implementation as a single lithium-ion battery charger. The MIC79050 uses an unregulated voltage source and provides an extremely accurate termination voltage. The output voltage varies only 0.75 % from nominal over the standard temperature range for Li-ion battery charging (-5°C to 60°C). The MIC79050 allows the charger to be disabled when the battery is fully charged and the current drawn by the battery has approached a minimum and/or the maximum charging time has elapsed. When the charger is disabled, the regulator output sinks a minimum of current when

the battery voltage is applied directly to its output. This current is typically 12 μA or less [30]. With a minimum of external components, accurate charging of Li-ion cells can be obtained. This is a simple cost effective solution for battery charging. The charging chip specifications require a minimum voltage of 4.7 V dc and a current of 100 mA. This implies an effective load of 47 Ω and load power of 470 mW. Considering other power losses, the design power was estimated to be 670 mW. The regulated output voltage of the battery charger chip is 4.2 volts at 100 mA. Figure 3.15 shows the block diagram of the battery charging chip. A mini prismatic polymer lithium-ion battery (PR-042025) manufactured by TCL Hyperpower Batteries Inc. is used for testing purposes. The battery has a nominal voltage of 3.7 V and 150 mAh capacity. Battery ratings and other specifications as provided by the manufacturer are attached in Appendix H.

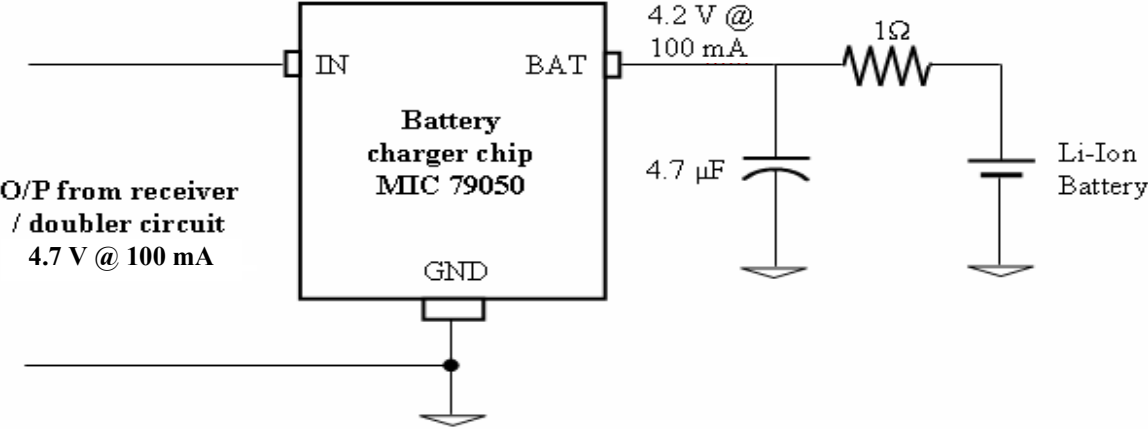


Figure 3.15: Block diagram of battery charging chip MIC 79050.

Having decided on the rectifier and regulator topology, it now becomes necessary to derive expressions for the transmitter circuit current, receiver circuit current and the ac power delivered to the load for the lumped equivalent model as shown in Fig. 3.16. This allows us to develop a model that is appropriate for simulation in Matlab. This model calculates power delivered to the coil while considering the effects of the parasitic coil capacitances. Fig. 3.16 is similar to Fig. F.1 if one replaces R_L in Fig. F.1 by $R_L/2$.

From Appendix F, the transmitter coil impedance Z_{TRA} for Fig. 3.16 can be written as:

$$Z_{TRA} = R_{TRA} + j X_{TRA}.$$

$$\text{Here, } R_{TRA} = \frac{\omega^2 (R_T + R_{REF}) C_T (1 - \omega^2 L_T C_{ST}) (C_T + C_{ST}) - [1 - \omega^2 L_T (C_T + C_{ST})] [\omega^2 C_T C_{ST} (R_T + R_{REF})]}{\omega^2 C_T^2 (1 - \omega^2 L_T C_{ST})^2 + \omega^4 C_T^2 C_{ST}^2 (R_T + R_{REF})^2},$$

$$X_{TRA} = - \left(\frac{\omega^3 C_T C_{ST} (R_T + R_{REF})^2 (C_T + C_{ST}) + \omega C_T [1 - \omega^2 L_T (C_T + C_{ST})] (1 - \omega^2 L_T C_{ST})}{\omega^2 C_T^2 (1 - \omega^2 L_T C_{ST})^2 + \omega^4 C_T^2 C_{ST}^2 (R_T + R_{REF})^2} \right). \quad \text{These are}$$

obtained from Eqns. (F.7A) and (F.7B).

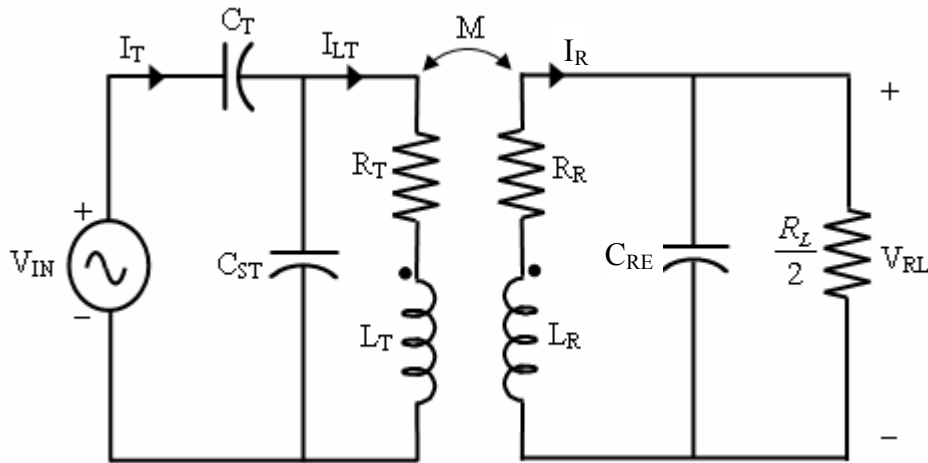


Figure 3.16: Simplified version of Fig. 3.14 from power dissipation consideration.

The transmitter coil compensation capacitor C_T for Fig. 3.16 is obtained from Eqn. (F.8) as:

$$C_T = \frac{2\omega_0^2 L_T C_{ST} - \omega_0^2 C_{ST}^2 (R_T + R_{REF})^2 - \omega_0^4 L_T^2 C_{ST}^2 - 1}{\omega_0^2 C_{ST} (R_T + R_{REF})^2 + \omega_0^4 L_T^2 C_{ST} - \omega_0^2 L_T}.$$

The value of R_{REF} in the above equations for Fig. 3.16 can be written by replacing R_L in Eqn. (F.6A) with $R_L/2$ as:

$$R_{REF} = \frac{\omega^2 M^2 \left(\omega^2 R_R C_{RE}^2 \frac{R_L^2}{4} + R_R + \frac{R_L}{2} \right)}{\left(R_R + \frac{R_L}{2} - \omega^2 L_R C_{RE} \frac{R_L}{2} \right)^2 + \left(\omega L_R + \omega R_R C_{RE} \frac{R_L}{2} \right)^2}.$$

The resonance frequency ω_{0r} for Fig. 3.16 can now be obtained from Eqn. (F.6C) as:

$$\omega_{0r} = \sqrt{\frac{C_{RE} \left(\frac{R_L}{2} \right)^2 - L_R}{L_R C_{RE}^2 \left(\frac{R_L}{2} \right)^2}} = \sqrt{\frac{C_{RE} R_L^2 - 4L_R}{L_R C_{RE}^2 R_L^2}}.$$

The corresponding value of C_{RE} is obtained from Eqn. (F.6D) as:

$$C_{RE} = \frac{\frac{R_L}{2} \pm \sqrt{\left(\frac{R_L}{2} \right)^2 - 4\omega_0^2 L_R^2}}{2\omega_0^2 L_R \frac{R_L}{2}} = \frac{R_L \pm \sqrt{R_L^2 - 16\omega_0^2 L_R^2}}{2\omega_0^2 L_R R_L}.$$

Applying KVL to the transmitter circuit and from Eqn. (F.3) a relation between I_T and I_{LT} can be obtained as:

$$I_{LT} = I_T \left[1 + \frac{C_{ST}}{C_T} \right] - V_{IN} (j\omega C_{ST}).$$

An expression for the receiver coil current can be obtained for Fig. 3.16 by replacing R_L with $R_L/2$ in Eqn. (F.5).

$$\text{Hence, } I_R = \frac{j\omega M I_{LT}}{j\omega L_R + R_R + \left(\frac{\frac{R_L}{2}}{1 + j\omega C_{RE} \frac{R_L}{2}} \right)} = \frac{j\omega M I_{LT}}{j\omega L_R + R_R + \left(\frac{R_L}{2 + j\omega C_{RE} R_L} \right)}.$$

The voltage V_{RL} and power P_{RL} across the load resistor $R_L/2$ are given by:

$$V_{RL} = I_R \left(\frac{R_L}{2 + j\omega C_{RE} R_L} \right),$$

$$P_{RL} = \frac{2|V_{RL}|^2}{R_L}.$$

CHAPTER 4

SIMULATIONS AND RESULTS

4.1 RPDS Simulation

In the previous chapter an analytical technique was developed to simulate the power delivery to the load by the present RPDS. This analytical model considers the effect of the parasitic coil resistances and capacitances. The model is simulated in Matlab and the results are discussed here.

Figure 4.1 shows the plot for the variation in power delivered to a 35Ω load resistance as a function of resonance frequency. This is for the case of transmitter circuit with series compensation and receiver circuit with parallel compensation (C_{R+}). It is evident from this plot that the variation in load power delivery follows the variation in link efficiency for the case of receiver circuit with parallel compensation (C_{R+}) as given in Fig. 3.13. As in the case of the link efficiency, the power delivery also starts to fall at higher frequencies greater than 30 kHz. Maximum power delivery occurs at 25 kHz. The input supply voltage (rms) applied to the transmitter coil for the following simulation is $V_{IN} = 1.55 V$. The calculated values for the transmitter and receiver coil parasitic capacitances used here are 47.6 pF and 2.1 pF respectively as obtained from $C_{ST} \approx 5.2 \times 10^{-14} D_T N_T = 5.2 \times 10^{-14} \times 16.05 \times 57 \approx 47.63$ pF for the transmitter coil and $C_{SR} \approx 5.2 \times 10^{-14} D_T N_T = 5.2 \times 10^{-14} \times 1.343 \times 30 \approx 2.1$ pF for the receiver coil [23]. The calculated values for the transmitter and receiver coil parasitic resistances are 0.24Ω and 0.107Ω respectively as obtained from sections 3.1.1 and 3.1.2. The Matlab code used for this simulation is produced in Appendix I. In the above plot, the parasitic coil capacitances and the coil resistances are assumed to be constant with frequency.

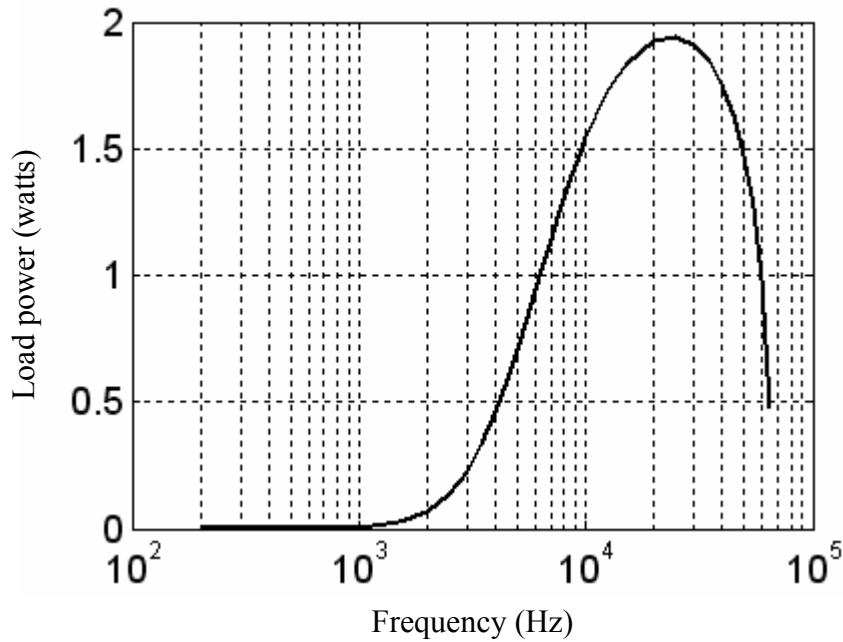


Figure 4.1: Load power delivered as a function of resonance frequency. Analytical model considers parasitic coil capacitances $C_{ST} = 47.63$ pF and $C_{SR} = 2.1$ pF. $V_{IN} = 1.55$ V rms, $R_L = 35 \Omega$.

In practical coil applications at high frequencies the parasitic coil capacitances and coil resistances vary with frequency. To predict the behavior of coils at high frequencies, accurate values of these coil parasitics are necessary. Figure 4.2 gives the variation in load power as a function of parasitic coil capacitances. Here parasitic coil capacitance values are increased. It is evident from Fig. 4.2 that, as the parasitic capacitance values increase, the power delivered to the load decreases. Figure 4.3 gives the variation in load power as a function of parasitic coil resistances. Here also, the load power decreases with increase in the parasitic coil resistance values.

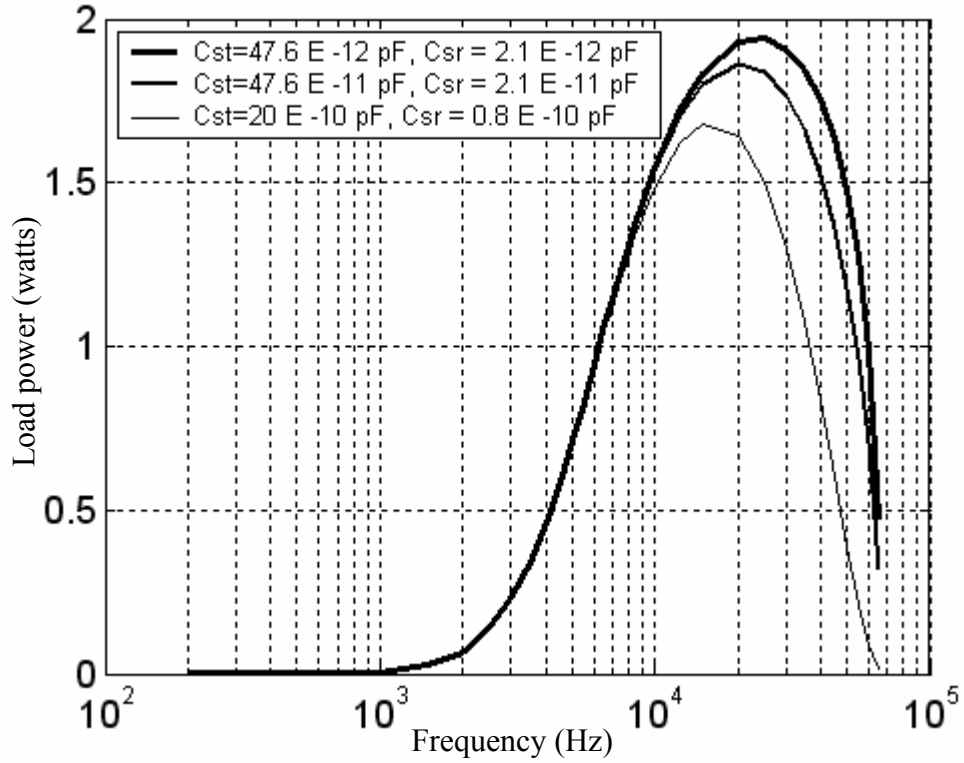


Figure 4.2: Load power delivered as a function of resonance frequency for different values of parasitic capacitances C_{ST} and C_{SR} . $V_{IN} = 1.55$ V rms, $R_L = 35 \Omega$.

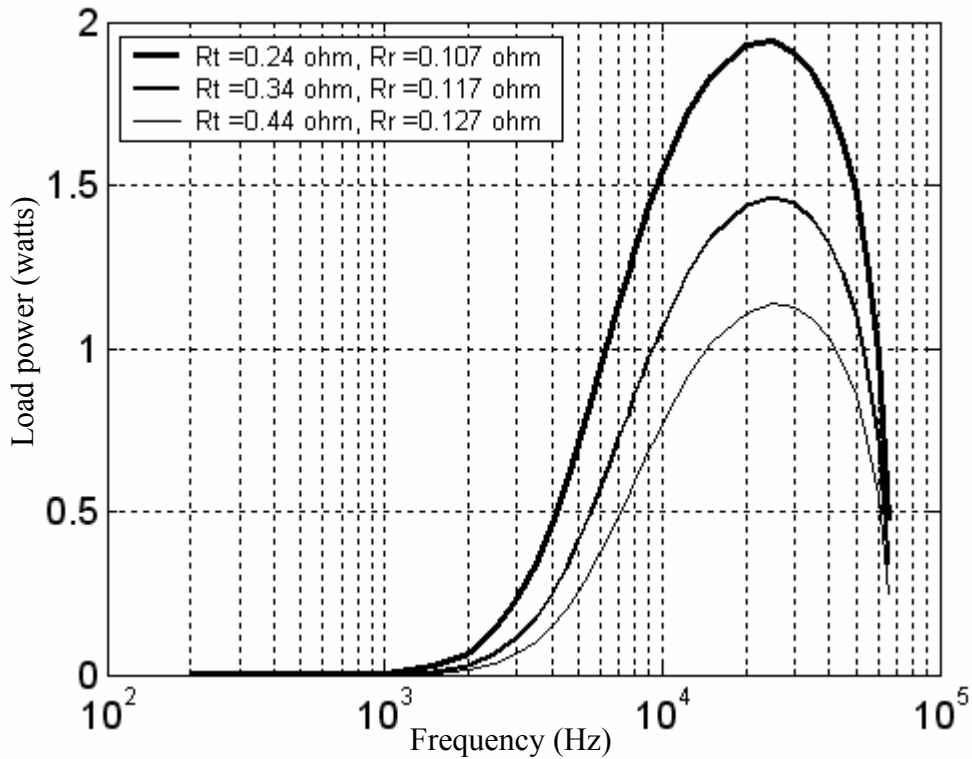


Figure 4.3: Load power delivered as a function of resonance frequency for different values of coil resistances R_T and R_R . $V_{IN} = 1.55$ V rms, $R_L = 35 \Omega$.

4.2 Coil Parasitics, Skin and Proximity Effect Model

Coil parasitics can dictate the behavior of coupled coils at high frequencies. The ac resistance of a solid copper wire can be quite different from its dc resistance due to skin effect. The wire acts as a high frequency current tube when ac current is passed at sufficiently high frequencies. The current passes preferentially near the surface of the wire and this is known as the skin effect. Skin effect can be calculated for isolated copper wires. When the wire is wound in a coil, there is an added loss in each turn associated with induced eddy currents due to fluctuating magnetic field. More energy is required to maintain these currents and this increases the effective resistance of the coil. There also occur some dielectric losses due to resulting distributed capacitances, but with a carefully chosen dielectric, these losses can be reduced to 10-20 % of the total losses. Designed link efficiencies and power output are often not met because of improper modeling of these parasitics. In this work, an attempt has been made to model skin and proximity effects at higher frequencies. A model has been developed and implemented with the help of a Matlab code for both the transmitter and the receiver coils.

Skin depth d for good conductors is given by $d = 5033 \sqrt{\frac{\rho}{\mu f}}$ cm. For copper, $d = \frac{6.62}{\sqrt{f}}$ in cm for f in Hz. Here, d , ρ , μ and f are the diameter (cm), resistivity (1.73×10^{-6} Ω -cm), relative permeability = 1 for copper and frequency (Hz) respectively. The ratio of the alternating current resistance to the direct current resistance (resistance ratio) of any such copper wire is:

$\frac{R_{AC}}{R_{DC}} \approx \frac{\pi r^2}{\pi(2r-d)d}$. Here, r is the radius of the wire. Calculation of copper losses in multilayer

coils, analyzed by Butterworth S. in 1926 and reproduced in [27] is as follows:

$$\frac{R_{AC}}{R_{DC}} = H + \frac{1}{4} \left[\left(\frac{Kbm}{D} \right)^2 \left(\frac{d_0}{C} \right)^2 G \right]. \quad (4.1)$$

Here, K is a constant depending on the type of winding (see Fig. J.1 in Appendix J), b is the axial length of winding, D is overall diameter, m is number of layers, d_0/C is diameter of wire/spacing between centers of adjacent turns in same layer, k is a constant depending upon the type of winding, H is the resistance ratio of wire when insulated (see Table J.1 in Appendix J) and G is the Proximity effect factor (see Table J.1 in Appendix J). H and G can be calculated for various values of x from Table J.1. The value of x is given by $x = 0.1078d_0\sqrt{f}$ where x is a parameter for defining the resistance ratio.

The dc resistance of the transmitter coil $R_T \approx \pi D_T N_T \approx 0.24 \Omega$. The dc resistance of the receiver coil $R_R = \pi D_R N_R / \rho \approx 0.107 \Omega$. The ac resistance of both the transmitter and the receiver coils can be calculated from Eqn. (4.1).

Figures 4.4 and 4.5 show variation in ac resistance with frequency for the transmitter and receiver coils respectively. Differences between the dc turn resistance values (of 0.24Ω for transmitter coil and 0.107Ω for receiver coil) and ac resistance values at higher frequencies are evident from both plots. This modeling for the ac resistance values has helped in the design of more accurate series and parallel compensation capacitors for the transmitter and receiver coils thereby optimizing power delivery to the receiver coil. Table J.1 was used to generate the values of H , the resistance ratio of wire when insulated and G , the Proximity effect factor. As shown in Fig. 4.3, the power delivered to the load does vary with variation in parasitic resistance of the coils.

Figure 4.6 shows the variation in the load power delivered using the derived analytical model, for dc values of parasitic coil resistances and ac parasitic coil resistance values from the skin effect model. It is evident that the load power decreases as the parasitic resistance increases

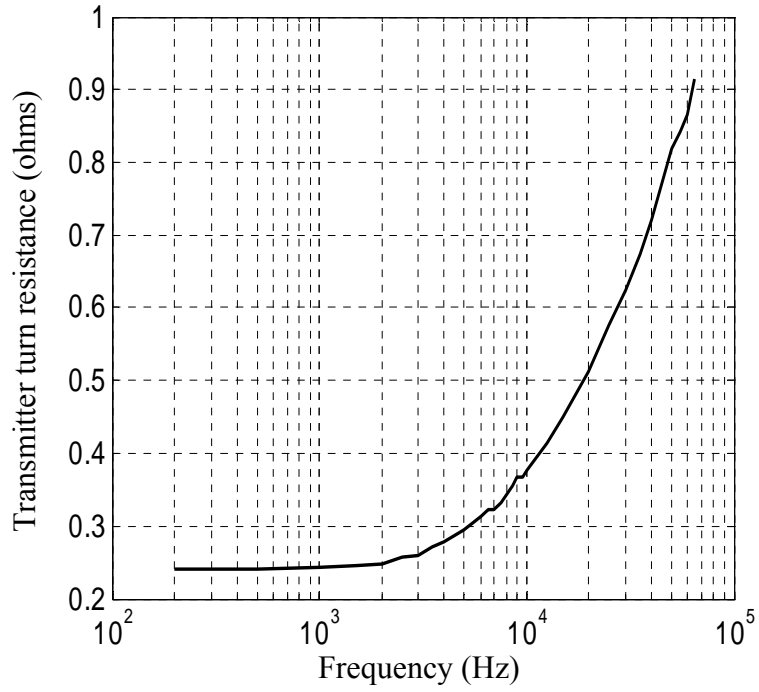


Figure 4.4: Variation in the transmitter coil resistance with frequency (skin/proximity effects).

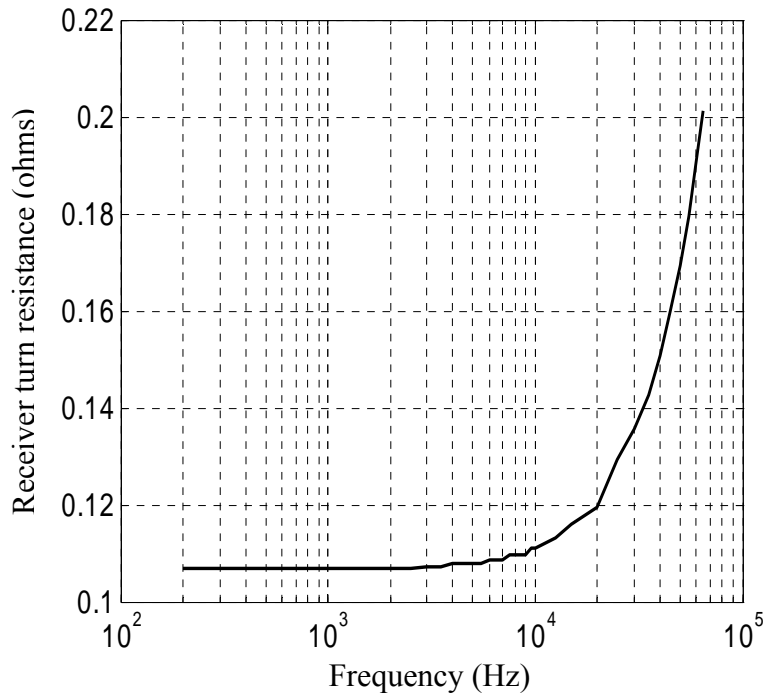


Figure 4.5: Variation in the receiver coil resistance with frequency (skin/proximity effects).

with frequency, confirming the previously plotted hypothetical situation in Fig. 4.3. Note that the resonance frequency ω_{0r} does not depend on the parasitic skin resistance value for this case. Figure 4.7 shows the variation in the link efficiency as a function of frequency for a series compensated transmitter and parallel compensated (C_{R+}) receiver circuit. It is evident from the figure that the efficiency decreases as the parasitic coil resistances increased.

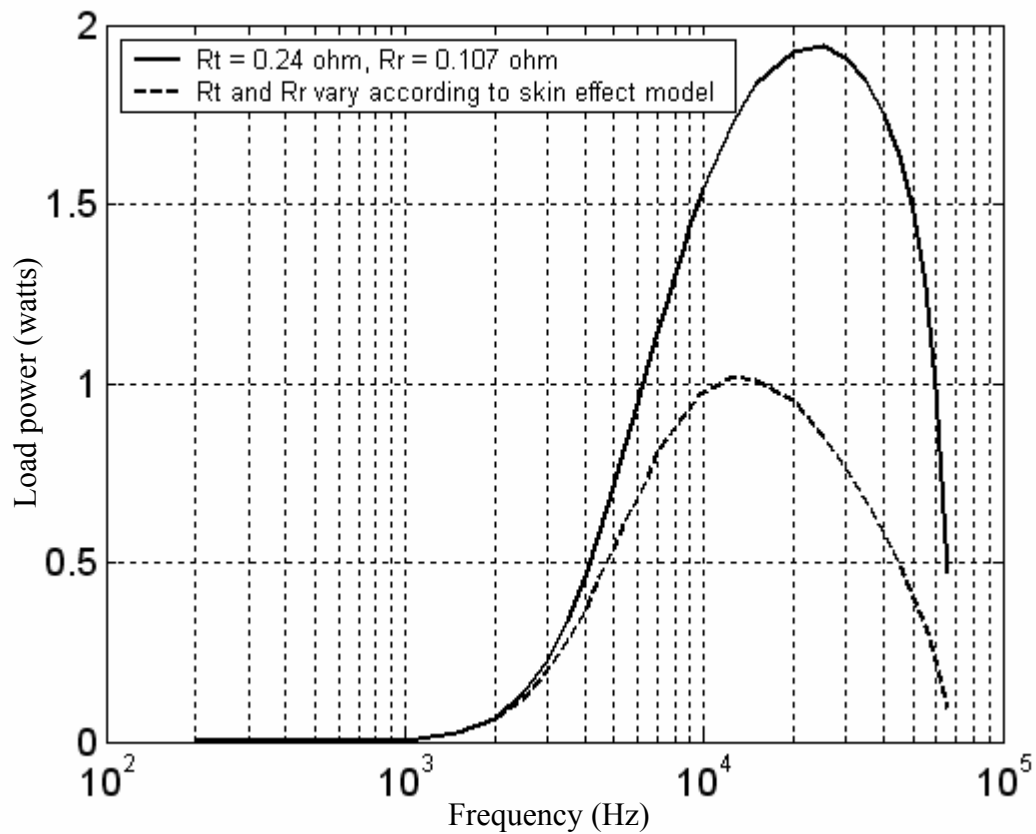


Figure 4.6: Load power delivered as a function of resonance frequency with and without using skin effect. $V_{IN} = 1.55$ V rms, $R_L = 35 \Omega$.

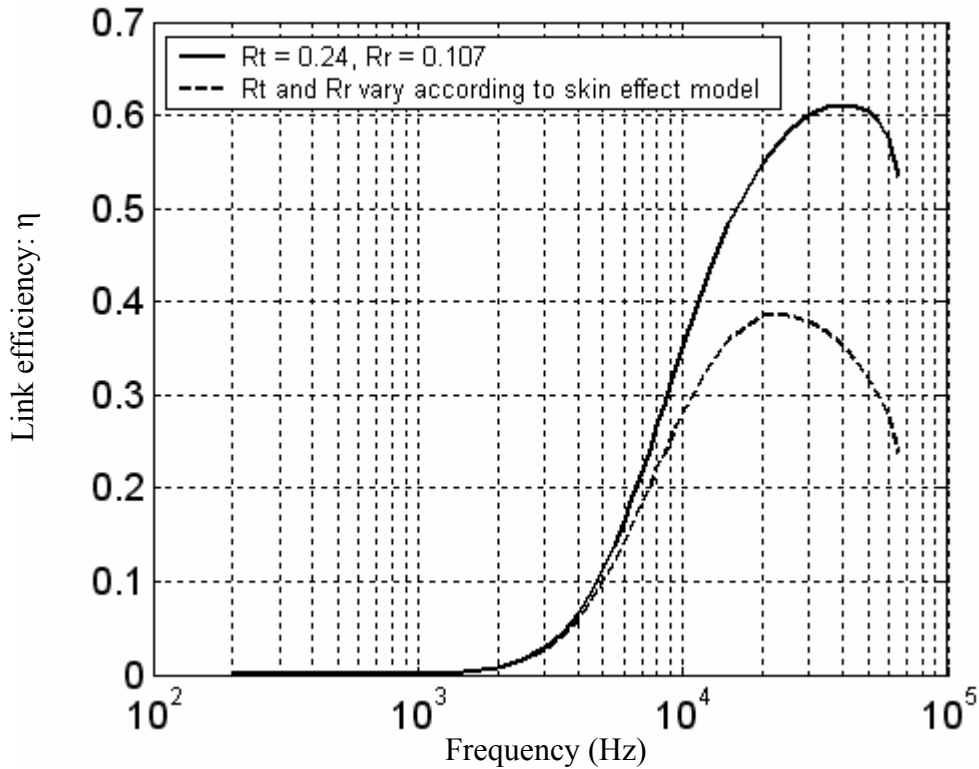


Figure 4.7: Link efficiency as a function of resonance frequency with and without using skin effect. $V_{IN} = 1.55$ V rms, $R_L = 35 \Omega$.

4.3 Results

Parasitic modeling employed in this work has resulted in the design of accurate series and parallel compensation capacitors for the transmitter and receiver coils thereby optimizing power delivery to the receiver coil. Simulation utilizing Matlab showed the maximum power delivery to occur near resonance frequency of 20 kHz. Test measurements on the coil concur with the design simulations. Figure 4.8 shows the variation in power delivery at 20 kHz and 40 kHz with coplanar radial displacement of the receiver coil axis with respect to the transmitter coil axis. Here, the receiver coil is moved inside the transmitter coil on a coplanar diametric line as shown in Fig. 4.9. The transmitter coil input voltage is $V_{IN} = 19.81$ V rms and $R_L = 65 \Omega$.

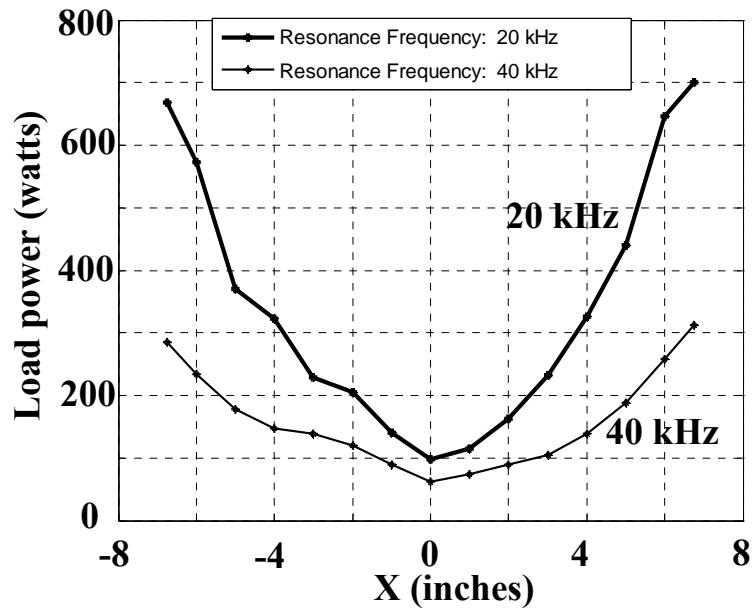


Figure 4.8: Power delivered to the load as a function of radial coplanar displacement X of the receiver coil axis with respect to the transmitter coil axis. $V_{IN} = 19.81$ V rms and $R_L = 65 \Omega$.

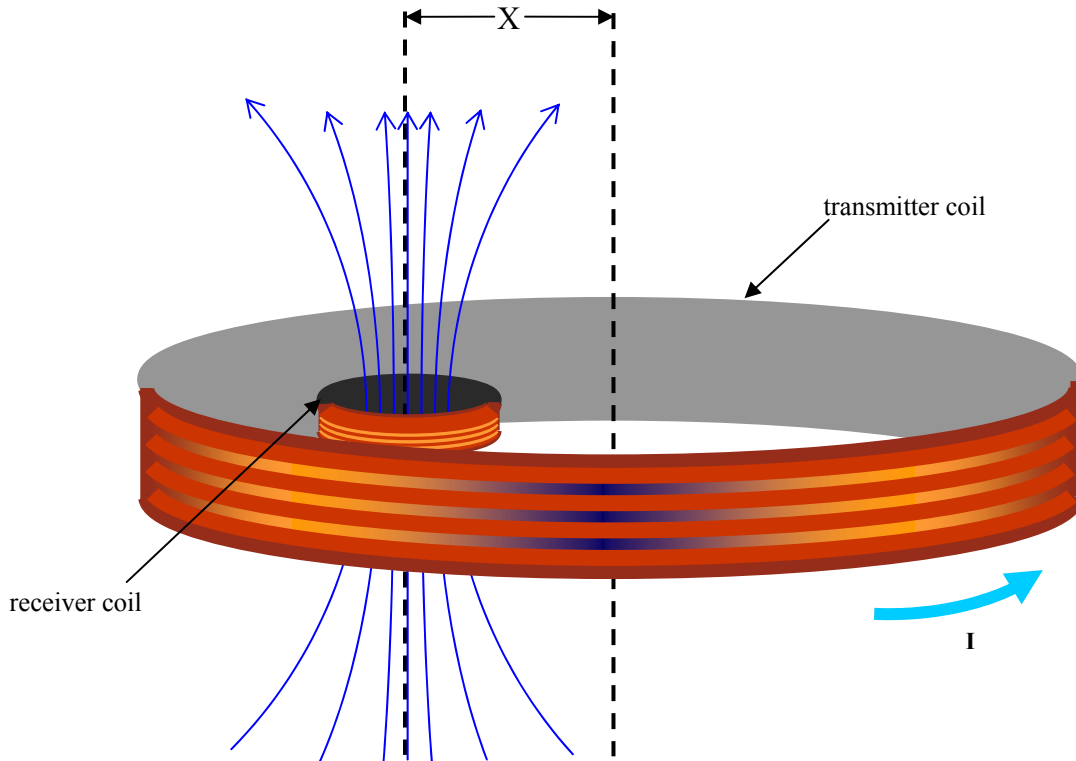


Figure 4.9: Schematic illustration of the radial coplanar displacement of the coil axes X .

Analytical model derived in section 3.3 is used in combination with the skin effect model to design the compensation capacitors to test the coils at 20 kHz and 40 kHz. Here, it is observed that the power delivered to the load increases as the receiver coil is moved diametrically towards the periphery of the transmitter coil. Table 4.1 gives the measured dc voltage and power obtained across a 65 Ω load resistance at various radial coplanar displacements of the coil axes at 20 kHz and 40 kHz for transmitter coil input voltage $V_{IN} = 19.81$ V rms. A maximum power of 1.33 W at 9.65 V and 137.5 mA was obtained for an input supply voltage of 17.67 V RMS, operating frequency of 20 kHz and a coplanar displacement of the receiver coil axis with respect to the transmitter coil axis of 7.5". The latter point is not indicated in Fig. 4.8.

Table 4.1: Variation in load voltage V_{dc} and load power P_{dc} with radial coplanar displacement X of the coil axes at 20 kHz and 40 kHz. $V_{IN} = 19.81$ V rms and $R_L = 65 \Omega$.

X (See Fig 4.9) (inches)	20 kHz		40kHz	
	V_{dc} (volts)	P_{dc} (milli watts)	V_{dc} (volts)	P_{dc} (milli watts)
6.75	6.75	700.96	4.5	311.54
6	6.48	646.01	4.1	258.62
5	5.35	440.35	3.5	188.46
4	4.60	325.54	3.0	138.46
3	3.88	231.61	2.6	104.00
2	3.25	162.50	2.4	88.62
1	2.73	114.66	2.2	74.46
0	2.53	98.48	2.0	61.54
-1	3.02	140.49	2.4	88.62
-2	3.65	204.96	2.8	120.62
-3	3.86	229.23	3.0	138.46
-4	4.58	322.72	3.1	147.85
-5	4.90	369.39	3.4	177.85
-6	6.10	572.47	3.9	234.00
-6.75	6.59	668.13	4.3	284.46

Figure 4.10 shows the overall circuit schematic used for Li-ion battery charging utilizing the RPDS. It consists of the lumped equivalent model for the transmitter and the receiver coils, a voltage doubler circuit and the battery charger circuitry. An operating frequency $f_0 = 20$ kHz and a radial coplanar displacement of the coil axes $X = 6$ inches were chosen for battery charging purposes. Calculated values for the transmitter and receiver coil parasitic capacitances are $C_{ST} = 47.63$ pF and $C_{SR} = 2.1$ pF respectively. The transmitter coil and receiver coil resistances as estimated by the skin and proximity effect model at 20 kHz are $R_T = 0.51 \Omega$ and $R_R = 0.119 \Omega$ respectively. The transmitter coil is series compensated with $C_T = 25.865$ nF and the receiver coil is parallel compensated with $C_R = 1.648$ μ F. Capacitor values for C_1 and C_2 are chosen to be 6 μ F each. The dc load voltage and power measured across a 65 Ω load for $V_{IN} = 19.81$ V rms are as given in Table 4.1. A 3.7 V nominal, 150 mAh polymer lithium-ion battery was charged in 50 minutes from an initial voltage of 3.48 V to 3.84 V. The battery charging period was 1 hour and 40 minutes from an initial voltage of 3.39 V to 4.12 V as per Fig. 4.11. Figure 4.11 gives the plot for battery voltage and charging current with time. This figure concurs with the actual technical specifications given in Appendix K.

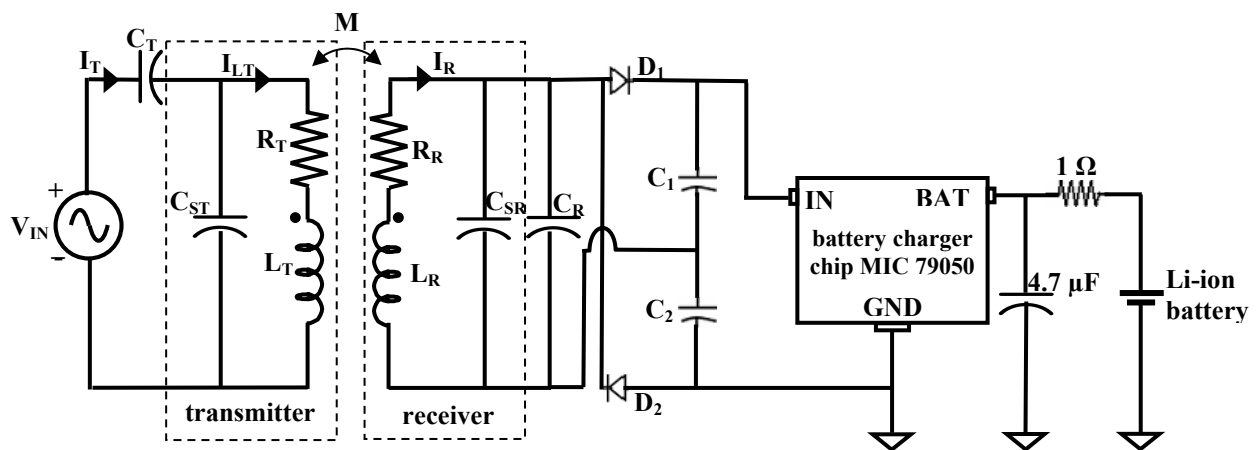


Figure 4.10: Circuit layout for the RPDS consisting of the lumped equivalent model, a voltage doubler circuit and a battery charger circuit. Transmitter coil is series compensated and receiver coil is parallel compensated.

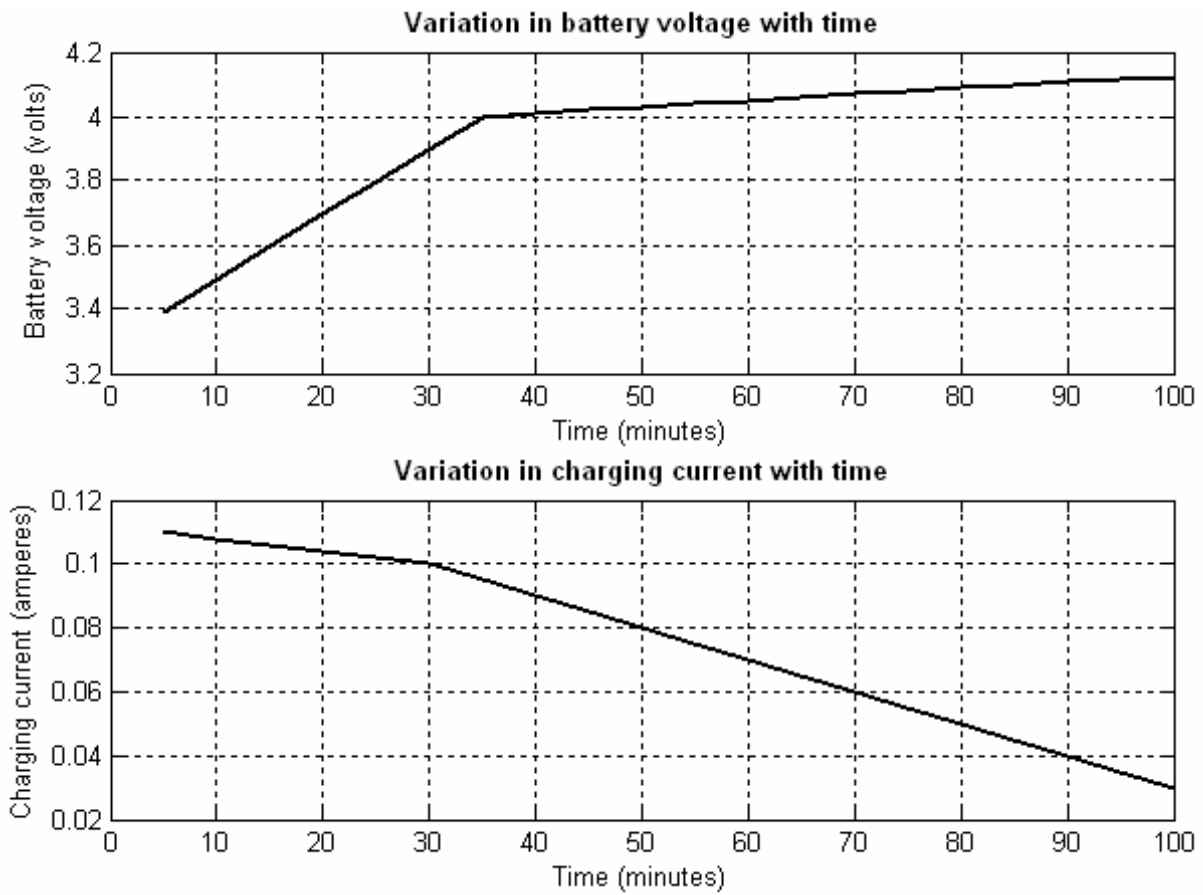


Figure 4.11: Variation in battery voltage and charging current with time. Resonance frequency of the coils is 20 kHz and radial coplanar displacement of the coil axes $X = 6$ inches.

CHAPTER 5

SUMMARY AND FUTURE WORK

5.1 Summary and Discussions

A remote power delivery system (RPDS) for a bio-implantable electrical stimulation system (BESS) has been successfully modeled and fabricated. This RPDS is a loosely coupled inductive system with very low link efficiency. A design process for the transmitter and the receiver coils has been described. Different models that simulate the variation in link efficiency with frequency have been analyzed. The use of a voltage doubling full wave rectifier and a battery charging chip (MIC 79050 from MICREL Inc.) are described. Load power delivery using an analytical model has been simulated. The importance of parasitic modeling at higher frequencies is realized. Parasitic modeling employed in this work has resulted in design of accurate series and parallel compensation capacitors for the transmitter and receiver coils thereby optimizing power delivery to the receiver coil. The variation in coil inductance, parasitic turn resistance and capacitance at higher frequencies may hinder total compensation. Optimization of the link efficiency is of primary importance in this loosely coupled inductive system. Simulation utilizing Matlab showed the maximum power delivery to occur near resonance frequency of 20 kHz. Test measurements on the coil concur with the design simulations. The charging chip specifications require a minimum voltage of 4.7 V dc and a current of 100 mA. This implies an effective load of 47Ω and load power of 470 mW. Considering other power losses, the design power was estimated to be 670 mW. The regulated output voltage of the battery charger chip is 4.2 volts at 100 mA. A maximum power of 1.33 W was obtained across a 65Ω load for an input supply voltage of 17.67 V RMS, resonance frequency of 20 kHz and a radial coplanar displacement of the coil axes $X = 7.5$ inches. This exceeds the design power value of 670 mW.

This may provide for flexibility in the choice of input supply voltage to the transmitter coil and/or choice of location for the bio-implanted receiver coil. A 3.7 V nominal, 150 mAh polymer lithium-ion battery was charged at an operating frequency $f_0 = 20$ kHz and a radial coplanar displacement of the coil axes $X = 6$ inches in 1 hour and 40 minutes from an initial voltage of 3.39 V to 4.12 V with an input voltage V_{IN} of 19.81 V rms. The remote power delivery system developed here can be utilized for a number of other bio-implantable devices, sensors and actuators. Actual measurements in implanted conditions have not been conducted in this project.

5.2 Future Work

There is need to further improve the coil high-frequency model specifically involving parasitic capacitance estimation for more accurately predicting the coil response at higher frequencies. A model to estimate linkage efficiency in finite size coplanar coils with radial-axial displacements needs to be developed. An electromagnetic simulation tool may be used for this purpose. Different coil sizes and positions can be experimented with. The use of a ferrite core in the receiver coil to increase the flux linkage is one possible option to induce higher voltages in the receiver circuit. Also, the coil driver efficiency and the rectifier efficiency have to be further analyzed.

REFERENCES

1. J. C. Schuder, J. H. Gold, and H. E. Stephenson Jr., "An Inductively Coupled RF System for the Transmission of 1 kW of power through the skin," *IEEE Trans. Biomed. Eng.*, vol. MNE-18, No. 4, pp. 265-273, July 1971.
2. W. H. Ko, S. P. Liang, and C. D. Fung, "Design of radio-frequency powered coils for implant instruments," *Med. & Biol. Eng. & Comput.*, vol. 15, pp. 634-640, 1977.
3. E. S. Hochmair, "System optimization for improved accuracy in Transcutaneous Signal and Power Transmission," *IEEE Trans. Biomed. Eng.*, vol. BME-31, No. 2, pp. 177-186, February 1984.
4. B. Smith, P. H. Peckham, M. W. Keith, and D. D. Roscoe, "An external powered, multichannel, implantable stimulator for versatile control of paralyzed muscle," *IEEE Trans. Biomed. Eng.*, vol. BME-34, No. 7, pp. 499-507, July 1987.
5. P. E. K. Donaldson, "Power for neurological prostheses: a simple inductive RF link with improved performance," *Journal of Biomedical Engineering*, Vol. 9, pp. 194-197, July 1986.
6. J. C. Schuder, and H. E. Stephenson, Jr., "Energy transport to a coil which circumscribes a ferrite core and is implanted within the body," *IEEE Trans. Biomed. Eng.*, vol. BME-12, Nos. 3 and 4, pp. 154-163, July/October 1965.
7. M. Soma, D. C. Galbraith, and R. L. White, "Radio-frequency coils in implantable devices: misalignment analysis and design procedure," *IEEE Trans. Biomed. Eng.*, vol. BME-34, No. 4, pp. 276-282, April 1987.
8. C. M. Zierhofer and E. S. Hochmair, "High efficiency coupling insensitive transcutaneous power and data transmission via an inductive link," *IEEE Trans. Biomed. Eng.*, vol. BME-37, No. 7, pp. 716-722, July 1990.
9. A. Ghahary, B. H. Cho, "Design of transcutaneous energy transmission system using a series resonant converter," *IEEE Trans. Power Electronics*, Vol. 7, No. 2, pp. 261-269, April 1992.

10. K. V. Schuylenbergh, and R. Puers, "Self tuning inductive powering for implantable telemetric monitoring systems," *8th International Conference on Solid-State Sensors and Actuators, and Eurosensors IX*, Stockholm, Sweden, pp. 55-58, June 25-29, 1995.
11. B. Ziaie, M. D. Nardin, A. R. Coghlan, and K. Najafi, "A single-channel implanted microstimulator for functional neuromuscular stimulator," *IEEE Trans. Biomed. Eng.*, vol. 44, No. 10, pp. 909-920, October 1997.
12. J. Hirai, T. W. Kim, A. Kawamura, "Study on intelligent battery charging using inductive transmission of power and information," *IEEE Trans. Power Electronics*, Vol. 15, No. 2, pp. 335-345, March 2000.
13. R. Puers, M. Catrysse, G. Vandevoorde, R. J. Collier, E. Louridas, F. Burny, M. Donkerwolcke, and F. Moulart, "A telemetry system for the detection of hip prosthesis loosening by vibration analysis," *Proceedings of the Eurosensors XIII*, Hague, Netherlands, pp. 757-760, 1999.
14. J. T. Boys, G. A. Covic and A. W. Green, "Stability and control of inductively coupled power transfer systems," *IEE Proc.-Electr. Power Appl.*, Vol. 147, No. 1, pp.37-43, January 2000.
15. J. Wu, V. Quinn and G. H. Bernstein, "A simple, wireless powering scheme for MEMS devices," *Proc. of SPIE*, pp. 43-52, Vol. 4559, 2001.
16. G. Vandevoorde and R. Puers "Wireless energy transfer for stand-alone systems: a comparison between low and high power applicability," *Sensors and Actuators A: Physical*, Vol. 92, pp. 305-311, August 2001.
17. O. H. Stielau and G. A. Covic, "Design of loosely coupled inductive power transfer systems," *Int. Conf. Power system Tech., Proc. Powercon 2000*, Vol. 1, pp. 85-90, 2000.
18. C. S. Wang, G. A. Covic and O. H. Stielau, "Power transfer capability and bifurcation phenomena of loosely coupled inductive power transfer systems," *IEEE Trans. Industrial Electronics*, Vol. 51, No. 1, pp. 148-157, February 2004.

19. C. S. Wang, G. A. Covic and O. H. Stielau, "Load models and their application in the design of loosely coupled inductive power transfer systems," *Int. Conf. Power system Tech., Proc. Powercon 2000*, Vol. 2, pp. 1053-1058, 2000.
20. W. Mokwa and U. Schnakenberg, "Micro-transponder systems for medical applications," *IEEE Trans. Inst. and Meas.*, Vol. 50, No. 6, pp. 1551-1555, December 2001.
21. MIT physics 8.02, "Electricity and Magnetism, Course Notes, Modules: Fields, Coulomb's law",
URL: <http://evangelion.mit.edu/802TEAL3D/visualizations/coursenotes/index.htm>
22. M. N. O. Sadiku, "Elements of Electromagnetics – Third Edition," *Oxford University Press*, pp. 104-107, 2001.
23. S. Kopparthi, "Remote power delivery and signal amplification for MEMS devices," M.S. thesis, Louisiana State University, 2003.
24. S. Kona, "Circuitry for a remotely powered bio-implantable gastric electrical stimulation system," M.S. thesis, Louisiana State University, 2003.
25. V. R. Gaddam, J. Yernagula, R. R. Anantha, S. Kona, S. Kopparthi, A. Chamakura, P. K. Ajmera and A. Srivastava, "Remote power delivery for hybrid integrated bio-implantable electrical stimulation system," *SPIE 12th Annual Int. Sym. on Smart Structures and Materials*, San Diego, California, U.S.A., March 07-10, 2005. in printing. F. Terman, "Radio engineers' handbook," *McGraw-Hill Book company, inc.*, ASIN: B0007DOWRW, pp. 60-82, 135-162, 1943.
26. J. Yernagula, "Contact effects in thermally evaporated pentacene thin films and aspects of microsystem hybrid integration," M.S. thesis, Louisiana State University, 2003.
27. F. Terman, "Radio engineers' handbook," *McGraw-Hill Book company, inc.*, ASIN: B0007DOWRW, pp. 60-82, 135-162, 1943.
28. F. W. Grover, "Inductance calculations: working formulas and tables," *The Instrumentation, Systems, and Automation Society*, ISBN: 0876645570, pp. 112-118, 1982.

29. K. Van Schuylenbergh, "Optimization of inductive powering of small biotelemetry implants," PhD dissertation, K. U. Leuven, pp. 47-51, 79-83, 1998.

30. http://www.micrel.com/_PDF/mic79050.pdf.

APPENDIX A

TABLE FOR VALUES OF Y_1 AND Y_2

Table A.1: Values of y_1 and y_2 for use in Eqn. (3.1). After reference [27].

Here $b \Rightarrow l$ (coil axial length), $c \Rightarrow t$ (coil radial thickness)

b/c or c/b	y_1	Differ- ence	c/b	y_2	Differ- ence	b/c	y_3	Differ- ence
0	0.5000	0.0253	0	0.125	0.002	0	0.597	0.002
0.025	0.5253	0.0237						
0.05	0.5490	0.0434	0.05	0.127	0.005	0.05	0.599	0.003
0.10	0.5924	0.0386	0.10	0.132	0.010	0.10	0.602	0.006
0.15	0.6310	0.0342	0.15	0.142	0.013	0.15	0.608	0.007
0.20	0.6652	0.0301	0.20	0.155	0.016	0.20	0.615	0.009
0.25	0.6953	0.0266	0.25	0.171	0.020	0.25	0.624	0.009
0.30	0.7217	0.0230	0.30	0.192	0.023	0.30	0.633	0.010
0.35	0.7447	0.0198	0.35	0.215	0.027	0.35	0.643	0.011
0.40	0.7645	0.0171	0.40	0.242	0.031	0.40	0.654	0.011
0.45	0.7816	0.0144	0.45	0.273	0.034	0.45	0.665	0.012
0.50	0.7960	0.0121	0.50	0.307	0.037	0.50	0.667	0.013
0.55	0.8081	0.0101	0.55	0.344	0.040	0.55	0.690	0.012
0.60	0.8182	0.0083	0.60	0.384	0.043	0.60	0.702	0.013
0.65	0.8265	0.0066	0.65	0.427	0.047	0.65	0.715	0.014
0.70	0.8331	0.0052	0.70	0.474	0.049	0.70	0.729	0.013
0.75	0.8383	0.0039	0.75	0.523	0.053	0.75	0.742	0.014
0.80	0.8422	0.0029	0.80	0.576	0.056	0.80	0.756	0.015
0.85	0.8451	0.0019	0.85	0.632	0.059	0.85	0.771	0.015
0.90	0.8470	0.0010	0.90	0.690	0.062	0.90	0.786	0.015
0.95	0.8480	0.0003	0.95	0.752	0.064	0.95	0.801	0.015
1.00	0.8483	1.00	0.816	1.00	0.816	

APPENDIX B

LINK EFFICIENCY FOR THE UNCOMPENSATED CASE

Figure B.1 shows an equivalent representation for an inductively coupled circuit. The alternating current flowing in the transmitter coil due to the voltage applied to this circuit, produces magnetic flux that induces a voltage in the coupled receiver coil. Here, the effect of the coupled receiver coil on the transmitter circuit is as if an impedance has been added in series with it (Fig. B.2). Also, the receiver coil current is the current that would flow if the induced voltage from the transmitter circuit were applied in series with the receiver circuit and if the transmitter circuit were absent [27].

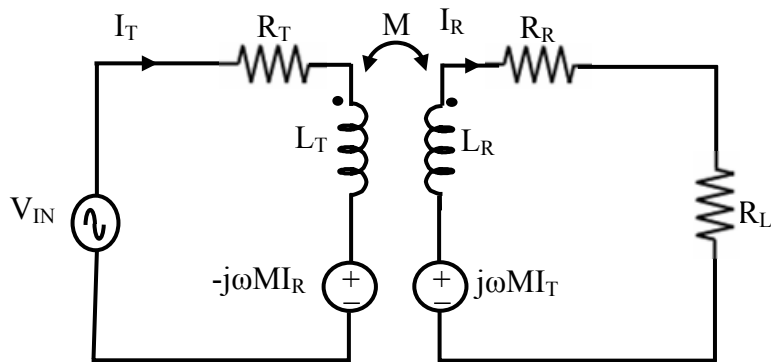


Figure B.1: Inductively coupled circuit with equivalent transmitter and receiver circuits.

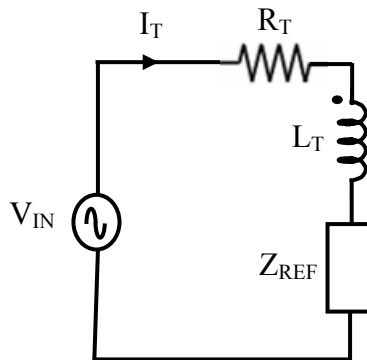


Figure B.2: Equivalent transmitter circuit.

The link efficiency of an uncompensated transmitter and receiver coil system is calculated as the product of the individual transmitter coil and receiver coil efficiencies. Applying KVL to the transmitter circuit we get:

$$V_{IN} - I_T(R_T + j\omega L_T) + j\omega MI_R = 0. \quad (B1)$$

Applying KVL to the receiver coil circuit we get:

$$-j\omega MI_T + [j\omega L_R + R_R + R_L]I_R = 0. \quad (B2)$$

Here, I_T and I_R are the transmitter circuit and the receiver circuit currents respectively. L_T and L_R are the self inductance values for the transmitter and the receiver coils respectively, R_T and R_R are the parasitic turn resistances of L_T and L_R respectively, ω is angular frequency and R_L is the load resistance.

The receiver circuit impedance Z_{REC} is given by: $Z_{REC} = (R_R + R_L) + j\omega L_R$. From Eqn. B2 we get:

$$I_R = \frac{j\omega MI_T}{j\omega L_R + R_R + R_L} \quad (B3)$$

$$\text{or } I_R = \frac{\omega^2 MI_T L_R}{(R_R + R_L)^2 + \omega^2 L_R^2} + j \frac{\omega MI_T (R_R + R_L)}{(R_R + R_L)^2 + \omega^2 L_R^2}.$$

Substituting Eqn. (B3) in Eqn. (B1) we get: $V_{IN} - I_T(R_T + j\omega L_T) + j\omega M \left(\frac{j\omega MI_T}{j\omega L_R + R_R + R_L} \right) = 0$.

$$V_{IN} - I_T \left(R_T + j\omega L_T + \frac{\omega^2 M^2}{j\omega L_R + R_R + R_L} \right) = 0. \quad \text{i.e.} \quad V_{IN} - I_T (R_T + j\omega L_T + Z_{REF}) = 0. \quad \text{Here,}$$

$Z_{REF} = \frac{\omega^2 M^2}{j\omega L_R + R_R + R_L}$ is the reflected impedance of the receiver circuit into the transmitter

circuit. On further simplification, $Z_{REF} = \frac{\omega^2 M^2 (R_R + R_L)}{(R_R + R_L)^2 + \omega^2 L_R^2} + j \left[\frac{-\omega^3 M^2 L_R}{(R_R + R_L)^2 + \omega^2 L_R^2} \right]$.

Here, $R_{REF} = \frac{\omega^2 M^2 (R_R + R_L)}{(R_R + R_L)^2 + \omega^2 L_R^2}$ and $X_{REF} = \frac{-\omega^3 M^2 L_R}{(R_R + R_L)^2 + \omega^2 L_R^2}$. Here R_{REF} and X_{REF} are the

reflected resistance and reactance of the receiver circuit into the transmitter circuit.

The link efficiency η for the transmitter coil and receiver coil can be obtained as

$\eta = \eta_T \times \eta_R$. Here, η_T and η_R are the transmitter coil and receiver coil efficiencies respectively.

Here, $\eta_T = \frac{\text{Power delivered to the receiver circuit}}{\text{Total power handled by the transmitter circuit}}$ and

$\eta_R = \frac{\text{Power delivered to the load}}{\text{Total power handled by the receiver circuit}}$.

Therefore, $\eta_T = \frac{I_T^2 R_{REF}}{I_T^2 (R_T + R_{REF})} = \frac{R_{REF}}{R_T + R_{REF}}$ and $\eta_R = \frac{I_R^2 R_L}{I_R^2 (R_R + R_L)} = \frac{R_L}{R_R + R_L}$.

$\eta = \eta_T \times \eta_R = \frac{R_{REF} R_L}{(R_T + R_{REF})(R_R + R_L)}$. Substituting the expressions for R_{REF} into the above

equation, and, since we already know that $\eta = \eta_T \times \eta_R$, we obtain

$\eta = \frac{\omega^2 M^2 R_L}{R_T [(R_R + R_L)^2 + \omega^2 L_R^2] + \omega^2 M^2 (R_R + R_L)}$. Parasitic capacitors for the transmitter and the

receiver coils have not been considered in this model for simplicity.

APPENDIX C

MATLAB CODE FOR THE UNCOMPENSATED CASE

Matlab code to generate a plot for the variation in link efficiency with operating frequency is produced here. This same code is used to generate the semi log scale plot and also its logarithmic inset shown in Fig. 3.4.

```
% Plot for link efficiency for the uncompensated case.

% clc
% clear all
% close all
format long

% Design values
Rt = 0.25;
Rr = 0.107;
Lt=2.5*10-3;
Lr=39*10-6;
M=4.7960*10-6;
Ro=32.5;

% Frequency setting
f = [200 500 1.0E+03 1.5E+03 2.0E+03 2.5E+03 3.0E+03 3.5E+03 4.0E+03 4.50E+03
5.0E+03 5.5E+03 6.0E+03 6.5E+03 7.0E+03 7.5E+03 8.0E+03 8.5E+03 9.0E+03 9.5E+03
10.0E+03 12.5E+03 15.0E+03 2.0E+04 2.5E+04 3.0E+04 3.5E+04 4.0E+04 4.5E+04 5.0E+04
5.5E+04 6.0E+04 6.5E+04];
w = 2*pi*f

% Link efficiency
n = (w.^2*M^2*Ro)./(Rt.*((Rr+Ro).^2+(w.^2.*Lr.^2))+((w.^2*M^2).*(Ro+Rr)))

% Plot (semilog scale)
semilogx(f,n);
grid on
hold on

% % Plot (log scale)
% loglog(f,n);
% grid on
% hold on
```

APPENDIX D

LINK EFFICIENCY FOR THE COMPENSATED CASE

As explained in section 3.2, coil compensation can be defined as the addition of a capacitor in either series or in parallel to the coil circuit. In the case of the RPDS that is designed here, series compensation has been chosen for the transmitter circuit and a choice has to be made between series or parallel compensation for the receiver circuit. Analytical models for transmitter coil compensation in series and receiver coil compensation in both series and parallel will be developed for comparison purposes.

Transmitter coil series compensation and receiver coil series compensation

Figure D.1 shows an inductively coupled circuit with equivalent transmitter and receiver circuits. Parasitic capacitors for the transmitter and the receiver coils have not been considered in this model for simplicity. Here both the transmitter and the receiver circuits have been compensated in series with capacitors C_T and C_R respectively.

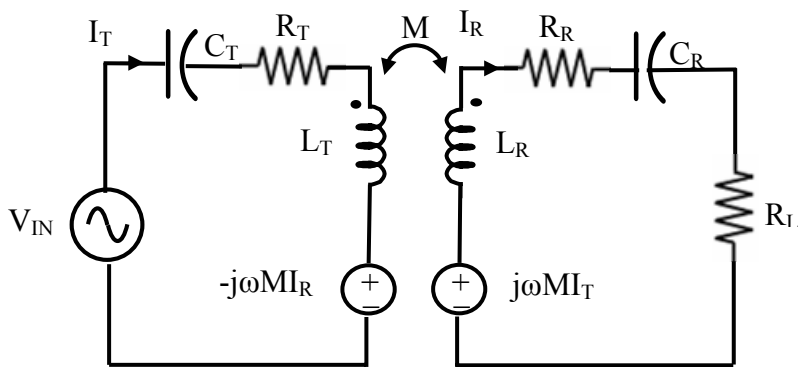


Figure D.1: Inductively coupled circuit with equivalent series compensated transmitter and receiver circuits.

The link efficiency of a compensated transmitter and receiver coil system is calculated as the product of the individual transmitter coil and receiver coil efficiencies.

Applying KVL to the transmitter circuit:

$$V_{IN} - I_T \left(R_T + j\omega L_T + \frac{1}{j\omega C_T} \right) + j\omega M I_R = 0. \quad (D1)$$

Applying KVL to the receiver coil circuit:

$$j\omega M I_T - \left[j\omega L_R + R_R + \frac{1}{j\omega C_R} + R_L \right] I_R = 0. \quad (D2)$$

Here, I_T and I_R are the transmitter circuit and the receiver circuit currents respectively. L_T and L_R are the self inductance values for the transmitter and the receiver coils respectively, R_T and R_R are the parasitic turn resistances of L_T and L_R respectively, ω is angular frequency and R_L is the load resistance. The receiver circuit impedance is given by: $Z_{REC} = (R_R + R_L) + j \left(\omega L_R - \frac{1}{\omega C_R} \right)$.

From Eqn. D2 we get:

$$I_R = \frac{j\omega M I_T}{(R_R + R_L) + j \left(\omega L_R - \frac{1}{\omega C_R} \right)}. \quad (D3)$$

Substituting Eqn. (D3) back in Eqn. (D1) we get:

$$V_{IN} - I_T \left(R_T + j\omega L_T + \frac{1}{j\omega C_T} \right) + j\omega M \left(\frac{j\omega M I_T}{(R_R + R_L) + j \left(\omega L_R - \frac{1}{\omega C_R} \right)} \right) = 0.$$

$$V_{IN} - I_T \left(R_T + j\omega L_T + \frac{1}{j\omega C_T} + \frac{\omega^2 M^2}{(R_R + R_L) + j \left(\omega L_R - \frac{1}{\omega C_R} \right)} \right) = 0.$$

$$V_{IN} - I_T \left(R_T + j\omega L_T + \frac{1}{j\omega C_T} + Z_{REF} \right) = 0. \quad \text{Here, } Z_{REF} = \frac{\omega^2 M^2}{(R_R + R_L) + j \left(\omega L_R - \frac{1}{\omega C_R} \right)} \quad \text{is the}$$

reflected impedance of the receiver circuit into the transmitter circuit. On further simplification,

$$Z_{REF} = \frac{\omega^2 M^2 (R_R + R_L)}{(R_R + R_L)^2 + \left(\omega L_R - \frac{1}{\omega C_R} \right)^2} + j \left[\frac{-\omega^2 M^2 \left(\omega L_R - \frac{1}{\omega C_R} \right)}{(R_R + R_L)^2 + \left(\omega L_R - \frac{1}{\omega C_R} \right)^2} \right].$$

$$\text{Here, } R_{REF} = \frac{\omega^2 M^2 (R_R + R_L)}{(R_R + R_L)^2 + \left(\omega L_R - \frac{1}{\omega C_R} \right)^2} \quad \text{and } X_{REF} = \frac{-\omega^2 M^2 \left(\omega L_R - \frac{1}{\omega C_R} \right)}{(R_R + R_L)^2 + \left(\omega L_R - \frac{1}{\omega C_R} \right)^2} \quad \text{are the}$$

reflected resistance and reactance of the receiver circuit into the transmitter circuit. Also, the resonance frequency ω_{or} of the receiver coil can be obtained by equating $X_{REC} = 0$ or $X_{REF} = 0$.

In either case we obtain $\omega_{or} = \frac{1}{\sqrt{L_R C_R}}$. When $\omega = \omega_{or}$, $Z_{REF} = R_{REF}$

$$= \frac{\omega_{or}^2 M^2}{(R_R + R_L)} = \frac{M^2}{L_R C_R (R_R + R_L)}. \quad C_T \text{ and } C_R \text{ are chosen such that both transmitter and receiver}$$

coils resonate at the same operating frequency $\omega_0 = \omega_{or} = \omega_{or}$. While conducting test

measurements on the coil, first an operating frequency is chosen and then the value of C_R is

calculated from the above equation for receiver coil resonance from $C_R = \frac{1}{\omega_0^2 L_R}$. The value of

C_T is calculated by choosing the same resonance frequency for the transmitter coil and equating

the transmitter coil reactance to zero. The transmitter coil impedance is given by

$$Z_{TRA} = R_T + j\omega L_T + \frac{1}{j\omega C_T} + Z_{REF}. \quad \text{Now, to calculate } C_T, \quad \omega_0 L_T - \frac{1}{\omega_0 C_T} = 0 \quad \text{or } C_T = \frac{1}{\omega_0^2 L_T}.$$

The link efficiency η for the transmitter coil and receiver coil can be obtained as $\eta = \eta_T \times \eta_R$. Here, η_T and η_R are the transmitter coil and receiver coil efficiencies

respectively. Where, $\eta_T = \frac{\text{Power delivered to the receiver circuit}}{\text{Total power handled by the transmitter circuit}}$ and

$$\eta_R = \frac{\text{Power delivered to the load}}{\text{Total power handled by the receiver circuit}}.$$

$$\eta_T = \frac{I_T^2 R_{REF}}{I_T^2 (R_T + R_{REF})} = \frac{R_{REF}}{R_T + R_{REF}} = \frac{\omega_0^2 M^2 (R_R + R_L)}{\omega_0^2 M^2 (R_R + R_L) + R_T \left[(R_R + R_L)^2 + \left(\omega_0 L_R - \frac{1}{\omega_0 C_R} \right)^2 \right]}.$$

$$\eta_R = \frac{I_R^2 R_L}{I_R^2 (R_R + R_L)} = \frac{R_L}{R_R + R_L}. \text{ Hence, } \eta = \frac{\omega_0^2 M^2 R_L}{R_T \left[(R_R + R_L)^2 + \left(\omega_0 L_R - \frac{1}{\omega_0 C_R} \right)^2 \right] + \omega_0^2 M^2 (R_R + R_L)}$$

$$\text{or } \eta = \frac{M^2 R_L}{(R_R + R_L) \left[R_T L_R C_R (R_R + R_L) + M^2 \right]} \text{ since } \omega_0^2 = \frac{1}{L_R C_R}.$$

Transmitter coil series compensation and receiver coil parallel compensation

Figure D.2 shows an inductively coupled circuit with equivalent transmitter and receiver circuits. Here the transmitter circuit has been compensated in series while the receiver circuit is compensated in parallel with capacitors C_T and C_R respectively. Parasitic capacitors for the transmitter and the receiver coils have been neglected in this model for simplicity. The link efficiency of a compensated transmitter and receiver coil system is calculated as the product of the individual transmitter coil and receiver coil efficiencies.

Applying KVL to the transmitter circuit:

$$V_{IN} - I_T \left(R_T + j\omega L_T + \frac{1}{j\omega C_T} \right) + j\omega M I_R = 0. \quad (D4)$$

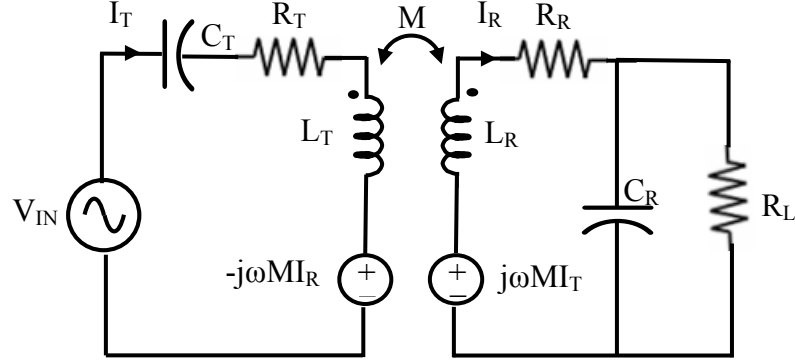


Figure D.2: Inductively coupled circuit with equivalent series compensated transmitter and parallel compensated receiver circuits.

Applying KVL to the receiver coil circuit:

$$j\omega M I_T - \left[j\omega L_R + R_R + \frac{R_L}{1 + j\omega C_R R_L} \right] I_R = 0. \quad (\text{D5})$$

Here the receiver circuit impedance is given by: $Z_{REC} = j\omega L_R + R_R + \frac{R_L}{1 + j\omega C_R R_L}$. On further

$$\text{simplification, } Z_{REC} = \frac{R_R + R_L + \omega^2 R_R C_R^2 R_L^2}{1 + \omega^2 C_R^2 R_L^2} + j \left[\frac{\omega L_R - \omega C_R R_L^2 + \omega^3 L_R C_R^2 R_L^2}{1 + \omega^2 C_R^2 R_L^2} \right].$$

Here, $R_{REC} = \frac{R_R + R_L + \omega^2 R_R C_R^2 R_L^2}{1 + \omega^2 C_R^2 R_L^2}$ and $X_{REC} = \frac{\omega L_R - \omega C_R R_L^2 + \omega^3 L_R C_R^2 R_L^2}{1 + \omega^2 C_R^2 R_L^2}$ are the

receiver circuit resistance and reactance respectively. From Eqn. D5 we get:

$$I_R = \frac{j\omega M I_T}{\left[j\omega L_R + R_R + \frac{R_L}{1 + j\omega C_R R_L} \right]}. \quad (\text{D6})$$

Substituting Eqn. (D6) in Eqn. (D4) we get:

$$V_{IN} - I_T \left(R_T + j\omega L_T + \frac{1}{j\omega C_T} \right) + j\omega M \left(\frac{j\omega M I_T}{j\omega L_R + R_R + \frac{R_L}{1 + j\omega C_R R_L}} \right) = 0 \text{ gives}$$

$$V_{IN} - I_T \left(R_T + j\omega L_T + \frac{1}{j\omega C_T} + \frac{\omega^2 M^2}{j\omega L_R + R_R + \frac{R_L}{1 + j\omega C_R R_L}} \right) = 0, \text{ or}$$

$$V_{IN} - I_T \left(R_T + j\omega L_T + \frac{1}{j\omega C_T} + Z_{REF} \right) = 0.$$

Here, $Z_{REF} = \frac{\omega^2 M^2}{j\omega L_R + R_R + \frac{R_L}{1 + j\omega C_R R_L}}$ is the reflected impedance of the receiver circuit into

the transmitter circuit. On further simplification,

$$Z_{REF} = \frac{\omega^2 M^2 (\omega^2 R_R C_R^2 R_L^2 + R_R + R_L)}{(R_R + R_L - \omega^2 L_R C_R R_L)^2 + (\omega L_R + \omega R_R C_R R_L)^2} + j \left[\frac{\omega^2 M^2 (\omega C_R R_L^2 - \omega^3 L_R C_R^2 R_L^2 - \omega L_R)}{(R_R + R_L - \omega^2 L_R C_R R_L)^2 + (\omega L_R + \omega R_R C_R R_L)^2} \right].$$

Here, $R_{REF} = \frac{\omega^2 M^2 (\omega^2 R_R C_R^2 R_L^2 + R_R + R_L)}{(R_R + R_L - \omega^2 L_R C_R R_L)^2 + (\omega L_R + \omega R_R C_R R_L)^2}$ and

$X_{REF} = \frac{\omega^2 M^2 (\omega C_R R_L^2 - \omega^3 L_R C_R^2 R_L^2 - \omega L_R)}{(R_R + R_L - \omega^2 L_R C_R R_L)^2 + (\omega L_R + \omega R_R C_R R_L)^2}$ are the reflected resistance and reactance

of the receiver circuit into the transmitter circuit. The resonance frequency ω_{or} of the receiver coil can be obtained by equating $X_{REF} = 0$ or $X_{REF} = 0$. In either case we obtain

$\omega_{or} = \sqrt{\frac{C_R R_L^2 - L_R}{L_R C_R^2 R_L^2}}$. When, $\omega = \omega_{or}$ then $Z_{REF} = R_{REF}$. Compensation capacitors C_T and C_R are

chosen such that both transmitter and receiver coils resonate at the same operating frequency $\omega_0 = \omega_{or} = \omega_{ot}$. While conducting test measurements on the coil, for an operating frequency, the value of C_R is calculated from the above equation for receiver coil resonance. We

obtain $C_R = \frac{R_L \pm \sqrt{R_L^2 - 4\omega_0^2 L_R^2}}{2\omega_0^2 L_R R_L}$. In order to limit C_R to physically reliable values,

$$R_L^2 - 4\omega_0^2 L_R^2 \geq 0 \text{ or}$$

$$\omega_0 \leq \frac{R_L}{2L_R}. \quad (\text{D7})$$

The value of C_T is calculated as in the previous case and $C_T = \frac{1}{\omega_0^2 L_T}$.

The link efficiency η for the transmitter coil and receiver coil can be obtained as $\eta = \eta_T \times \eta_R$.

Here, η_T and η_R are the transmitter coil and receiver coil efficiencies respectively.

$$\text{As before, } \eta_T = \frac{I_T^2 R_{REF}}{I_T^2 (R_T + R_{REF})} = \frac{R_{REF}}{R_T + R_{REF}} \text{ or}$$

$$\eta_T = \frac{\omega_0^2 M^2 (\omega_0^2 R_R C_R^2 R_L^2 + R_R + R_L)}{\omega_0^2 M^2 (\omega_0^2 R_R C_R^2 R_L^2 + R_R + R_L) + R_T \left[(R_R + R_L - \omega_0^2 L_R C_R R_L)^2 + (\omega_0 L_R + \omega_0 R_R C_R R_L)^2 \right]}$$

$$\text{and } \eta_R = \frac{I_R^2 \operatorname{Re} \left[\frac{R_L}{1 + j\omega C_R R_L} \right]}{I_R^2 \operatorname{Re} \left[j\omega L_R + R_R + \frac{R_L}{1 + j\omega C_R R_L} \right]}. \text{ Since } \omega = \omega_0,$$

$$\operatorname{Re} \left[j\omega L_R + R_R + \frac{R_L}{1 + j\omega C_R R_L} \right] = \frac{R_R + R_L + \omega_0^2 R_R C_R^2 R_L^2}{1 + \omega_0^2 C_R^2 R_L^2} \text{ and } \eta_R = \frac{R_L}{R_R + R_L + \omega_0^2 R_R C_R^2 R_L^2}.$$

$$\text{Now, } \eta = \frac{\omega_0^2 M^2 R_L}{R_T \left\{ (R_R + R_L - \omega_0^2 L_R C_R R_L)^2 + (\omega_0 L_R + \omega_0 R_R C_R R_L)^2 \right\} + \omega_0^2 M^2 (R_R + R_L + \omega_0^2 R_R C_R^2 R_L^2)} \text{ or}$$

$$\eta = \frac{M^2 R_L}{R_T \left\{ \frac{L_R (L_R + R_R C_R R_L)^2}{(C_R R_L^2 - L_R)} + (L_R + R_R C_R R_L)^2 \right\} + M^2 \left\{ \frac{(R_R + R_L) L_R + (C_R R_L^2 - L_R) R_R}{L_R} \right\}}$$

APPENDIX E

MATLAB CODE FOR THE COMPENSATED CASE

Matlab code to generate plots for variation in link efficiency as a function of operating frequency in semi-log and logarithmic scales. Here, series compensation has been chosen for the transmitter circuit and a comparison is made between series and parallel (C_{R-} and C_{R+}) compensation for the receiver circuit.

```
% Plot for link efficiency with receiver coil series and parallel (Cr- and Cr+)
compensation.

% clc
% clear all
% close all
format long

% Design values
Rt = 0.25;
Rr = 0.107;
Lt=2.5*10^-3;
Lr=39*10^-6;
M=4.7960*10^-6;
Ro=32.5;

% Frequency setting
f = [200 500 1.0E+03 1.5E+03 2.0E+03 2.5E+03 3.0E+03 3.5E+03 4.0E+03 4.50E+03
5.0E+03 5.5E+03 6.0E+03 6.5E+03 7.0E+03 7.5E+03 8.0E+03 8.5E+03 9.0E+03 9.5E+03
10.0E+03 12.5E+03 15.0E+03 2.0E+04 2.5E+04 3.0E+04 3.5E+04 4.0E+04 4.5E+04 5.0E+04
5.5E+04 6.0E+04 6.5E+04];
w = 2*pi*f

% Receiver circuit series/parallel compensation capacitance values
% parallel
Cr = (Ro^2-(Ro^4-(4*(w*Ro*Lr).^2)).^0.5)./(2*(w*Ro).^2*Lr)
% series
Crser = 1./(w.^2*Lr)

% Link efficiency
% parallel
ncomp = (w.^2*M^2*Ro)./(Rt.*((Rr+Ro-
w.^2.*Lr.*Cr*Ro).^2+(w.*Lr+w.*Rr.*Cr*Ro).^2)+((w.^2*M^2).*(Ro+Rr+w.^2.*Rr.*Cr.^2*Ro^2)))
% series
ncompser = (w.^2*M^2*Ro)./(Rt.*((Rr+Ro)^2+(w*Lr-1./(w.*Crser)).^2)+((w.^2*M^2)*(Ro+Rr)))

% Plot (semilog scale)
semilogx(f,ncomp);
hold on
```

```
semilogx(f,ncompser);  
grid on  
hold on  
  
% % Plot (log scale)  
% loglog(f,ncomp);  
% hold on  
% loglog(f,ncompser);  
% grid on  
% hold on
```

APPENDIX F

LINK EFFICIENCY FOR THE COMPENSATED CASE – CONSIDERING COIL PARASITIC CAPACITANCES

Figure F.1 shows an inductively coupled circuit with equivalent transmitter and receiver circuits. Here, the transmitter circuit has been compensated in series and the receiver circuit in parallel with capacitors C_T and C_R respectively, C_{ST} and C_{SR} are the transmitter coil and the receiver coil parasitic capacitances respectively and $C_{RE} = C_{SR} + C_R$.

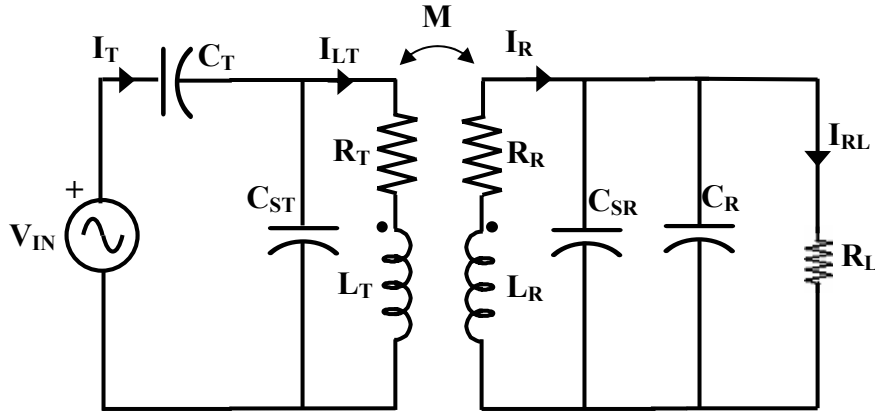


Figure F.1: Inductively coupled circuit with series compensated transmitter and parallel compensated receiver coils.

The link efficiency of a compensated transmitter and receiver coil system is calculated as the product of the individual transmitter coil and receiver coil efficiencies.

Applying KVL to the transmitter circuit:

$$V_{IN} - \frac{I_T}{j\omega C_T} - I_{LT}(R_T + j\omega L_T) + j\omega M I_R = 0 \quad (F1)$$

$$\text{and } \frac{(I_T - I_{LT})}{j\omega C_{ST}} - I_{LT}(R_T + j\omega L_T) + j\omega M I_R = 0 \quad (F2)$$

From Eqns. (F1) and (F2),

$$-V_{IN} + \frac{I_T}{j\omega C_T} = -\frac{I_T}{j\omega C_{ST}} + \frac{I_{LT}}{j\omega C_{ST}},$$

$$\text{or } I_{LT} = I_T \left[1 + \frac{C_{ST}}{C_T} \right] - V_{IN} (j\omega C_{ST}). \quad (\text{F3})$$

Applying KVL to the receiver circuit:

$$j\omega M I_{LT} - I_R \left(j\omega L_R + R_R + \frac{R_L}{1 + j\omega C_R R_L} \right) = 0, \quad (\text{F4})$$

$$\text{or } I_R = \frac{j\omega M I_{LT}}{j\omega L_R + R_R + \left(\frac{R_L}{1 + j\omega C_R R_L} \right)}. \quad (\text{F5})$$

Here the receiver circuit impedance is given by $Z_{REC} = j\omega L_R + R_R + \frac{R_L}{1 + j\omega C_{RE} R_L}$. This is

similar to the parallel compensation case in Appendix D but with C_R now replaced by C_{RE} . On

further simplification, $Z_{REC} = \frac{R_R + R_L + \omega^2 R_R C_{RE}^2 R_L^2}{1 + \omega^2 C_{RE}^2 R_L^2} + j \left[\frac{\omega L_R - \omega C_{RE} R_L^2 + \omega^3 L_R C_{RE}^2 R_L^2}{1 + \omega^2 C_{RE}^2 R_L^2} \right]$. Here,

$R_{REC} = \frac{R_R + R_L + \omega^2 R_R C_{RE}^2 R_L^2}{1 + \omega^2 C_{RE}^2 R_L^2}$ and $X_{REC} = \frac{\omega L_R - \omega C_{RE} R_L^2 + \omega^3 L_R C_{RE}^2 R_L^2}{1 + \omega^2 C_{RE}^2 R_L^2}$ are the receiver

circuit resistance and reactance respectively. Substituting Eqn. (F5) in (F1):

$$V_{IN} - \frac{I_T}{j\omega C_T} - I_{LT} \left[R_T + j\omega L_T + \frac{\omega^2 M^2}{j\omega L_R + R_R + \frac{R_L}{1 + j\omega C_R R_L}} \right] = 0,$$

$$\text{or } V_{IN} - \frac{I_T}{j\omega C_T} - I_{LT} [R_T + j\omega L_T + Z_{REF}] = 0.$$

Here, the reflected impedance of the receiver circuit into the transmitter circuit is obtained similar to the parallel compensation case in Appendix D but with C_R now replaced by C_{RE} .

$$Z_{REF} = \frac{\omega^2 M^2 (\omega^2 R_R C_{RE}^2 R_L^2 + R_R + R_L)}{(R_R + R_L - \omega^2 L_R C_{RE} R_L)^2 + (\omega L_R + \omega R_R C_{RE} R_L)^2} + j \left[\frac{\omega^2 M^2 (\omega C_{RE} R_L^2 - \omega^3 L_R C_{RE}^2 R_L^2 - \omega L_R)}{(R_R + R_L - \omega^2 L_R C_{RE} R_L)^2 + (\omega L_R + \omega R_R C_{RE} R_L)^2} \right]$$

$$\text{Here, } R_{REF} = \frac{\omega^2 M^2 (\omega^2 R_R C_{RE}^2 R_L^2 + R_R + R_L)}{(R_R + R_L - \omega^2 L_R C_{RE} R_L)^2 + (\omega L_R + \omega R_R C_{RE} R_L)^2} \text{ and} \quad (F6A)$$

$$X_{REF} = \frac{\omega^2 M^2 (\omega C_{RE} R_L^2 - \omega^3 L_R C_{RE}^2 R_L^2 - \omega L_R)}{(R_R + R_L - \omega^2 L_R C_{RE} R_L)^2 + (\omega L_R + \omega R_R C_{RE} R_L)^2} \quad (F6B)$$

are the reflected resistance and reactance of the receiver circuit into the transmitter circuit. The resonance frequency ω_{or} of the receiver coil can be obtained by equating $X_{REC} = 0$ or $X_{REF} = 0$.

In either case we obtain

$$\omega_{or} = \sqrt{\frac{C_{RE} R_L^2 - L_R}{L_R C_{RE}^2 R_L^2}}. \quad (F6C)$$

When $\omega = \omega_{or}$, then $Z_{REF} = R_{REF}$. C_T and C_{RE} are chosen such that both transmitter and receiver coils resonate at the same operating frequency $\omega_0 = \omega_{or} = \omega_{0r}$. While conducting test measurements on the coil for an operating frequency the value of C_{RE} is calculated from the above equation for receiver coil resonance. We obtain

$$C_{RE} = \frac{R_L \pm \sqrt{R_L^2 - 4\omega_0^2 L_R^2}}{2\omega_0^2 L_R R_L}. \quad (F6D)$$

In order to limit C_{RE} to real values, $R_L^2 - 4\omega_0^2 L_R^2 \geq 0$ or $\omega_0 \leq \frac{R_L}{2L_R}$.

Figure F.2 shows the equivalent transmitter side circuit with the receiver side reflected impedance. The value of C_T is calculated by first deriving an expression for the transmitter coil

impedance Z_{TRA} . Now, $Z_{TRA} = \frac{1}{j\omega C_T} + \frac{(R_T + R_{REF}) + j\omega L_T}{1 + (R_T + R_{REF})j\omega C_{ST} - \omega^2 L_T C_{ST}}$. On further simplification,

$$Z_{TRA} = \frac{\omega^2 (R_T + R_{REF}) C_T (1 - \omega^2 L_T C_{ST}) (C_T + C_{ST}) - [1 - \omega^2 L_T (C_T + C_{ST})] [\omega^2 C_T C_{ST} (R_T + R_{REF})]}{\omega^2 C_T^2 (1 - \omega^2 L_T C_{ST})^2 + \omega^4 C_T^2 C_{ST}^2 (R_T + R_{REF})^2} + j \left(\frac{\omega^3 C_T C_{ST} (R_T + R_{REF})^2 (C_T + C_{ST}) + \omega C_T [1 - \omega^2 L_T (C_T + C_{ST})] (1 - \omega^2 L_T C_{ST})}{\omega^2 C_T^2 (1 - \omega^2 L_T C_{ST})^2 + \omega^4 C_T^2 C_{ST}^2 (R_T + R_{REF})^2} \right).$$

$$\text{Here, } R_{TRA} = \frac{\omega^2 (R_T + R_{REF}) C_T (1 - \omega^2 L_T C_{ST}) (C_T + C_{ST}) - [1 - \omega^2 L_T (C_T + C_{ST})] [\omega^2 C_T C_{ST} (R_T + R_{REF})]}{\omega^2 C_T^2 (1 - \omega^2 L_T C_{ST})^2 + \omega^4 C_T^2 C_{ST}^2 (R_T + R_{REF})^2} \quad (F7A)$$

$$\text{and } X_{TRA} = - \left(\frac{\omega^3 C_T C_{ST} (R_T + R_{REF})^2 (C_T + C_{ST}) + \omega C_T [1 - \omega^2 L_T (C_T + C_{ST})] (1 - \omega^2 L_T C_{ST})}{\omega^2 C_T^2 (1 - \omega^2 L_T C_{ST})^2 + \omega^4 C_T^2 C_{ST}^2 (R_T + R_{REF})^2} \right) \quad (F7B)$$

are the transmitter coil resistance and reactance respectively. The transmitter coil compensation capacitor C_T can be calculated by equating $X_{TRA} = 0$. The expression obtained is:

$$C_T = \frac{2\omega_0^2 L_T C_{ST} - \omega_0^2 C_{ST}^2 (R_T + R_{REF})^2 - \omega_0^4 L_T^2 C_{ST}^2 - 1}{\omega_0^2 C_{ST} (R_T + R_{REF})^2 + \omega_0^4 L_T^2 C_{ST} - \omega_0^2 L_T}. \quad (F8)$$

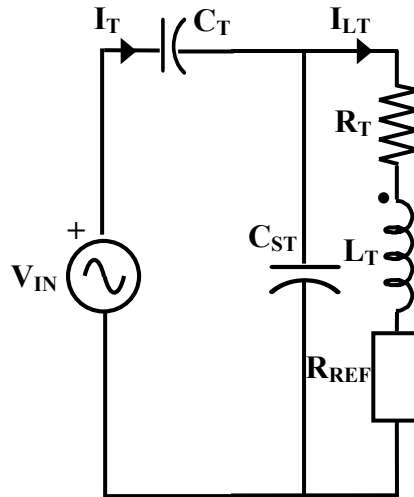


Figure F.2: Equivalent circuit on the transmitter side of an inductively coupled circuit.

The link efficiency η for the transmitter coil and receiver coil can be obtained as $\eta = \eta_T \times \eta_R$.

Here, η_T and η_R are the transmitter coil and receiver coil efficiencies respectively. As before,

$$\eta_T = \frac{R_{REF}}{R_T + R_{REF}} \text{ or}$$

$$\eta_T = \frac{\omega_0^2 M^2 (\omega_0^2 R_R C_{RE}^2 R_L^2 + R_R + R_L)}{\omega_0^2 M^2 (\omega_0^2 R_R C_{RE}^2 R_L^2 + R_R + R_L) + R_T \left[(R_R + R_L - \omega_0^2 L_R C_{RE} R_L)^2 + (\omega_0 L_R + \omega_0 R_R C_{RE} R_L)^2 \right]}$$

The receiver circuit efficiency is calculated as $\eta_R = \frac{1}{1 + \frac{R_R}{R_L} \left\{ \frac{|I_R|}{|I_{RL}|} \right\}^2}$ or

$$\eta_R = \frac{R_L}{R_R + R_L + \omega_0^2 R_R C_{RE}^2 R_L^2}.$$

The overall link efficiency is given by $\eta = \eta_T \times \eta_R$, or

$$\eta = \frac{\omega_0^2 M^2 R_L}{R_T \left\{ (R_R + R_L - \omega_0^2 L_R C_{RE} R_L)^2 + (\omega_0 L_R + \omega_0 R_R C_{RE} R_L)^2 \right\} + \omega_0^2 M^2 (R_R + R_L + \omega_0^2 R_R C_{RE}^2 R_L^2)} \quad \text{or}$$

$$\eta = \frac{M^2 R_L}{R_T \left\{ \frac{L_R (L_R + R_R C_{RE} R_L)^2}{(C_{RE} R_L^2 - L_R)} + (L_R + R_R C_{RE} R_L)^2 \right\} + M^2 \left\{ \frac{(R_R + R_L) L_R + (C_{RE} R_L^2 - L_R) R_R}{L_R} \right\}}.$$

APPENDIX G

MATLAB CODE FOR THE COMPENSATED CASE – CONSIDERING COIL PARASITIC CAPACITANCES

Matlab code to generate a plot for variation in link efficiency as a function of operating frequency. Here the transmitter coil is compensated in series and the receiver coil is compensated in parallel (C_{R+} and C_{R-}). Parasitic capacitances are considered in this code.

```
% Plot for link efficiency for the compensated case, considering coil parasitics (Cr+ and Cr-).

% clc
% clear all
% close all
format long

% Design values
Rt = 0.25;
Rr = 0.107;
Lt=2.5*10^-3;
Lr=39*10^-6;
M=4.7960*10^-6;
Ro=32.5;

% Frequency setting
f = [200 500 1.0E+03 1.5E+03 2.0E+03 2.5E+03 3.0E+03 3.5E+03 4.0E+03 4.50E+03
5.0E+03 5.5E+03 6.0E+03 6.5E+03 7.0E+03 7.5E+03 8.0E+03 8.5E+03 9.0E+03 9.5E+03
10.0E+03 12.5E+03 15.0E+03 2.0E+04 2.5E+04 3.0E+04 3.5E+04 4.0E+04 4.5E+04 5.0E+04
5.5E+04 6.0E+04 6.5E+04];
w = 2*pi*f

% Transmitter and receiver parasitic capacitance values
Cst = [47.6*10^-12 47.6*10^-12 47.6*10^-12 47.6*10^-12 47.6*10^-12 47.6*10^-12
47.6*10^-12 47.6*10^-12 47.6*10^-12 47.6*10^-12 47.6*10^-12 47.6*10^-12 47.6*10^-12
47.6*10^-12 47.6*10^-12 47.6*10^-12 47.6*10^-12 47.6*10^-12 47.6*10^-12 47.6*10^-12
47.6*10^-12 47.6*10^-12 47.6*10^-12 47.6*10^-12 47.6*10^-12 47.6*10^-12 47.6*10^-12
47.6*10^-12 47.6*10^-12 47.6*10^-12 47.6*10^-12 47.6*10^-12 47.6*10^-12];
Csr = [2.1*10^-12 2.1*10^-12 2.1*10^-12 2.1*10^-12 2.1*10^-12 2.1*10^-12 2.1*10^-12
2.1*10^-12 2.1*10^-12 2.1*10^-12 2.1*10^-12 2.1*10^-12 2.1*10^-12 2.1*10^-12
2.1*10^-12 2.1*10^-12 2.1*10^-12 2.1*10^-12 2.1*10^-12 2.1*10^-12 2.1*10^-12
2.1*10^-12 2.1*10^-12 2.1*10^-12 2.1*10^-12 2.1*10^-12 2.1*10^-12 2.1*10^-12
2.1*10^-12 2.1*10^-12];

% Transmitter and receiver compensation capacitor values
Cre = (Ro^2+(Ro^4-(4*(w*Ro*Lr).^2)).^0.5)./(2*(w*Ro).^2*Lr)
```

```

Cr = Cre-Csr
Rref = (w.^2*M^2.*(w.^2.*Rr.*Cr.^2*Ro^2+Rr+Ro))./((Rr+Ro-
w.^2.*Lr.*Cr*Ro).^2+(w.*Lr+w.*Rr.*Cr*Ro).^2);
Ct = (2*w.^2.*Lt.*Cst-w.^2.*Cst.^2.*(Rt+Rref).^2-w.^4.*Lt.^2.*Cst.^2-
1)./(w.^2.*Cst.*(Rt+Rref).^2+w.^4.*Lt.^2.*Cst-w.^2.*Lt);

% Link efficiency
ntruecomp = ( ((Rref.*((1-w.^2.*Lt.*Cst).^2-w.^2.*Cst.^2.*(Rt+Rref).^2))./(1-
w.^2.*Lt.*Cst).^2+w.^2.*Cst.^2.*(Rt+Rref).^2).*(Ro./(Rr+Ro+w.^2.*Rr.*Cr.^2*Ro^2)) )./(
((w.^2.*(Rt+Rref).*Ct.*(1-w.^2.*Lt.*Cst).*(Ct+Cst)-(1-
w.^2.*Lt.*(Ct+Cst)).*(w.^2.*Ct.*Cst.*(Rt+Rref)))./(w.^2.*Ct.^2.*(1-
w.^2.*Lt.*Cst).^2+w.^4.*Ct.^2.*Cst.^2.*(Rt+Rref).^2)))

% Plot (semilog scale)
semilogx(f,ntruecomp);
grid on
hold on

% % Plot (log scale)
% loglog(f,ntruecomp);
% grid on
% hold on

```

APPENDIX H

LI-ION BATTERY RATINGS

Mini-prismatic polymer lithium-ion battery (PR-042025) manufactured by TCL Hyperpower Batteries Inc. Battery ratings as provided by the manufacturer are listed in Table H1 below.

Table H1: Polymer Li-ion battery (PR-042025) ratings from TCL Hyperpower Batteries Inc.

Item		Rating	Note
3.1	Capacity	150mAh	Discharge:0.2CmA (30mA) cut off Voltage:3V for cell
3.2	Nominal Voltage	Average 3.7V	Discharge:0.2CmA (30mA) cut off Voltage:3V for cell
3.3	AC Impedance Resistance	$\leq 260m\ \Omega$	
3.4	Discharge Cut-off Voltage	3.00V	
3.5	Charge Current	150mA	Standard Charge
3.6	Charge Voltage	4.2V	
3.7	Max. Charge Voltage	4.23V	
3.8	Charge Time	Approx 2.5h	Charge: 1.0CmA(150mA)
3.9	Max. Charge Current	225mA	1.5CmA
3.10	Max. Discharge Current	300mA	2.0CmA
3.11	Weight	Approx 3.0g	
3.12	Operating Temperature	Charge	0~+45°C
		Discharge	-20~+60°C
3.13	Storage Temperature	less than 1 month	-20~+45°C
		less than 6 months	-20~+35°C
			Recommended storage temperature: 20°C ,at the shipment state

APPENDIX I

MATLAB CODE TO CALCULATE POWER DELIVERED TO THE LOAD

Matlab code to generate a plot for variation in power delivered to the load as a function of operating frequency. Receiver circuit has been compensated in parallel (C_{R+}). Parasitic coil capacitances are considered in this code.

Plot for load power delivery

```
clear all
% close all

format long

% assigning values common to all three cases

Vin=1.55;

Rl=65;
Ro=Rl/2;
Lt=2.5*10-3;
Rt=0.24;
Cst=47.6*10-12;
% Cst=30*10-9;
Lr=39*10-6;
Rr=0.107;
Csr=2.1*10-12;
% Cst=3*10-9;
M=4.7960*10-6;

% freq
f = [200 500 1.0E+03 1.5E+03 2.0E+03 2.5E+03 3.0E+03 3.5E+03 4.0E+03 4.50E+03
5.0E+03 5.5E+03 6.0E+03 6.5E+03 7.0E+03 7.5E+03 8.0E+03 8.5E+03 9.0E+03 9.5E+03
10.0E+03 12.5E+03 15.0E+03 2.0E+04 2.5E+04 3.0E+04 3.5E+04 4.0E+04 4.5E+04 5.0E+04
5.5E+04 6.0E+04 6.5E+04];
w = 2*pi*f

% Calculation of receiver coil capacitance: Cr
Cr=(Rl2+(Rl4-(16.*(w.*Rl.*Lr).^2)).0.5)/(2.*(w.*Rl).^2.*Lr)

% Calculation of receiver coil impedance: Zr
% addrr = (2*Rl/(4+(w*Cr*Rl)2));
rr = Rr+(2*Rl/(4+(w.*Cr.*Rl).^2));
xr = w.*Lr-((w.*Cr.*Rl2)/(4+(w.*Cr.*Rl).^2));
```

```

Zr = rr + i.*xr
% Zrabs = abs(Zr);

% Calculation of Load. Load is Cr parallel to Ro
Zl = Rl*2./(4+(w.*Cr.*Rl).^2)-i.*((w.*Cr.*Rl.^2)./(4+(w.*Cr.*Rl).^2))
% rIZl = real(Zl);
% imgZl = imag(Zl);
% Zlabs = abs(Zl);

% Calculation of transmitter coil capacitance: Ct
Rte=Rt+((w.^4.*M^2.*Rr.*Cr.^2.*Rl^2)+(4*w.^2.*M^2.*Rr)+(2*w.^2.*M^2.*Rl))./(((2*Rr)+Rl-(w.^2.*Lr.*Cr.*Rl)).^2+((2*w.*Lr)+(w.*Rr.*Cr.*Rl)).^2);
Xte=(w.*Lt)+((w.^3.*M^2.*Cr.*Rl^2)-(w.^5.*M^2.*Lr.*Cr.^2.*Rl^2)-(4*w.^3.*M^2.*Lr))./(((2*Rr)+Rl-(w.^2.*Lr.*Cr.*Rl)).^2+((2*w.*Lr)+(w.*Rr.*Cr.*Rl)).^2);
Ct = ((1-w.*Cst.*Xte).^2+(w.*Cst.*Rte).^2)./((w.*Xte)-((w.^2).*Cst.*(Rte.^2+Xte.^2)))

% Calculation of transmitter coil impedance: Zt
rt=Rte./((1-w.*Cst.*Xte).^2+(w.*Cst.*Rte).^2);
Xt=-(1./(w.*Ct)).*(1+((w.^2.*Ct.*Cst.*(Rte.^2+Xte.^2))-(w.*Ct.*Xte))./((1-w.*Cst.*Xte).^2+(w.*Cst.*Rte).^2));
Zt=rt+i.*Xt
Zabs=abs(Zt);

% Calculation of transmitter coil current: It & Ilt
It=Vin./Zt
Ilt=It.*(1+(Cst./Ct))-Vin.*(i.*(w.*Cst))
% It=Vin/(abs(Zt));

% Calculation of receiver coil current: Ir
Ir = (i.*(w.*M.*Ilt))./Zr
rIIR = real(Ir);
imgIr = imag(Ir);
Irabs = abs(Ir);

% Calculation of dc voltage at load: Vo and dc power at load: Po
Vo = Zl.*Ir
% rIVo = real(Vo);
% imgVo = imag(Vo);
% Voabs = abs(Vo);
Po = Vo.^2./Ro
rIPo = real(Po);
Poabs = abs(Po);
semilogx(f,Po)
grid on
hold on

```

APPENDIX J

TABLE AND CHART FOR SKIN EFFECT MODEL

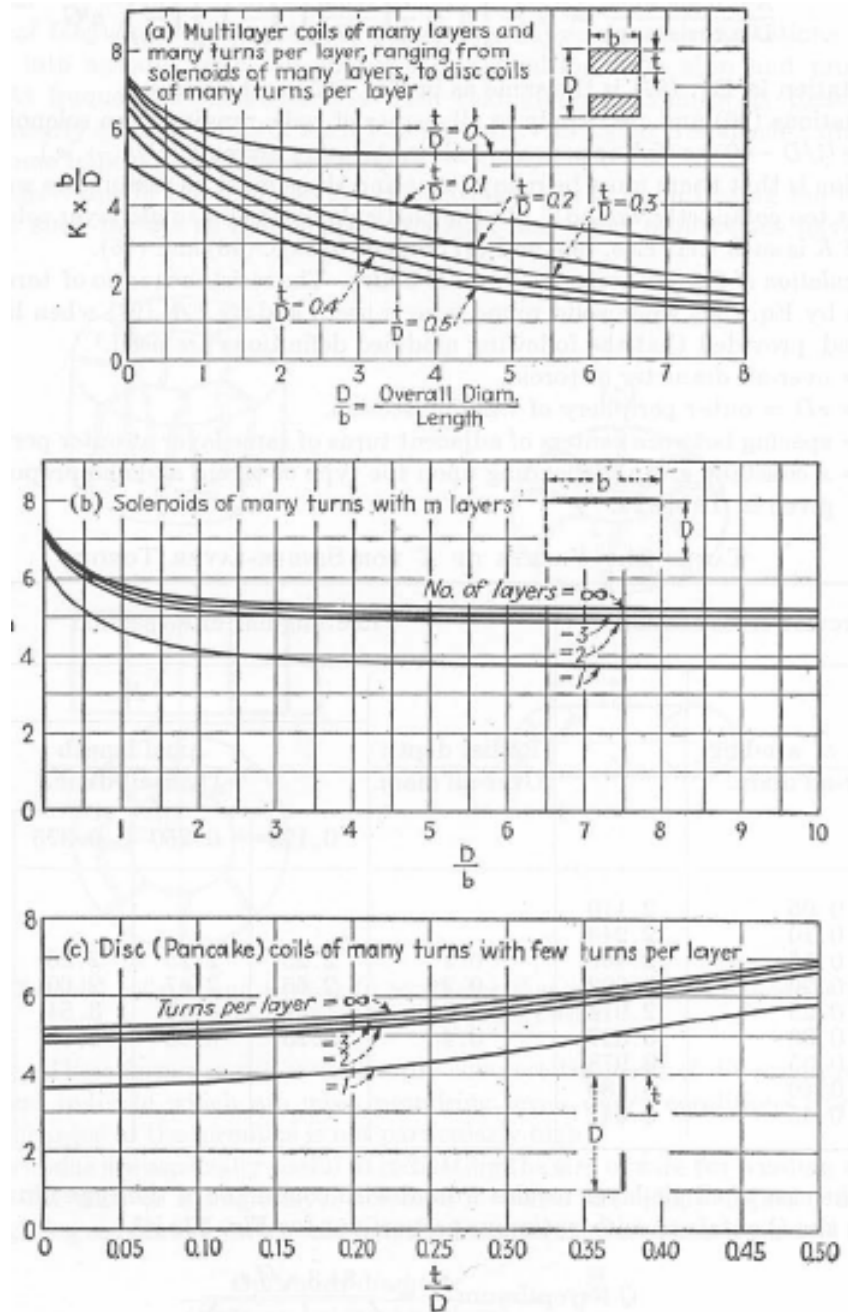


Figure J.1: Plots for various values of K for multilayer coils. After reference [27].

Table J.1: Values for functions H and G. After reference [27].

VALUES OF THE FUNCTIONS *H* AND *G*

d = diameter of wire, cm; ρ = resistivity, cgs units; *f* = frequency, cycles per sec;
 $x = \pi d \sqrt{2f/\rho}$. For copper of resistivity 1,700 cgs units $x = 0.1078 d \sqrt{f}$

<i>x</i>	<i>H</i>	<i>G</i>	<i>x</i>	<i>H</i>	<i>G</i>	<i>x</i>	<i>H</i>	<i>G</i>	<i>x</i>	<i>H</i>	<i>G</i>
0.0	1.000	$x^4/64$	2.5	1.175	0.2949	5.0	2.043	0.755	10.0	3.799	1.641
0.1	1.000		2.6	1.201	0.3184	5.2	2.114	0.790	11.0	4.151	1.818
0.2	1.000		2.7	1.228	0.3412	5.4	2.184	0.826	12.0	4.504	1.995
0.3	1.000		2.8	1.256	0.3632	5.6	2.254	0.861	13.0	4.856	2.171
0.4	1.000		2.9	1.286	0.3844	5.8	2.324	0.896	14.0	5.209	2.348
0.5	1.000		0.00097	3.0	1.318	0.4049	6.0	2.394	0.932	15.0	5.562
0.6	1.001	0.00202	3.1	1.351	0.4247	6.2	2.463	0.967	16.0	5.915	2.702
0.7	1.001	0.00373	3.2	1.385	0.4439	6.4	2.533	1.003	17.0	6.268	2.879
0.8	1.002	0.00632	3.3	1.420	0.4626	6.6	2.603	1.038	18.0	6.621	3.056
0.9	1.003	0.01006	3.4	1.456	0.4807	6.8	2.673	1.073	19.0	6.974	3.233
1.0	1.005	0.01519	3.5	1.492	0.4987	7.0	2.743	1.109	20.0	7.328	3.409
1.1	1.008	0.02196	3.6	1.529	0.5160	7.2	2.813	1.144	21.0	7.681	3.586
1.2	1.011	0.03059	3.7	1.566	0.5333	7.4	2.884	1.180	22.0	8.034	3.763
1.3	1.015	0.04127	3.8	1.603	0.5503	7.6	2.954	1.216	23.0	8.388	3.940
1.4	1.020	0.0541	3.9	1.640	0.5673	7.8	3.024	1.251	24.0	8.741	4.117
1.5	1.026	0.0691	4.0	1.678	0.5842	8.0	3.094	1.287	25.0	9.094	4.294
1.6	1.033	0.0863	4.1	1.715	0.601	8.2	3.165	1.322	30.0	10.86	5.177
1.7	1.042	0.1055	4.2	1.752	0.618	8.4	3.235	1.357	40.0	14.40	6.946
1.8	1.052	0.1265	4.3	1.789	0.635	8.6	3.306	1.393	50.0	17.93	8.713
1.9	1.064	0.1489	4.4	1.826	0.652	8.8	3.376	1.428	60.0	21.46	10.48
2.0	1.078	0.1724	4.5	1.863	0.669	9.0	3.446	1.464	70.0	25.00	12.25
2.1	1.094	0.1967	4.6	1.899	0.686	9.2	3.517	1.499	80.0	28.54	14.02
2.2	1.111	0.2214	4.7	1.935	0.703	9.4	3.587	1.534	90.0	32.07	15.78
2.3	1.131	0.2462	4.8	1.971	0.720	9.6	3.657	1.570	100.0	35.61	17.55
2.4	1.152	0.2708	4.9	2.007	0.738	9.8	3.728	1.605			
2.5	1.175	0.2949	5.0	2.043	0.755	10.0	3.799	1.641	Large	$\frac{\sqrt{2x+1}}{4}$	$\frac{\sqrt{2x-1}}{8}$

APPENDIX K

PERFORMANCE CHARACTERISTICS OF LI-ION BATTERY

UBC641730/ Performance Characteristics

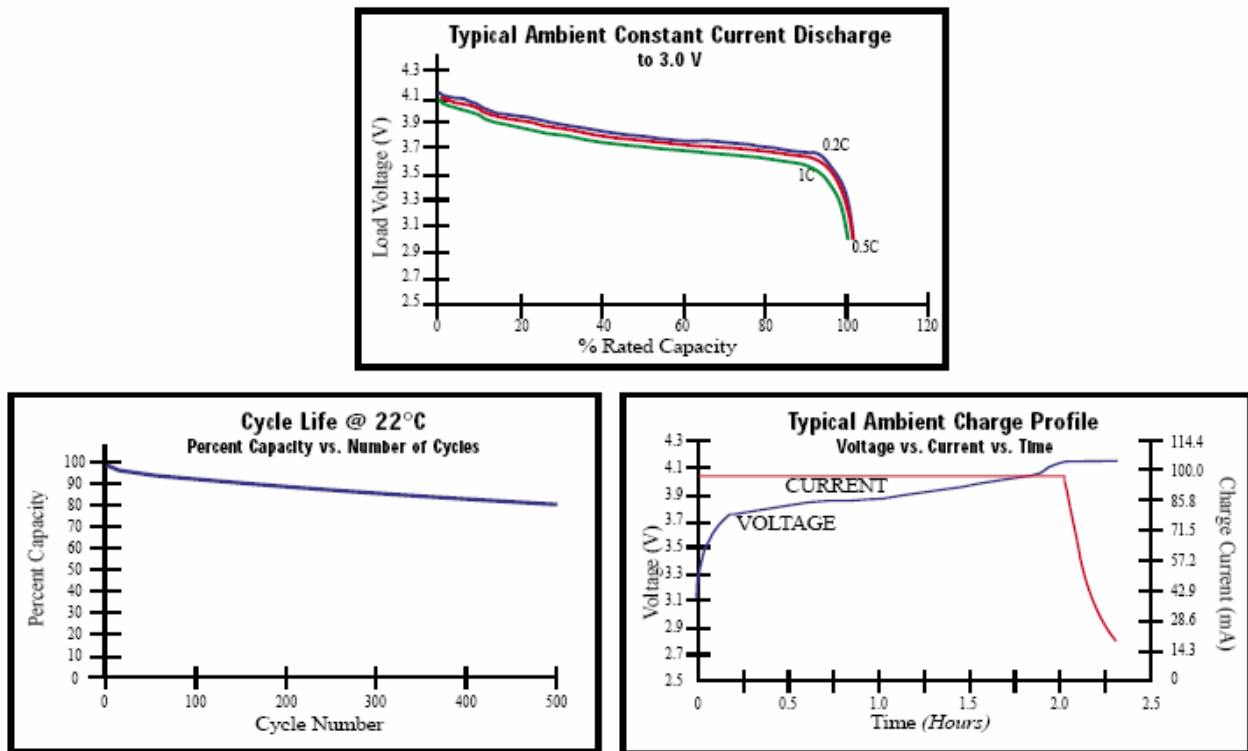


Figure K.1: The performance characteristics of an Ultralife polymer rechargeable battery. The actual battery used for experimental purposes was a similar Powerizer polymer Li-ion rechargeable battery. No data sheets were made available by Powerizer for their product.

VITA

Venkat Reddy Gaddam was born on December 27, 1978, in Hyderabad, India. He graduated from Bapuji Institute of Engineering and Technology, Davangere, India, where he earned a bachelor's degree of engineering in electronics and communication engineering in December 2002. Later in August 2002, he was enrolled in the Department of Electrical and Computer Engineering at Louisiana State University, Baton Rouge, Louisiana and has worked as a graduate research assistant in the field of remote power deliver systems for bio-implantable purposes. He is presently a candidate for the degree of Master of Science in Electrical Engineering at Louisiana State University.